

### 13. UPPER OCEAN TEMPERATURE AND NUTRIENT CONTRASTS INFERRED FROM PLEISTOCENE PLANKTONIC FORAMINIFER $\delta^{18}\text{O}$ AND $\delta^{13}\text{C}$ IN THE EASTERN EQUATORIAL PACIFIC<sup>1</sup>

J.W. Farrell,<sup>2</sup> D.W. Murray,<sup>3</sup> V.S. McKenna,<sup>3</sup> and A.C. Ravelo<sup>4</sup>

#### ABSTRACT

We present Pleistocene oxygen and carbon isotope records from two planktonic foraminifer species (*Globigerinoides sacculifer* and *Neoglobobulimina dutertrei*) from Ocean Drilling Program Site 847 (0°16'N, 95°19'W; 3334 m water depth). An average sample resolution of 4500 yr was obtained by sampling at an interval of 15 cm through a continuous 35-m section from 0 to 1.15 Ma. Our  $\delta^{18}\text{O}$ -based chronology is similar to that derived independently by astronomically tuning the gamma-ray attenuation porosity evaluator (GRAPE) record (Shackleton et al., this volume), though offsets as large as  $\pm 30$  k.y. occur on occasion.

The surface waters at eastern equatorial Pacific Site 847, 380 km west of the Galápagos, are characterized by strong and constant upwelling, elevated nutrient concentrations, and high productivity. The isotopic composition of *G. sacculifer* (300–355  $\mu\text{m}$ ) reflects conditions in the thin-surface mixed layer, and the composition of *N. dutertrei* (355–425  $\mu\text{m}$ ) monitors the subsurface waters of the permanent shallow (10–40 m) thermocline. The Pleistocene  $\delta^{18}\text{O}$  difference (*N. dutertrei* minus *G. sacculifer*,  $\Delta\delta^{18}\text{O}_{\text{d-s}}$ ) averages 0.9‰ and ranges from 0‰ to 1.7‰. Neglecting species effects and shell size, the average Pleistocene  $\delta^{13}\text{C}$  difference (*G. sacculifer* minus *N. dutertrei*,  $\Delta\delta^{13}\text{C}_{\text{s-d}}$ ) is 0.0‰ and ranges from -0.5‰ to 0.5‰. The  $\Delta\delta^{18}\text{O}_{\text{d-s}}$  and  $\Delta\delta^{13}\text{C}_{\text{s-d}}$  records are used to infer vertical contrasts in upper ocean water temperature and nutrient concentration, though  $\delta^{13}\text{C}$  may also be influenced by other factors, such as  $\text{CO}_2$  gas exchange. Variations in the isotopic differences are often synchronous with glacial/interglacial climate change. Glacial periods are characterized by smaller vertical contrasts in both temperature and nutrient concentration, and by notably greater accumulation rates of *N. dutertrei* and  $\text{CaCO}_3$ . We attribute these responses to greater upwelling at the equatorial divergence. Superimposed on the glacial/interglacial  $\Delta\delta^{18}\text{O}_{\text{d-s}}$  pattern is a long-term trend possibly associated with the advection of Peru Current waters. The temporal fluctuations in the isotopic contrasts are strikingly similar to those observed at Site 851 (Ravelo and Shackleton, this volume), suggesting that the inferred changes in thermal and chemical profiles occurred over a broad region in the equatorial Pacific.

#### INTRODUCTION

A principal objective of ODP Leg 138 was to recover complete sequences of late Neogene age sediments to address fundamental questions regarding the paleoenvironment in the eastern equatorial Pacific (EEP) Ocean. To this end, we constructed a continuous record of undisturbed late Neogene age sediments, with a high accumulation rate (averaging 3.3 cm/k.y.), from the multiple advanced hydraulic piston cores from four offset holes at Site 847, located on the equator, 380 km west of the Galápagos Archipelago (Fig. 1). This sedimentary record provides an opportunity to evaluate oceanic and climatic evolution along the equator, for the site has maintained the same latitude since forming at about 7 Ma (Mayer, Pisias, Janecek, et al., 1992). A database of continuous and detailed paleoenvironmental indices has been synthesized. Our focus in this study is on the thermal and chemical gradients in the upper water column, inferred from the oxygen and carbon isotope records from two species of planktonic foraminifers that inhabited different depths in the photic zone. Two companion reports focus on the variations in the Pleistocene planktonic foraminifer fauna (McKenna et al., this volume), and on biogenic sedimentation (Murray et al., this volume) at Site 847.

#### REGIONAL SETTING

##### Oceanographic and Climatic Setting

Surface-water circulation in the equatorial Pacific is largely controlled by the westward-blowing trade winds, which are centered on the intertropical convergence zone (ITCZ), just north of the equator. Site 847 sits beneath the westward-flowing south equatorial current (SEC), which is forced by the southeast trade (SET) winds (Fig. 1). The SEC is fed by the Peru current (PC), which advects cool, nutrient-rich waters from the southeast Pacific into the Galápagos Region; and by the north equatorial countercurrent (NECC), which carries eastward the return-flow surface waters from the western equatorial "warm-pool." At the equator, the surface-water transport diverges poleward and continuity necessitates that displaced surface waters are replaced by subsurface waters, which upwell from no more than 40–100 m (Bryden and Brady, 1985). These cool, nutrient-rich waters, which are separated from the thin overlying mixed layer by the permanent shallow thermocline, fuel biological productivity at one of the highest levels in the open ocean (Chavez and Barber, 1987). The upwelling at Site 847 maintains an annual mean sea surface temperature (SST) of 23.9°C (Levitus, 1982), about 5°C colder than surface waters in the western equatorial Pacific (WEP). A strong thermocline exists between 10 and 40 m throughout the year near Site 847 (Hayes et al., 1986). The precise thermocline depth has been defined in a variety of ways, and we describe three (Fig. 2A). Robinson (1976) mapped the annual mean "top of the thermocline" at ~13 m near Site 847, which is the depth where the temperature was 2°F colder than the surface. The second estimate of 37 m was derived by applying the 20°C isotherm definition ("upper thermocline") of McPhaden and Hayes (1990) to the Levitus (1982) data. The third estimate of 20 m (Hayes et al., 1986) also used the 20°C isotherm definition, but was based on different data. Since Site 847 is always south of the ITCZ, precipitation in this region is relatively low compared to the tropical regions

<sup>1</sup> Pisias, N.G., Mayer, L.A., Janecek, T.R., Palmer-Julson, A., and van Andel, T.H. (Eds.), 1995. *Proc. ODP, Sci. Results*, 138: College Station, TX (Ocean Drilling Program).

<sup>2</sup> Department of Geological Sciences, Brown University, Providence, RI 02912-1846, U.S.A. (present address: Department of Oceanography, University of British Columbia, Vancouver, B.C., V6T 1Z4, Canada).

<sup>3</sup> Department of Geological Sciences, Brown University, Providence, RI 02912-1846, U.S.A.

<sup>4</sup> Marine Sciences Board, University of California, Santa Cruz, CA 95064, U.S.A.

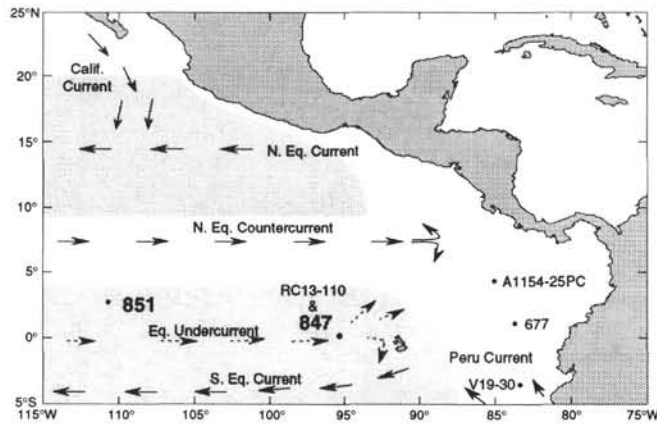


Figure 1. Location of Site 847 and other sites within the modern surface current system of the eastern equatorial Pacific. Shaded areas indicate the extent of the South and North Equatorial Current systems. The Equatorial Undercurrent flows subsurface, as indicated by dashed arrows.

to the north and east (Taylor, 1973). For example, the annual mean rainfall at Site 847 is about 70 cm/yr and varies on a monthly basis from a low of 1 cm/month in the fall, to a high of 20 cm/month in the spring. In contrast, monthly precipitation in the Panama Basin (5°N, 81°W) ranges from 25 to 40 cm/month, for an annual mean of 430 cm/yr. This volume of fresh water is large enough to significantly affect the isotopic composition of Panama Basin foraminifers (Curry et al., 1983).

Although Site 847 always lies beneath the SET winds and the SEC, there is seasonal variability in the oceanographic conditions that reflects the climatic forcing from the hemisphere in winter (Wyrtki, 1966). During February–April, the ITCZ, which marks the boundary between the northeast and southeast trade winds, moves to its most southerly location of the year, near 3°N. This prevents the NECC from developing. Since SET winds are weak at this time, the SEC diminishes, and the northern extent recedes to about 2°N. The SSTs at Site 847 are the highest of the year and surface salinity values are the lowest (Fig. 2C), because precipitation is at a maximum (Taylor, 1973). During May–July, the ITCZ shifts northward of 10°N as boreal winter begins. The NECC forms and the SEC strengthens and pushes northward. At Site 847, the SST drops from 26°C to about 23°C, surface salinity values climb to 34.5‰, and the thermocline descends below 40 m, the annual deep (Figs. 2A–2C). During August–January, the ITCZ reaches as far as 17°N, the most northerly position of the year. The SET and the SEC are at their strongest, and the NECC is fully developed. Relatively strong upwelling at this time of year results in a shallow thermocline and cool (22°–23°C) surface waters at Site 847.

### Interannual Variability (El Niño)

Although the amplitude of the seasonal changes in oceanographic conditions near Site 847 are distinct, they pale by comparison to the interannual perturbations induced by the El Niño Southern Oscillations (ENSO), which affect global climate conditions. The pronounced interannual changes are attributed to shifts between warmer climate phases (El Niño) and cooler ones (La Niña) that arise from instabilities in the coupled ocean-atmosphere of the tropical Pacific (Philander, 1990). El Niños in the EEP are characterized by a relaxation of the SET winds, a weakened SEC, reduced evaporation, higher SST, and significantly greater rainfall. As an El Niño evolves, the SST remains high because of the eastward advection of warm, nutrient-depleted WEP surface waters. These “backwashed” waters thicken the EEP mixed layer and significantly depress the thermocline.

The 1982–83 El Niño is an ideal example of the dramatic changes that occur in the oceanic, climatic, and ecological conditions along the

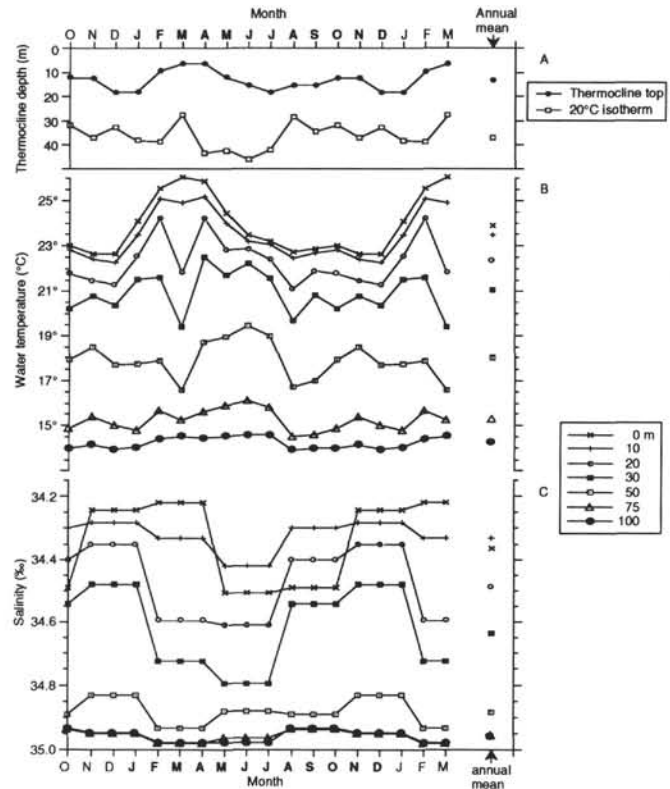


Figure 2. Monthly variations and annual averages of the oceanographic conditions in the upper 100 m near Site 847 (0°N, 95°W). Thermocline depths (A) have been estimated from the maps in Robinson (1976) and from the Levitus (1982) data by applying the 20°C isotherm definition of McPhaden and Hayes (1990). Water temperature (B) and salinity (C) are from Levitus (1982).

equatorial Pacific. Anomalous EEP SST and surface currents associated with this El Niño were first observed in August 1982 (Cane, 1983; Barber and Chavez, 1983; Halpern, 1987). By December, there was a tremendous thickening of the mixed layer near Site 847 and the thermocline (20°C isotherm) deepened from its average position of 37 m to almost 150 m, which is well below the photic zone (Halpern, 1987). The upper water column was nearly isothermal (Fig. 3B). The El Niño had a drastic impact on the biota. A fivefold decline in productivity was observed in the surface waters near Site 847. This was related to a sharp decline in the mixed layer nitrate concentrations that resulted from the upwelling of nutrient-depleted waters from the base of the mixed layer rather than the thermocline (Barber and Chavez, 1983). Farther to the west, biogenic particle fluxes were lower by a factor of two in sediment traps (139°W, 1°N) (Dymond and Collier, 1988).

### Subsurface Water

The subsurface water along the equator is the equatorial undercurrent (EUC), which flows from west to east, as a narrow ribbon between 2°N and 2°S (Lukas, 1986). The nutrient-rich EUC supplies the upwelling region in the equatorial Pacific and along coastal Peru (Wooster and Gilmartin, 1961; Wyrtki, 1967; Fiedler and Philbrick, 1991). The importance of this current cannot be underestimated, for it exerts a great influence upon the biological, physical, and chemical oceanography of the EEP. The current is composed of two water masses. The upper tier is the core of the current and is characterized by higher flow velocities, temperatures of 20°–21°C, and salinities of 35.2‰–35.4‰ (Tsuchiya, 1968). The lower tier is the “Equatorial 13°C Water” (Montgomery and Stroup, 1962), which forms a thermostat in the thermocline. Compared to the overlying tier, the waters in

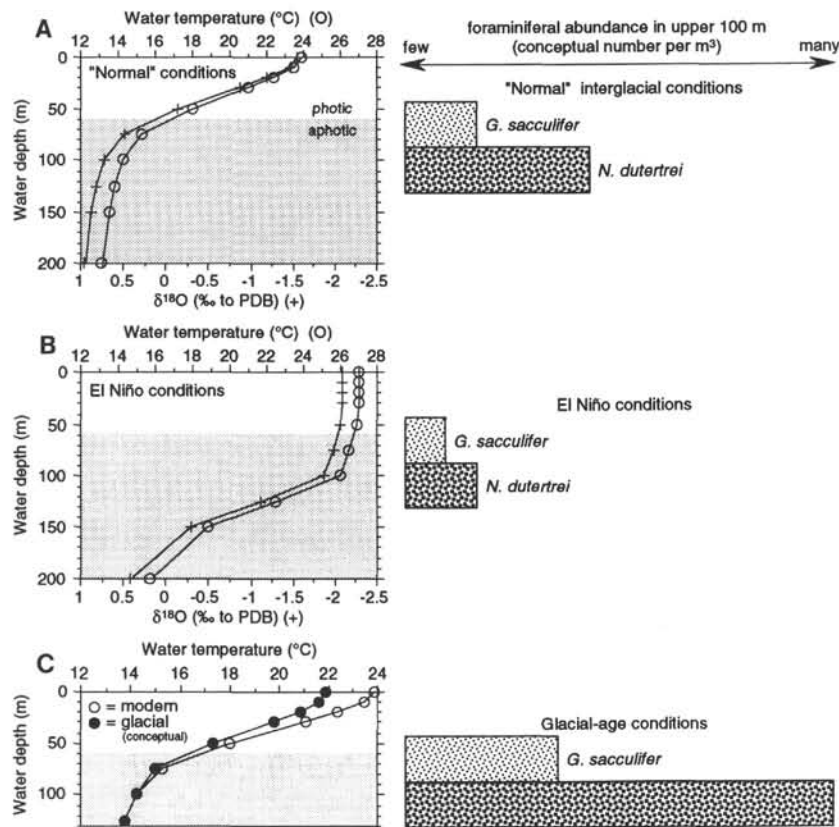


Figure 3. Conceptual ecological response of foraminifers during (A) "normal" divergent conditions, (B) El Niño conditions, and (C) glacial-age conditions in the eastern equatorial Pacific. The water temperature profile in Figure 3A is the annual average at 0°N, 95°W from Levitus (1982). The temperature profile in Figure 3B existed during December 1982 (Halpern, 1987). The photic zone extends to approximately 60 m (shaded area at depth is aphotic). The profiles of equilibrium  $\text{CaCO}_3\text{-}\delta^{18}\text{O}$  were calculated from the Levitus (1982) and Halpern (1987) temperature and salinity data by using the Fairbanks et al. (1982) salinity equation and the Erez and Luz (1983) paleotemperature equation. The hypothetical glacial temperature profile in Figure 3C is based on a 2°C cooler SST (Lyle et al., 1992) and a smaller thermal contrast inferred herein. *N. dutertrei* thrive in the upper thermocline (30–50 m) (Fig. 3A), which coincides with the nutricline during normal conditions. During the El Niño (Fig. 3B), their abundance declines because the formation of the thick, warm mixed layer depresses the thermocline into the aphotic zone where productivity decreases and the food supply shrinks. Enhanced upwelling and greater productivity during glacial times favored increased production of foraminifers, especially *N. dutertrei*. *G. sacculifer* inhabit the thin-surface mixed layer at all times. Lower *G. sacculifer* abundances during El Niños are attributed to a decline in primary productivity, whereas higher abundances during glacial times are inferred from increased productivity and from higher accumulation rates of tests at Site 847.

this one are nutrient rich, better oxygenated, cooler, and slightly fresher (13.9°C, 34.99‰ at 100 m at 0°N, 95°W; Lukas, 1986). This water shoals from below 150 m in the western Pacific to less than 30 m in the Galápagos region. Current speeds just west of the Galápagos are usually not faster than 70 cm/s (Lukas, 1986). Although the Galápagos Islands are an obstacle, the current splits, flows around them, upwells off the coast of Peru (Wyrki, 1963; Toggweiler et al., 1991), and ultimately feeds back into the SEC. The EUC feeds the SEC at subsurface, supplying most of its water, but the PC and the NECC also contribute (Wyrki, 1966).

The origin of the EUC has received considerable attention during the past 10 yr, particularly after it was recognized that this water mass may play an important role in ENSO events (Wooster and Guillen, 1974). The water in the upper tier originates within the central and eastern South Pacific Ocean (Tsuchiya et al., 1990). At the equator, it shoals to the east and is mixed into the surface waters between 110° and 95°W, thereby forming the center of the equatorial SST "cold

tongue" (Wyrki et al., 1981; Bryden and Brady, 1985). Based on pre-bomb  $\Delta^{14}\text{C}$  in seawater and corals, Toggweiler et al. (1991) proposed that the lower tier of the EUC forms as ~8°C water far across the ocean in the subantarctic region of the southwest Pacific, possibly from the "lighter variety" of subantarctic mode water (7°–10°C) (McCartney, 1982). The water moves north to the equator and then eastward, forming the bulk of the EUC. As it flows, the water grows warmer and less saline by diapycnal alteration. This lower tier water is the major source of upwelled waters along the equator, particularly in the EEP.

Flow of the EUC is controlled by the trade winds. The EUC is strongest and shallowest between March and September, when the trade winds blow vigorously. The current is weakest and deepest between November and January, when the trade winds diminish. Interannual climate perturbations also affect the EUC. For example, the EUC stopped completely during one part of the 1982–83 El Niño because the volume of warm water that accumulated in the EEP was

large enough to reverse the sea-surface pressure gradient along the equator (Cane, 1983).

Given the importance of this current, we suspect that paleoceanographic variability observed in the EEP sedimentary record may reflect changes in the formation and circulation rate of the EUC and/or the initial chemical and physical properties of the South Pacific source waters that ultimately ventilate the thermocline in the EEP.

## FORAMINIFER ECOLOGY AND ISOTOPIC COMPOSITION

### Foraminifer Ecology

Detailed studies of the ecology, vertical distribution, flux, and isotopic composition of foraminifers collected in sediment traps, plankton tows, and surface sediments have been undertaken in the eastern tropical Pacific, but almost exclusively in the Panama Basin (near 5°N, 81°W) (Fairbanks et al., 1982; Curry et al., 1983; Thunell et al., 1983; Thunell and Reynolds, 1984; Bé et al., 1985). Since the oceanographic and climatic regimes in this region are significantly different from those in the EEP, the results of these studies are not always applicable to Site 847. The planktonic foraminifer species in the Panama Basin, and most likely the EEP, can be divided into two major assemblages that are depth-related, and thus temperature-related (Bé et al., 1985). The thermocline separates these two assemblages. The surface waters (0–25 m) are populated by *G. ruber*, *G. glutinata*, *G. bulloides*, and *G. sacculifer* (without sacs). In the subsurface waters (25–50 m), where primary production peaks, the assemblage is dominated by *N. dutertrei*, *G. aequilateralis*, *H. pelagica*, and *G. menardii*. When the mixed layer is thick, and the thermocline is depressed, the shallow water assemblage dominates over the deeper one. Conversely, the deeper assemblage thrives at the expense of the shallower one when the mixed layer thins and the thermocline shoals up into the photic zone (Bé et al., 1985).

*G. sacculifer* is one of the shallowest dwelling species within the warm surface mixed layer (Fairbanks et al., 1982). Specimens without sacs live in greatest abundance in the upper 20 m, whereas those with sacs live in slightly deeper waters (Bé et al., 1985). In general, the standing stock of *G. sacculifer* and the flux out of the mixed layer is greatest when surface waters are warm, the thermocline is deep, and thermocline dwellers such as *N. dutertrei* are less abundant (Bé et al., 1985; Watkins et al., 1993) (Fig. 3). Hence, we speculate that the *G. sacculifer* flux at Site 847 may be slightly higher from January to May, when SST rises by 1° or 2°C. The flux is probably independent of seasonal variations in thermocline depth because they are minor. Given the oceanographic conditions at Site 847, we suspect that *G. sacculifer* are not abundant, especially in comparison to *N. dutertrei*. This is partly based on the observation that *N. dutertrei* comprise 45% of the average Pleistocene faunal assemblage at Site 847 whereas *G. sacculifer* average only 3% (McKenna et al., this volume).

*N. dutertrei* is a thermocline dweller that is most abundant in upwelling regions and along the margins of highest productivity areas (Hemleben et al., 1989). A pronounced maximum in the abundance of this species was observed in the Panama Basin at the depth of the steepest thermocline, greatest primary productivity, and the deep chlorophyll maximum (Fairbanks et al., 1982). Observations based on plankton tows and seasonal flux patterns (Thunell and Reynolds, 1984; Bé et al., 1985) show that *N. dutertrei* abundance increases when the thermocline shoals (Fig. 3). The closer the thermocline moves toward the surface, the greater the volume of nutrient-rich, cool, subsurface water that becomes available to elevate phytoplankton production in the photic zone. From February to May, when the thermocline is shallow in the Panama Basin, the *N. dutertrei* flux is at least three times greater than during the rest of the year (Thunell and Reynolds, 1984). Because the thermocline is shallow and relatively invariant at Site 847, we think *N. dutertrei* thrives throughout the year. This nonspinose species is widely thought to be free of algal symbionts, but recent work

suggests that during phytoplankton blooms, *N. dutertrei* may use algal cells as facultative symbionts (Hemleben et al., 1989), because phytoplankton cell division has been observed within the host vacuoles, indicating a healthy algal state (Gastrich, 1988).

### Isotopic Composition of *G. sacculifer*

The question of whether spinose species, such as *G. sacculifer*, calcify in oxygen isotopic equilibrium with ambient seawater is still debated despite the efforts of many investigators over the past 30 yr. Several studies suggest that equilibrium calcification occurs (Williams et al., 1979; Curry and Matthews, 1981; Deuser et al., 1981; Erez and Honjo, 1981; Erez and Luz, 1982), although in many cases, scatter in the data allows for disequilibrium of up to  $\pm 0.5\%$ . Compelling support for equilibrium calcification is presented by Erez and Luz (1983), who showed experimental data from laboratory-cultured *G. sacculifer* (containing symbiotic algae) that demonstrated equilibrium calcification with ambient water over a range of temperatures. Nevertheless, many studies based on plankton tows, culture experiments, sediment traps, and core tops suggest that spinose species such as *G. sacculifer* fractionate in disequilibrium on the order of  $-0.35\%$  to  $-0.6\%$  because of metabolic effects (Shackleton et al., 1973; Kahn, 1979; Fairbanks et al., 1980, 1982; Duplessy et al., 1981; Williams et al., 1981; Deuser, 1987; Spero, 1992; Spero and Lea, 1993).

Foraminifers in the surface sediments are often enriched in  $\delta^{18}\text{O}$  compared to those caught in plankton tows in the overlying waters. There are several ways to explain a 0.9‰ enrichment observed in core top *G. sacculifer* (Duplessy et al., 1981). First, living foraminifers may not have grown in the same environment as those that accumulated in the surface sediments, which most likely represent the average conditions of thousands of years. Second, differential dissolution may remove those specimens with thin tests that grew in warmer waters (Berger, 1971; Wu and Berger, 1989). Third, gametogenic calcification in deeper and colder waters may add a significant mass of calcite, thereby pushing the  $\delta^{18}\text{O}$  composition of the total shell toward values higher than those observed in shallow-dwelling members of the same species (Bé, 1980; Erez and Honjo, 1981; Duplessy et al., 1981; Spero and Lea, 1993). The foraminifers caught in plankton tows and at shallow depths occasionally have calcite crusts covering their tests, whereas crusts are commonly observed on seafloor specimens. This observation and several recent studies (e.g., Erez et al., 1991; Lohmann, 1992, 1993) suggest that calcification occurs over a wide range of water depths and thus shell chemistry records ocean properties extending from the mixed layer down to subthermocline waters. The impact of this crust on the isotopic composition of the bulk foraminifer is considered significant, for it may consist of 30%–50% of the total shell mass (Erez et al., 1991; Lohmann, 1993).

A strong positive correlation exists between *G. sacculifer* size and shell  $\delta^{13}\text{C}$  (Berger et al., 1978; Duplessy et al., 1981; Oppo and Fairbanks, 1989). A negative offset from the carbon isotopic composition of the dissolved inorganic carbon ( $\delta^{13}\text{C}$  of  $\Sigma\text{CO}_2$ ) in smaller specimens has been attributed to the incorporation of  $^{12}\text{C}$ -enriched metabolic  $\text{CO}_2$  (Williams et al., 1977), presumably derived from foraminiferal respiration. On the other hand, photosynthesis by symbiotic algae raises shell  $\delta^{13}\text{C}$  because preferential uptake of  $^{12}\text{C}$ -enriched inorganic carbon by the algae enriches the foraminiferal microenvironment in  $\text{H}^{13}\text{CO}_3^-$  (Spero and Williams, 1988). This mechanism may explain the positive correlation between shell size and  $\delta^{13}\text{C}$  (Oppo and Fairbanks, 1989) because larger shells often have a greater density of symbiotic algae. Ontological vital effects also may contribute in raising shell  $\delta^{13}\text{C}$  (Spero, 1992), thus bringing the test value closer to the equilibrium value. Because the isotopic composition of foraminifers is size dependent, we limited our analysis of *G. sacculifer* to those in the 300- to 355- $\mu\text{m}$  size range as often as was possible and we avoided specimens with the final sac.

## Isotopic Composition of *N. dutertrei*

Evidence suggests that *N. dutertrei* fractionates in  $\delta^{18}\text{O}$  equilibrium with seawater and calcifies within a narrow depth interval (Fairbanks et al., 1980, 1982). Sediment trap results suggest that this species calcifies at a constant temperature (19°C in the Panama Basin) and adjusts water depth on a seasonal basis to maintain this preferred temperature (Curry et al., 1983). Calcification at a constant, though regionally different, temperature is also supported by studies of core top specimens (Curry and Matthews, 1981; Ravelo and Fairbanks, 1992).

Opinion regarding calcification of *N. dutertrei* within a narrow temperature range is not unanimous. *N. dutertrei* may have lived at shallower depths, in warmer waters during glacial periods (Shackleton, 1977; Curry and Crowley, 1987). This interpretation is based on an assumed preference that *N. dutertrei* has for a particular water density and the fact that compared to the isotopic composition of mixed layer species and benthic foraminifers, the amplitude of *N. dutertrei*  $\delta^{18}\text{O}$  on a glacial/interglacial time scale is smaller. Other investigators (Kahn, 1979; Duplessy et al., 1981; Erez and Honjo, 1981; Bouvier-Soumagnac and Duplessy, 1985) argued that *N. dutertrei* secrete a significant amount of calcite (perhaps 20% to 50% of the total shell weight) in the deeper and colder waters below the thermocline during gametogenic calcification. If this secondary calcification is quantitatively significant, as some suspect (Lohmann, 1993), interpretation of seafloor *N. dutertrei*  $\delta^{18}\text{O}$  in terms of calcification at a constant water temperature becomes more complicated. The  $\delta^{18}\text{C}$  of *N. dutertrei* is positively correlated with size (Bouvier-Soumagnac and Duplessy 1985), and to minimize this effect on the isotope record, we limited our analysis to those specimens in the 355- to 425- $\mu\text{m}$  range.

## DATA AND METHODS

Listed in Appendixes A and B are the isotope results from 614 analyses performed on 236 samples taken at ~15-cm intervals from 138-847C-1H-1, 0 cm, through -4H-2, 137 cm (0.01–31.87 mbsf), and from various "patch" sections within Holes 847B and 847D.

### Depth Scales

Out of necessity, we report the data with respect to four depth scales: (1) conventional shipboard nominal depth (meters below seafloor [mbsf]); (2) shipboard composite depth (meters composite depth [mcd]); (3) revised composite depth (rmcd); and (4) Brown composite depth (Bmcd). The first three depth scales are described elsewhere (Hagelberg et al., this volume; Shackleton et al., this volume). The fourth scale is discussed in Murray et al. (this volume). In brief, the fourth scale was developed because the first three do not represent the stratigraphy of our sample suite accurately. This is based on our examination and interhole correlation of shipboard stratigraphies of sediment density (GRAPE), magnetic susceptibility, and color in Holes 847A, 847B, 847C, and 847D. Our composite depth section for Site 847 is based primarily on the first nine cores from Hole 847C. Missing intervals from this hole have been replaced with "patch" intervals from adjacent Holes 847B and 847D (Murray et al., this volume). All depths referred to in the remainder of this study are in "Bmcd" unless otherwise noted.

### Sample Preparation

All samples were subsampled, retaining approximately 1 cm<sup>3</sup> for %CaCO<sub>3</sub> and %opal analyses (Murray et al., this volume). The remainder was freeze-dried, weighed, disaggregated in tap water, wet-sieved through a 150- $\mu\text{m}$  sieve, and dried at 50°C. The fine fraction (<150  $\mu\text{m}$ ) was allowed to settle for 24 hr. The water was siphoned off to within about 1 cm of the sediment-water interface, and the fine residue was dried, weighed, and saved for future studies. The coarse fraction (>150  $\mu\text{m}$ ) was divided equally into two aliquots: one for

faunal analysis (McKenna, et al., this volume), and the other for stable isotope analysis.

### Stable Isotope Analysis

Foraminiferal  $\delta^{13}\text{C}$  and  $\delta^{18}\text{O}$  were measured in the Brown University Benedum Stable Isotope Laboratory between 13 August 1992 and 10 January 1993. In an attempt to minimize the noise from ontogenetic variation on the isotopic composition (Berger et al., 1978; Curry and Matthews, 1981; Duplessy et al., 1981), we selected specimens of *G. sacculifer* without the final sac and from the 300- to 355- $\mu\text{m}$  size range whenever possible. In samples having fewer specimens, the size range was extended to 425  $\mu\text{m}$  and those having sacs were used. The average number of tests used per isotope analysis was 13 for *N. dutertrei* and 12 for *G. sacculifer*. Specimens of *N. dutertrei* having low or flat trochospire, considered *N. eggeri* by Thompson and Saito (1974), were not preferentially avoided when selecting tests for isotopic analysis. In a Pleistocene record from the Panama Basin, Pedersen et al. (1991) documented that the  $\delta^{18}\text{O}$  of these morphotypes is about 0.1‰ greater than those with low trochospire. Selected foraminifer samples were transferred into stainless steel boats filled with ethyl alcohol and were crushed with a glass pestle. We prefer ethanol over the more commonly used methanol, because Keigwin and Jones (1990) suggested that pulverizing in methanol lowers the  $\delta^{18}\text{O}$  by 0.22‰ by variable partitioning of <sup>16</sup>O and <sup>18</sup>O between the water and CO<sub>2</sub> reaction products. The steel boats were placed in a drying oven at 75°C for at least 1 hr. Dry samples were roasted in vacuo at 300°C for 1 hr to remove possible organic contaminants. In the extraction line, each CaCO<sub>3</sub> sample was reacted with orthophosphoric acid at 90°C for 14 min. The extracted carbon dioxide was analyzed on a fully automated, online VG Sira 24 Micromass mass spectrometer. Isotopic composition is expressed as a deviation per mil from the PeeDee belemnite (PDB) standard (Craig, 1957).

The Benedum Stable Isotope Laboratory's mass spectrometry reference gas (BIG-5) is calibrated to PDB by analysis of National Bureau of Standards (NBS) 19 and 20. The Benedum values for NBS-19 are -2.10‰ ( $\delta^{18}\text{O}$ ) and 1.91‰ ( $\delta^{13}\text{C}$ ), which compares to values reported by the NBS (I.L. Barnes, pers. comm., 1985) of -2.19‰ ( $\delta^{18}\text{O}$ ) and 1.92‰ ( $\delta^{13}\text{C}$ ). The Benedum values for NBS-20 are -4.18‰ ( $\delta^{18}\text{O}$ ) and -1.00‰ ( $\delta^{13}\text{C}$ ), which compares to NBS values of -4.14‰ ( $\delta^{18}\text{O}$ ) and -1.06‰ ( $\delta^{13}\text{C}$ ) (I.L. Barnes, pers. comm., 1985).

Duplicate or triplicate analyses were performed on 67 samples of *N. dutertrei* and on 24 samples of *G. sacculifer*. Based on these replicates, the analytical precision is  $\pm 0.08\text{‰}$  (average  $\frac{1}{2} \Delta \delta^{18}\text{O}$ ) and  $\pm 0.06\text{‰}$  (average  $\frac{1}{2} \Delta \delta^{13}\text{C}$ ) for *N. dutertrei* and  $\pm 0.12\text{‰}$  (average  $\frac{1}{2} \Delta \delta^{18}\text{O}$ ) and  $\pm 0.11\text{‰}$  (average  $\frac{1}{2} \Delta \delta^{13}\text{C}$ ) for *G. sacculifer*. To estimate the variance of normally distributed errors for populations represented by replicate analyses, we used the formula in Popp et al. (1986) and calculated an analytical precision (1 s) of  $\pm 0.17\text{‰}$  for  $\delta^{18}\text{O}$  and  $\pm 0.14\text{‰}$  for  $\delta^{13}\text{C}$  (*N. dutertrei*), and  $\pm 0.20\text{‰}$  for  $\delta^{18}\text{O}$  and  $\pm 0.20\text{‰}$  for  $\delta^{13}\text{C}$  (*G. sacculifer*).

## RESULTS

### Isotope Stratigraphy

Isotope values are plotted vs. depth in Figure 4. These Pleistocene  $\delta^{18}\text{O}$  records clearly show the glacial and interglacial climate cycles, which are characterized by high amplitudes (1‰ to 1.5‰) at about every 250–350 cm (~100-k.y.). The onset of the high-amplitude cycles is near 29 Bmcd in both records, although some relatively large-amplitude fluctuations are observed in the *N. dutertrei* record between 29 and 35 m. The *G. sacculifer*  $\delta^{18}\text{O}$  record (based on sample means) ranges from -1.22‰ to 0.54‰ around a mean value of -0.35‰. The *N. dutertrei* values range from -0.46‰ to 1.61‰ about a mean of 0.56‰. The  $\delta^{13}\text{C}$  values of the two species are similar. The *G. sacculifer*  $\delta^{13}\text{C}$  values range from 0.87‰ to 2.37‰ around a mean value of 1.50‰, whereas the *N. dutertrei* values range from 0.51‰ to

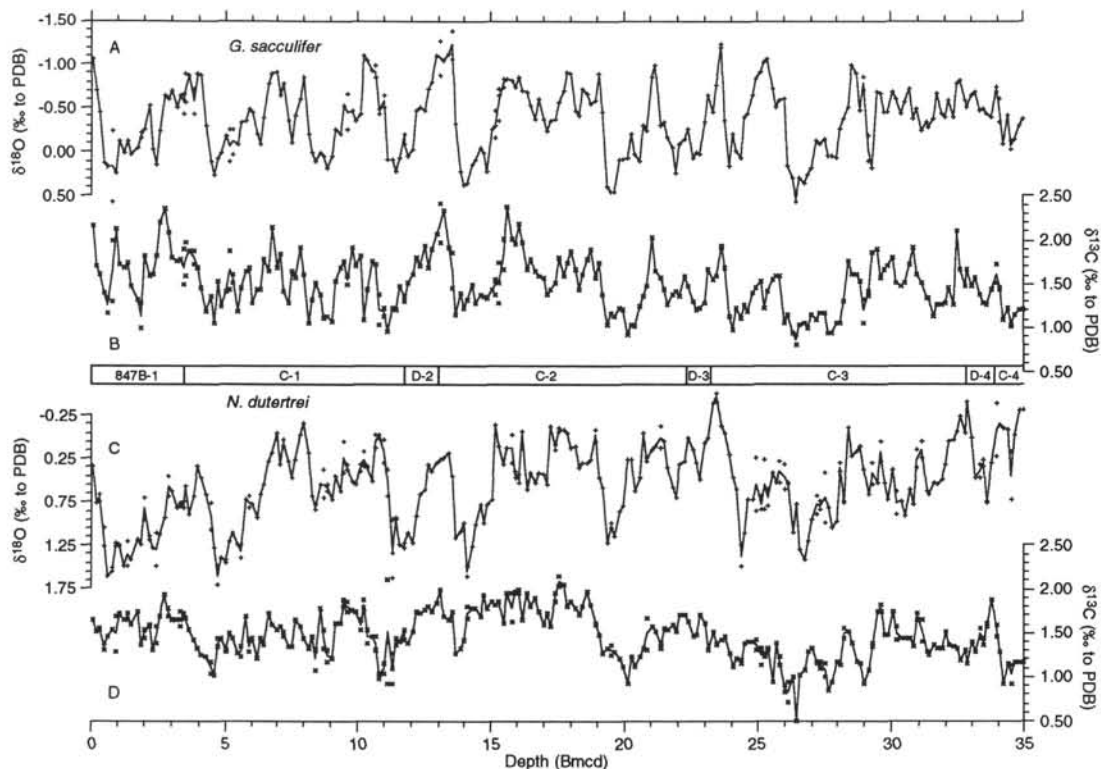


Figure 4. Planktonic foraminifer (*G. sacculifer* and *N. dutertrei*) stable isotope records from Site 847 vs. depth. All values from the Site 847 composite record are presented. The lines connect the mean values of the individual analyses at each depth. The sedimentary intervals used to construct this composite record include eight cores from three holes, which are identified in the middle of the figure.

2.09‰ around a mean of 1.47‰. Glacial stages are generally characterized by heavy  $\delta^{18}\text{O}$  and light  $\delta^{13}\text{C}$ , and interglacials by the opposite.

### Chronostratigraphy

A major accomplishment of the Leg 138 Shipboard Scientific Party was the construction of a new time scale and detailed age models for the drill sites based on astronomical tuning of the GRAPE stratigraphy (Shackleton et al., this volume). In this section, we evaluate the GRAPE age model at Site 847 by comparing it to our independently derived chronostratigraphy based on  $\delta^{18}\text{O}$ . We also consider the potential impact of coring-induced compaction of the sediments and of foraminiferal faunal abundance changes on the sedimentation rate and the chronostratigraphy.

#### The GRAPE Age Model

The GRAPE age model was constructed by correlating the sediment density stratigraphy (GRAPE, in rmcd) to variations in Northern Hemisphere summer insolation (Shackleton et al., this volume). Maxima in the GRAPE record, an index of weight percent calcium carbonate (Herbert and Mayer, 1991; Mayer, 1991), are aligned with insolation maxima (Berger and Loutre, 1991). For Site 847, the GRAPE age model has 28 control points within the 0–35 Bmcd interval. The depths of these control points were converted from rmcd to Bmcd and are shown in Figure 5. In the final version of their manuscript, Shackleton et al. (this volume) present a revised version of the GRAPE age model that includes adjustments which make it consistent with  $\delta^{18}\text{O}$  isotope data that has been generated at several Leg 138 sites. This revised age model is not discussed here. Instead, we focus on the original GRAPE age model, most of which was

constructed independent of the  $\delta^{18}\text{O}$  data, because we wish to compare a “pure” GRAPE age model to a  $\delta^{18}\text{O}$  age model.

#### $\delta^{18}\text{O}$ Chronostratigraphy

We developed  $\delta^{18}\text{O}$  age models for both the *N. dutertrei* and the *G. sacculifer* records (Table 1 and Fig. 5) by visually correlating to the SPECMAP stack global average  $\delta^{18}\text{O}$  record (Imbrie et al., 1984; Prell et al., 1986) over the interval from isotope stages 1 through 16.23 (0–631 ka), and to the ODP Site 677  $\delta^{18}\text{O}$  record (Shackleton et al., 1990) in the earlier interval. Before stage 16.23, the Site 677 ages assigned to the stages are older than the SPECMAP stack ages by 3%–12%. This divergence arises because Imbrie et al. (1984) accepted the 730 ka potassium-argon age for the Brunhes/Matuyama geomagnetic field reversal whereas Shackleton et al. (1990) did not. By orbitally tuning the  $\delta^{18}\text{O}$ , Shackleton et al. (1990) estimated a Brunhes/Matuyama age of approximately 780 ka, which agrees with two independent estimates based on  $^{40}\text{Ar}/^{39}\text{Ar}$  studies (Baksi et al., 1992; Hall and Farrell, 1993), and is consistent with an earlier astronomical estimate (Johnson, 1982).

Correlation to the SPECMAP stack and to the Site 677 record was unambiguous over the upper 29 m of the Site 847 record, which spans isotopic events 1 through 25 (Figs. 5–6). The record is sufficiently detailed to clearly resolve all the major isotope stages and many sub-stages. The good correlation to the isotope reference sections attests to the continuity and detail of the Site 847 composite depth record. Between 29 and 35 Bmcd, the structure in the *N. dutertrei* record is correlated to the Site 677 record, though with more difficulty than in the upper section. The deep structure in the *G. sacculifer* record is ambiguous, however, and cannot be easily matched to the Site 677 record, nor to other isotopic records spanning this time interval. As a result, the isotopic control points assigned to the *G. sacculifer* record

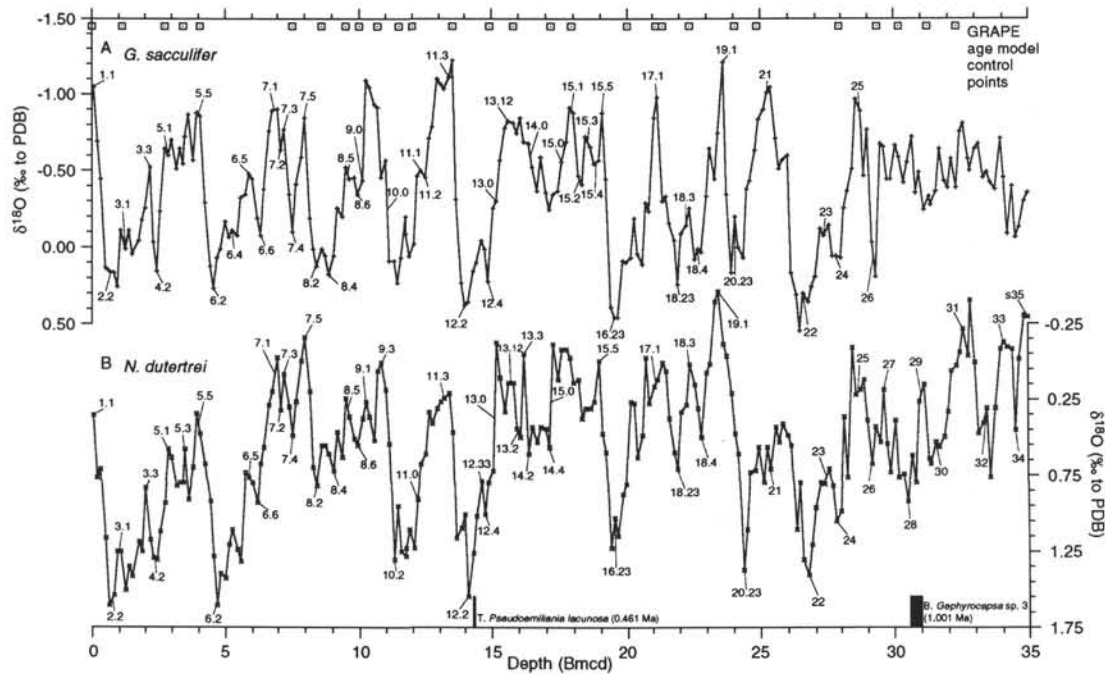


Figure 5. Oxygen isotope records from *G. sacculifer* and *N. dutertrei* vs. depth. Independent age models were developed for both records, and the isotopic events selected as chronostratigraphic control points in each are identified following the nomenclature of Prell et al. (1986) and Shackleton et al. (1990). For comparison, the control points from the GRAPE age model (Shackleton et al., this volume) are shown as squares. Nannofossil biostratigraphic datums are from I. Raffi (pers. comm., 1992).

between 30 and 35 Bmcd (events 27 through the transition to event s35, where “s” is for the “shoulder” of event 35) are simply those assigned to the *N. dutertrei* record.

#### *G. sacculifer* and *N. dutertrei* $\delta^{18}\text{O}$ Chronostratigraphies

The isotopic events in the *G. sacculifer* record do not always occur at the same depths as those in the *N. dutertrei* record. In other words, we see the same isotopic event in both records, but they occur at slightly different depths. Such an offset is noticeable at 10–11 m ( $\delta^{18}\text{O}$  stage 9), 15–19 m (stages 13–15), and 24–27 m (stages 20–22) (Figs. 4–5). The lead-lag pattern is not consistent. In some intervals, such as stages 20–22 and stage 9, the isotopic structure in *N. dutertrei* occurs deeper in the hole than in the *G. sacculifer* record. In other intervals, such as stages 13–15, the reverse is observed; the *G. sacculifer* structure stratigraphically precedes the *N. dutertrei* structure. The offset is not a sampling artifact since both species were selected from the same sample. The offset is attributed to either the sedimentologic interplay between variations in species abundance and bioturbation (Hutson, 1980), or to the fact that discretely sampled records do not necessarily show the full range or character of a signal (Prell et al., 1986). Similar offsets have been previously observed and modeled (e.g., Bé and Duplessy, 1976; Duplessy, 1978; Hutson, 1980; Schiffelbein, 1984, 1985). Variations in the absolute abundance of the two species, based on the data presented by McKenna et al. (this volume), do not show a pattern that is consistent with the leads and lags in the isotope records.

The two isotope age models (Table 1) were used to assign two age estimates and sedimentation rates to each of the 236 samples by linear interpolation between control points. Comparison of the estimates at each depth shows that the greatest depth/age discrepancy occurs in isotope stage 15, where the *G. sacculifer* structure leads the *N. dutertrei* structure by 37.5 cm (13 k.y.) (Fig. 7). The largest discrepancy in the opposite direction occurs in stage 20, and is 30 cm (10 k.y.). We chose the *G. sacculifer* age model as the preferred  $\delta^{18}\text{O}$  chronology for Site 847 based on its close match in relative amplitude to the SPECMAP stack.

#### Comparison of GRAPE and $\delta^{18}\text{O}$ Age Models

We compared the Site 847 *G. sacculifer*  $\delta^{18}\text{O}$  age model to the GRAPE model by applying both to the *G. sacculifer*  $\delta^{18}\text{O}$  data (Fig. 8). To a first approximation, the two models agree well. For the suite of 236 samples, the mean age difference ( $\delta^{18}\text{O}$  minus GRAPE) is only  $-1800$  yr, and at no point do they diverge by more than 30,000 yr. The similarity of the two models, and their independence, demonstrates not only the consistency and utility of the GRAPE correlations among widely spaced drill sites, but also the validity of tuning the GRAPE density to orbital insolation (Shackleton et al., this volume). Although portions of the GRAPE age model were revised, based on  $\delta^{18}\text{O}$  records from Site 849 (Mix et al., this volume), no  $\delta^{18}\text{O}$  data from Site 847 were used to modify the original Site 847 GRAPE age model. Adjustments to the GRAPE age model that were based on Site 849  $\delta^{18}\text{O}$  data were projected into the Site 847 age model only by GRAPE correlation. Compared to the Site 847 isotope age model, the GRAPE model was constructed in a fraction of the time, with less effort, and at significantly reduced expense.

Differences between the models do exist, however, and are large enough to affect studies of processes that occur over time scales of  $10^4$  to  $10^5$  yr. The largest lead-lag discrepancy between the models is  $-30$  k.y., which occurs for Sample 138-847B-1H-1, 123 cm, at 1.23 Bmcd. The GRAPE age assigned to the sample is 58 ka, but the (*G. sacculifer*)  $\delta^{18}\text{O}$  age is 28 ka, corresponding to  $\delta^{18}\text{O}$  stage 3.1. Because the discretely sampled  $\delta^{18}\text{O}$  record (15-cm spacing) does not necessarily capture the full range of the  $\delta^{18}\text{O}$  maxima or minima, we can only identify this particular event to within  $\pm 22$  cm (one and a half sample spaces to either side of Sample 138-847B-1H-1, 123 cm). Accordingly, the age estimate is thus  $\sim 28 \pm 5$  ka. The GRAPE age of 58 ka corresponds to the  $\delta^{18}\text{O}$  transition between stages 3 and 4, which occurs at least 80 cm deeper in the Site 847 record. The largest discrepancy in the other direction, that is, where the  $\delta^{18}\text{O}$  age assigned to a sample is older than the GRAPE age, occurs at 16.98 Bmcd for Sample 138-847C 2H-3, 107 cm. Here, the  $\delta^{18}\text{O}$  age of 546 ka is about 25 k.y. older than the GRAPE age of 521 ka. Based on the  $\delta^{18}\text{O}$  struc-

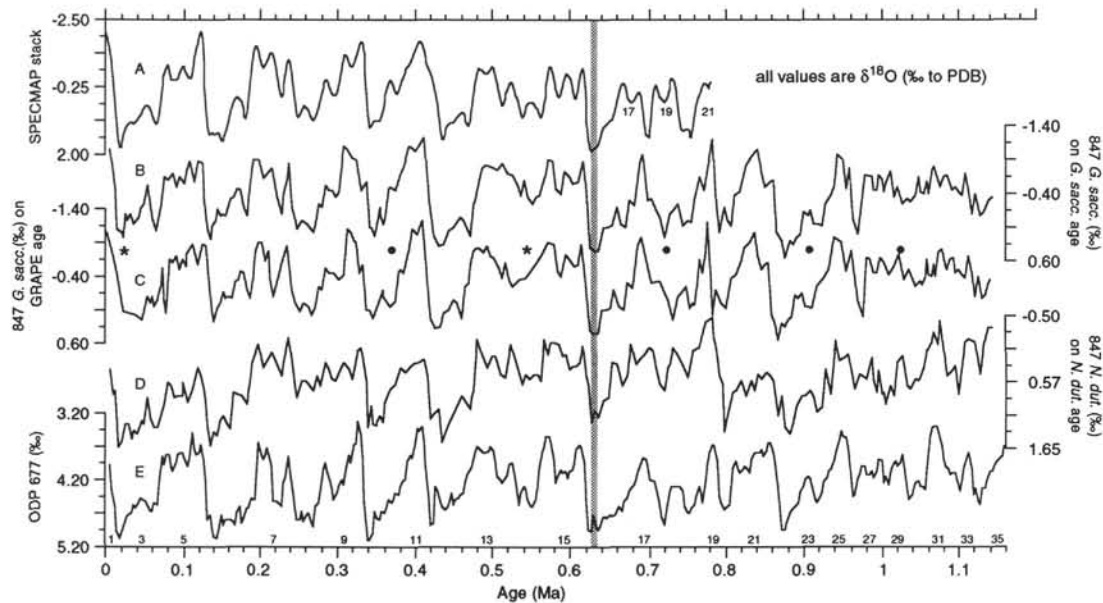


Figure 6. Oxygen isotope records from the SPECMAP stack and from Sites 847 and 677 vs. age. The SPECMAP stack (A) is in standard deviation units. The *G. sacculifer* record is plotted with respect to its  $\delta^{18}\text{O}$  age model (B) and its GRAPE age model (C). Large offsets between these two age models are identified by a solid star (★) and smaller ones by a solid circle (●). The *N. dutertrei* record is plotted vs. its  $\delta^{18}\text{O}$  age model (D) and the benthic isotope record from Site 677 (E) is from Shackleton et al. (1990). Odd numbers denote interglacial stages. The band at 630 ka marks the point below which the age  $\delta^{18}\text{O}$  estimates of Shackleton et al. (1990), which were adopted in this study, diverge toward older values than those in the SPECMAP stack.

ture, this interval falls within stage 14, between events 14.2 and 14.4, which have been assigned ages of 538 and 563 ka, respectively. The GRAPE age of 521 ka is too young for this isotope structure. This age corresponds to the isotopic transition from stage 13 to 14, that occurs at a shallower depth in the  $\delta^{18}\text{O}$  record. We attribute the largest differences between the GRAPE and the  $\delta^{18}\text{O}$  age models to difficulties in identifying obliquity peaks and valleys in the GRAPE density record. This results in miscorrelations to the orbital insolation curve and age estimate errors. Although discrepancies between the age models do occur, they do not show a consistent pattern, nor does one model progressively diverge from the other. Despite differences as large as 30 k.y., there are many intervals where the two models agree exactly, such as interglacial  $\delta^{18}\text{O}$  stages 5, 7, 11, 15.5, 17, 19, and 25 (Fig. 8).

#### Sediment Core Shortening and Lengthening

We noted with interest that the mean sedimentation rate at Site 847 is 30% higher than at nearby piston core Site RC13-110 (0°06'N, 95°39'W, 3231 m). The rate for the 0- to 630-k.y. interval at Site 847 is 3.4 cm/k.y., which is 1.0 cm/k.y. greater than that of 2.4 cm/k.y. in Core RC13-110, which is based on a detailed and orbitally tuned benthic foraminifer isotope record (Mix et al., 1991). We think that the sedimentation rate difference largely results from technique differences between ODP advanced piston coring and traditional piston coring. Ten percent of the difference may be attributed to expansion of the ODP sedimentary section (Hagelberg et al., 1992) because of elastic rebound (MacKillop et al., this volume) and other factors, relative to the "true" depth in the hole (Harris et al., this volume). Another ten percent results from the shortening (possibly on account of compression) of Core RC13-110, based on drilling reports (A. Mix, pers. comm., 1993). The final 10% cannot easily be accounted for by drilling disturbances and may reflect a true difference in the sedimentation rate between the two sites. Such a difference may result from variable bottom topography, which facilitates winnowing of fine sediment from one area and focusing in another. Given the small distance separating the sites, we do not think that the sedimentation rate difference is caused by a steep spatial gradient in the rain rate of particles from the

surface ocean. Karlin et al. (1992) suspect that sediments recovered by traditional piston cores, but not gravity cores, are compressed by plastic deformation. If different coring techniques distort sediments in different ways (Blomqvist, 1991), then this needs to be accounted for when comparing sedimentation rates and/or sediment mass fluxes between ODP sites and other sites drilled by piston or gravity cores.

## DISCUSSION

### Comparison with Other Pacific $\delta^{18}\text{O}$ Records

#### *N. dutertrei* $\delta^{18}\text{O}$

The relative amplitude of the Site 847 *N. dutertrei*  $\delta^{18}\text{O}$  record differs significantly from that of the *G. sacculifer* record and from other  $\delta^{18}\text{O}$  reference sections, such as the SPECMAP stack and the Site 677 record (Fig. 6). For example, the *N. dutertrei*  $\delta^{18}\text{O}$  values in stages 1–5 are notably heavier than those in stages 7–9. Likewise, the *N. dutertrei* values are relatively light in stages 13–15, and 17–19 and heavy in stage 21 compared to the other records (Figs. 4–6). To demonstrate that the Site 847 *N. dutertrei*  $\delta^{18}\text{O}$  record is representative of the EEP, rather than a local anomaly, we compared it to other *N. dutertrei* records from Cores RC13-110 (A. Mix, pers. comm., 1993), V19-30 (N. Shackleton, pers. comm., 1993), and A1154-25PC (Pedersen et al., 1991) (Figs. 1 and 9). The  $\delta^{18}\text{O}$  values in Cores V19-30 and RC13-110 and at Site 847 are nearly identical, most likely reflecting similar thermocline temperatures. The values from Core A1154-25PC are lighter, which is consistent with a warmer thermocline in the Panama Basin (Pedersen et al., 1991). The Site 847 *N. dutertrei*  $\delta^{18}\text{O}$  record is clearly not a local anomaly. Therefore, the apparent deviations in the relative amplitude of the *N. dutertrei*  $\delta^{18}\text{O}$  records are real, and represent either a species effect or isotopic variability in the thermocline that is not observed in the surface or bottom waters, as indicated by *G. sacculifer* and the Site 677 benthic isotope records.

If *N. dutertrei* calcifies the bulk of its test at a fixed temperature, or over a narrow temperature range in the thermocline (Curry and Matthews, 1981; Curry et al., 1983), then the  $\delta^{18}\text{O}$  record can be interpreted as an index of mean global seawater  $\delta^{18}\text{O}$ , a reflection of

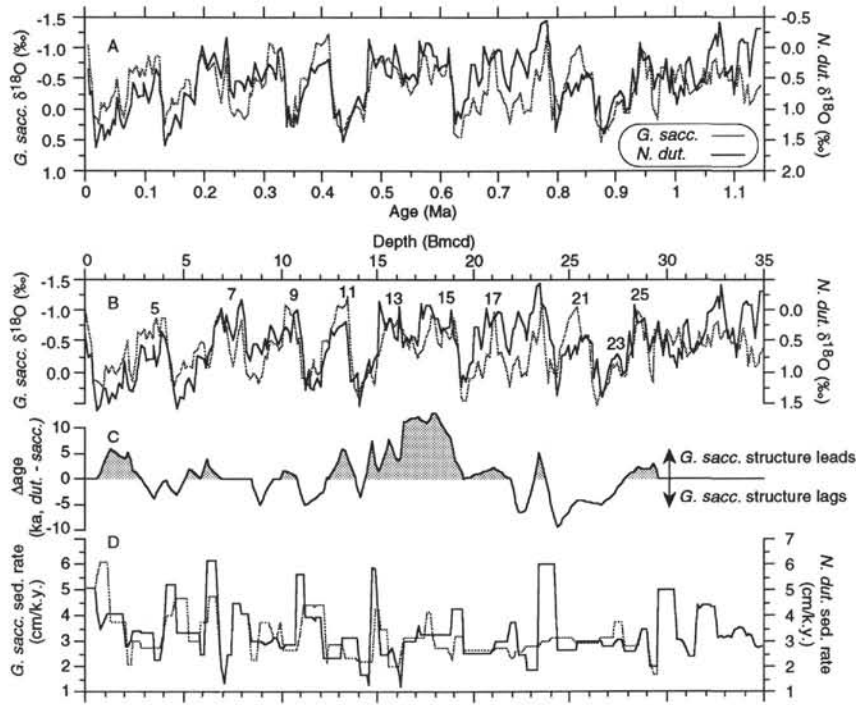


Figure 7. Comparison between the *G. sacculifer* and *N. dutertrei*  $\delta^{18}\text{O}$  age models. A.  $\delta^{18}\text{O}$  records from the two species are presented with respect to their independent age models, which minimizes the apparent stratigraphic offsets in isotopic structure. B. Same records plotted with respect to depth (Bmcd). Here, the offsets are clear, especially in stage 3 and in stages 13 through 15. C. Offset in isotopic structure expressed in terms of  $\Delta\text{age}$  vs. depth. D. Sedimentation rates resulting from the two isotope age models vs. depth.

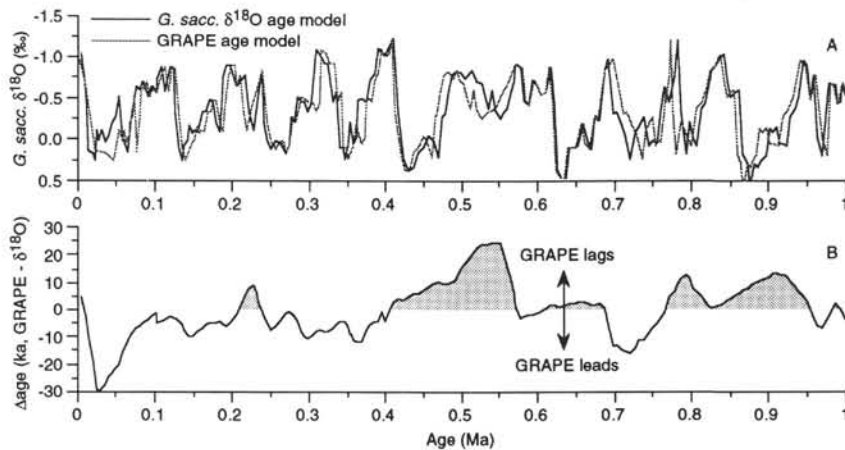


Figure 8. A. Leads and lags in the Site 847 *G. sacculifer*  $\delta^{18}\text{O}$  record compared with itself resulting from GRAPE age model estimates (Shackleton et al., this volume) that differ from those based on the *G. sacculifer*  $\delta^{18}\text{O}$  age model. The age estimates are similar, to a first approximation. B. Age offsets calculated as GRAPE minus  $\delta^{18}\text{O}$  age vs. age (based on *G. sacculifer*  $\delta^{18}\text{O}$ ).

ice volume. This presumes equilibrium fractionation and minimal gametogenic calcification below the thermocline. Despite the differences in hydrographic conditions between the Panama Basin and the equatorial divergence region, the similarity in the relative amplitudes of the *N. dutertrei* records (Fig. 9) supports the contention of calcification at relatively constant temperatures, though regionally offset.

On the other hand, the amplitudes of *G. sacculifer* records from WEP Cores RC17-177 (Shackleton, 1987) and V28-238 (Shackleton and Opdyke, 1973) are also considered a reliable index of ice volume, because SST is assumed to have remained generally invariant in this

region (e.g., Matthews and Poore, 1980; Shackleton, 1987; Prentice and Matthews, 1988). Because the shape and amplitude of the  $\delta^{18}\text{O}$  records from EEP *N. dutertrei* differ significantly from the WEP *G. sacculifer* records (Figs. 9–10), both cannot accurately reflect ice volume. If the *N. dutertrei* record is the accurate one, then the significant deviation of the *G. sacculifer*  $\delta^{18}\text{O}$  structure implies a temperature overprint on the WEP records, including Core V28-238, the linchpin of the SPECMAP stack. Alternatively, if the WEP *G. sacculifer* record is accurate, then the hypothesis of constant calcification temperature for *N. dutertrei* may not hold true. This implies either a

**Table 1. Chronostratigraphic control points for the  $\delta^{18}\text{O}$  records.**

<i>G. sacculifer</i> age model				<i>N. dutertrei</i> age model			
$\delta^{18}\text{O}$ stage	Composite depth (Bmcd)	Age (Ma)	Sedimentation rate (cm/k.y.)	$\delta^{18}\text{O}$ stage	Composite depth (Bmcd)	Age (Ma)	Sedimentation rate (cm/k.y.)
1.1	0.020	0.006	5.08	1.1	0.020	0.006	5.08
2.2	0.680	0.019	6.11	2.2	0.680	0.019	3.50
3.1	1.230	0.028	3.76	3.1	0.995	0.028	4.10
3.3	2.170	0.053	2.08	3.3	2.020	0.053	2.83
4.2	2.420	0.065	3.00	4.2	2.360	0.065	3.40
5.1	2.870	0.080	2.75	5.1	2.870	0.080	3.32
5.5	4.025	0.122	4.04	5.3	3.500	0.099	2.28
6.2	4.550	0.135	4.69	5.5	4.025	0.122	5.19
6.4	5.300	0.151	3.00	6.2	4.700	0.135	3.33
6.5	5.900	0.171	3.75	6.5	5.900	0.171	2.50
6.6	6.350	0.183	4.77	6.6	6.200	0.183	6.14
7.1	6.875	0.194	2.05	7.1	6.875	0.194	2.05
7.2	7.100	0.205	1.36	7.2	7.100	0.205	1.36
7.3	7.250	0.216	2.50	7.3	7.250	0.216	2.50
7.4	7.550	0.228	4.50	7.4	7.550	0.228	4.50
7.5	8.000	0.238	4.09	7.5	8.000	0.238	4.09
8.2	8.450	0.249	2.25	8.2	8.450	0.249	3.00
8.4	8.900	0.269	3.75	8.4	9.050	0.269	2.92
8.5	9.575	0.287	3.13	8.5	9.575	0.287	3.13
8.6	9.950	0.299	3.75	8.6	9.950	0.299	2.73
9	10.100	0.303	2.71	9.1	10.250	0.310	2.86
10	11.075	0.339	4.43	9.3	10.850	0.331	5.63
11.1	12.360	0.368	2.14	10.2	11.300	0.339	3.96
11.2	12.510	0.375	2.90	11	12.210	0.362	2.33
11.3	13.380	0.405	2.33	11.3	13.210	0.405	3.17
12.2	14.055	0.434	2.23	12.2	14.130	0.434	1.67
12.4	14.880	0.471	4.29	12.33	14.580	0.461	1.30
13	15.180	0.478	3.46	12.4	14.710	0.471	5.79
13.12	15.630	0.491	2.02	13	15.115	0.478	2.46
14	16.295	0.524	3.13	13.13	15.705	0.502	2.73
15	17.580	0.565	4.17	13.2	16.005	0.513	1.95
15.1	17.955	0.574	2.73	13.3	16.210	0.524	1.17
15.2	18.255	0.585	2.73	14.2	16.380	0.538	3.00
15.3	18.555	0.596	2.73	14.4	17.130	0.563	3.75
15.4	18.855	0.607	2.25	15	17.205	0.565	3.32
15.5	19.080	0.617	3.21	15.5	18.930	0.617	4.29
16.23	19.530	0.631	2.66	16.23	19.530	0.631	2.56
17.1	21.180	0.693	2.78	17.1	21.115	0.693	3.02
18.23	21.930	0.720	2.33	18.23	21.930	0.720	3.75
18.3	22.210	0.732	2.61	18.3	22.380	0.732	2.50
18.4	22.680	0.750	2.82	18.4	22.830	0.750	1.91
19.1	23.610	0.783	3.00	19.1	23.460	0.783	6.00
20.23	24.060	0.798	3.15	20.23	24.360	0.798	2.69
21	25.290	0.837	2.93	21	25.410	0.837	3.00
22	26.610	0.882	3.13	22	26.760	0.882	2.81
23	27.360	0.906	3.75	23	27.435	0.906	3.12
24	27.810	0.918	2.81	24	27.810	0.918	2.58
25	28.710	0.950	3.50	25	28.635	0.950	3.50
26	29.235	0.965	1.70	26	29.160	0.965	2.05
27	29.610	0.987	5.00	27	29.610	0.987	5.00
28	30.510	1.005	3.03	28	30.510	1.005	3.03
29	31.025	1.022	2.43	29	31.025	1.022	2.43
30	31.560	1.044	4.38	30	31.560	1.044	4.38
31	32.610	1.068	3.15	31	32.610	1.068	3.15
32	33.460	1.095	3.50	32	33.460	1.095	3.50
33	34.090	1.113	3.21	33	34.090	1.113	3.21
34	34.540	1.127	2.81	34	34.540	1.127	2.81
s35	34.990	1.143		s35	34.990	1.143	

Notes: Isotope stage nomenclature follows that of Prell et al. (1986) and Ruddiman et al. (1989). Ages for stages 1.1 through 16.23 are from Imrie et al. (1984). Ages for older events are estimated from Shackleton et al. (1990). *G. sacculifer* events in italics are taken from the *N. dutertrei* age model. Event s35 is the shoulder preceding the interglacial stage 35.

temperature effect or a  $\delta^{18}\text{O}_{\text{water}}$  effect on the *N. dutertrei*  $\delta^{18}\text{O}$ , which is entirely plausible in the EEP because small vertical changes in the calcification depth of *N. dutertrei* will affect the isotopic composition given the steeply dipping water temperature profile in the thermocline. Nevertheless, given the consistency of the EEP *N. dutertrei* records (Fig. 9), such vertical migrations would have had to be synchronous over a large region with diverse hydrographic regimes. Unless postdepositional processes are responsible for the differences in the relative amplitude of the *N. dutertrei* and the *G. sacculifer*  $\delta^{18}\text{O}$  records, we conclude that estimates of ice volume based on *N. dutertrei* are inconsistent with those based on low latitude "warm pool" *G. sacculifer*. Although we cannot discern which record, if either, provides a meaningful estimate of ice volume, we examine the *G. sacculifer* approach more closely in the next section.

### *G. sacculifer* $\delta^{18}\text{O}$

Stable isotope records from *G. sacculifer* are rare in the EEP because this species is highly susceptible to dissolution and occurs in low abundance. Such records are valuable, however, because this species is one of the few that calcifies predominantly in the mixed layer and thus provides an indication of surface ocean conditions. To examine temporal changes in the east-west temperature difference along the equatorial Pacific, and to further investigate the use of the WEP *G. sacculifer*  $\delta^{18}\text{O}$  record as an ice volume index, we compared the Site 847 *G. sacculifer*  $\delta^{18}\text{O}$  record to that from Core RC17-177 (1°45'N, 159°27'E, 2600 m) (Shackleton, 1987), one of the best records in the WEP (Fig. 10). To make this comparison, we adjusted the original age model of Core RC17-177 below stage 16.23 to the

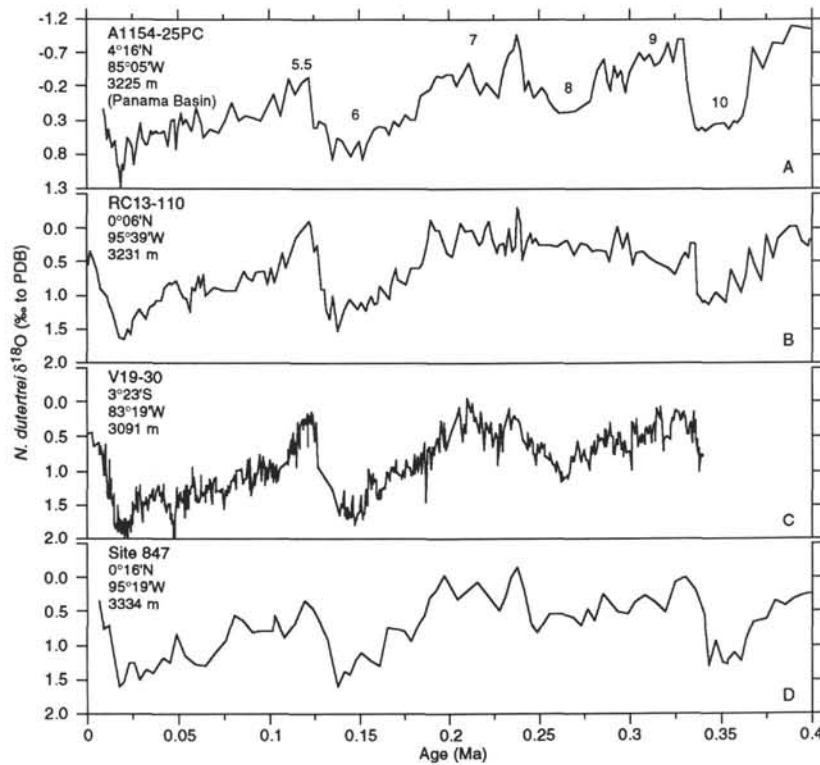


Figure 9. Comparison of *N. dutertrei*  $\delta^{18}\text{O}$  records from the eastern equatorial Pacific shows that the shapes of the records are similar, as are the absolute values in Cores RC13-110 and V19-30 and at Site 847. The lighter values in Core A1154-25PC reflect the warmer thermocline temperatures in the Panama Basin (Pedersen et al., 1991). Note the relatively light values in glacial stage 8. This structure differs significantly from that in the SPECMAP stack and in most *G. sacculifer*  $\delta^{18}\text{O}$  records, where stage 8 values are significantly greater than those in stage 5.

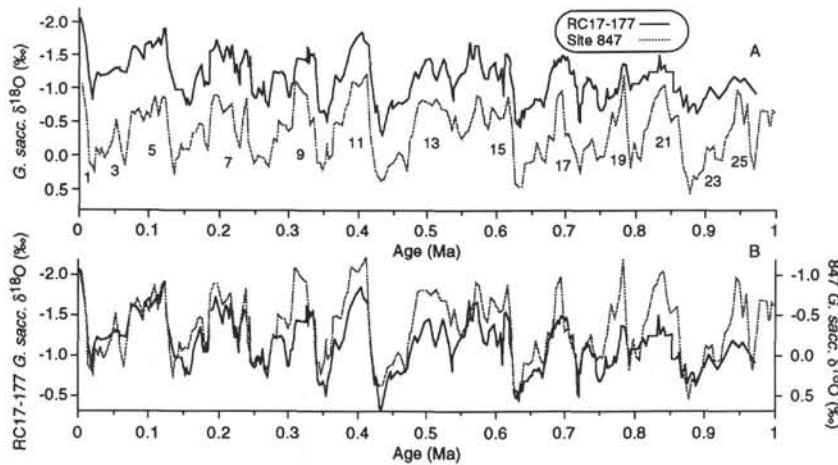


Figure 10. Comparison between eastern (Site 847) and western (RC17-177) equatorial Pacific *G. sacculifer*  $\delta^{18}\text{O}$  records. **A.** Site 847 values are uniformly heavier because of calcification in surface waters that today are  $5^{\circ}\text{C}$  colder on average. **B.** Isotopic alignment of the records over the top 250 k.y., showing the similarity of the amplitudes in the upper portion of the records, but relatively lighter interglacials in the Site 847 record before 250 ka. This is attributed to relatively warmer surface waters at Site 847, better carbonate preservation, or higher sedimentation rates.

Site 677 chronology (Shackleton et al., 1990). The two records are similarly resolved, and they are easily correlated (Fig. 10A). The Site 847  $\delta^{18}\text{O}$  values are uniformly heavier because of the cooler SST in the EEP. For the 0- to 250-ka interval, the mean  $\delta^{18}\text{O}$  value in the Site 847 record is 1.06‰ heavier than in the RC17-177 record, but the relative amplitudes of the records are strikingly similar (Fig. 10B).

This 1.06‰ isotopic difference translates into a temperature contrast of  $4.8^{\circ}\text{C}$  (Erez and Luz, 1983), closely approximating the present SST difference between these two sites ( $24^{\circ}\text{C}$  at Site 847 and  $29^{\circ}\text{C}$  at RC17-177). The similar amplitude of the two records is interesting because it argues against any significant change in the east-west temperature difference. Because the isotopic difference remained con-

stant, and presuming the WEP SST was relatively constant (Matthews and Poore, 1980), then the EEP SST most likely remained the same.

We note two significant differences between the EEP and WEP *G. sacculifer*  $\delta^{18}\text{O}$  records. First, the WEP record shows a long-term increase in  $\delta^{18}\text{O}$  from the core top, down into the middle of the Brunhes Chron (stage 12), which is not observed in the EEP record. This trend coincides with increasing dissolution, commonly referred to as the "mid-Brunhes dissolution trend" (Adelseck, 1977; Farrell and Prell, 1989). Second, before stage 8, the WEP glacial/interglacial amplitude is muted compared to that in the EEP. When the isotopic values from the two records are aligned over the top 8 isotope stages (0–250 ka) (Fig. 10B), we see that the pre-stage 8 interglacial amplitudes are relatively, and significantly, lighter in the EEP than in the WEP (Fig. 10B). At the same time, however, the post-stage 8 glacial amplitudes are essentially identical. Similar results were obtained by comparing the Site 847 *G. sacculifer* record to other WEP records such as that from Core V28-238. This EEP-WEP amplitude difference may be attributed to relatively greater dissolution in the WEP than in the EEP, particularly during interglacial times. Carbonate preservation may be better at Site 847, in part because the sedimentation rate is two times higher than at Site RC17-177. If dissolution is not the cause, and if the WEP records reflect global ice volume, then the relatively lighter interglacial values in the pre-stage 8 portion of the Site 847 record suggests a warmer interglacial SSTs (given the curve alignment). The outstanding question is why the thermal difference was constant from 0 to 250 ka, but differed before that.

### Dissolution Effects on the Isotope Records

Since carbonate dissolution distorts  $\delta^{18}\text{O}$  records, it must be considered when interpreting paleoenvironmental conditions (Erez, 1979). Dissolution preferentially removes the fragile and porous foraminifer tests (generally those enriched in  $^{16}\text{O}$ ) from the faunal assemblage, and concentrates the thicker and denser tests ( $^{18}\text{O}$ -enriched), that are less susceptible to dissolution (Berger, 1971; Berger and Killingly, 1977). In much of the Pacific, this effect is especially prevalent during interglacials, when dissolution intensity was greater than during glacials. Superimposed on the glacial/interglacial dissolution pattern are dissolution and preservation extrema centered on the transitions between climate states. Deglacials are characterized by greatly enhanced preservation, whereas periods of ice growth are marked by severe dissolution. This Pacific dissolution pattern reduces the glacial/interglacial amplitudes in  $\delta^{18}\text{O}$  because during interglacials, the tests with low  $\delta^{18}\text{O}$  are preferentially removed by dissolution and during glacials they are preserved (Erez, 1979). The amplitude is also reduced by the combined effects of bioturbation and sediment accumulation rates, which move specimens from the better preserved, and thicker, intervals (glacials) into the poorly preserved, thinner interglacial intervals.

Carbonate preservation appears to be better at Site 847 than at most other sites from the central and western equatorial Pacific. A clear and simple example of this is that a sufficient number of *G. sacculifer*, a dissolution susceptible species, were available for isotopic analysis throughout the record. This is not the case in the central equatorial Pacific (CEP), where *G. sacculifer* are rare, and instead, dissolution-resistant species, such as *G. tumida*, are used to generate isotope records (Chuey et al., 1987; Murray, 1987). The better preservation at EEP Site 847 is attributed to deposition in somewhat less corrosive (shallower) waters, and to significantly higher sedimentation rates, which tends to remove the carbonate sediment more rapidly from contact with corrosive bottom waters. The effect of temporal variations in dissolution intensity on the  $\delta^{18}\text{O}$  record in the WEP recently has been reviewed in detail (Wu and Berger, 1989, 1991; Wu et al., 1990; Le and Shackleton, 1992). These studies show that variations in preservation tend to shift the lightest  $\delta^{18}\text{O}$  values toward preservation spikes and the heaviest values toward dissolution maxima. This shift is especially noticeable when sedimentation rates are low and dissolution is severe

(Wu et al., 1990), which is not the case at Site 847. Thus, because of better preservation, the Site 847 *G. sacculifer* record more accurately reflects temperature and the  $\delta^{18}\text{O}$  of seawater.

Carbonate preservation indices from Site 847 are presented for three Pleistocene intervals by Murray (this volume) and McKenna et al. (this volume) (Fig. 11). A general pattern of enhanced preservation during glacial stages is shown by: (1) greater percentages of whole planktonic foraminifer tests (%whole planktonic), indicating less breakage caused by dissolution; (2) higher coarse fraction (weight percent >150  $\mu\text{m}$ ), also indicating less breakage; (3) higher percentages of those foraminifer species that are more easily susceptible to dissolution; and (4) higher foraminifer fluxes. Superimposed on the glacial/interglacial pattern is evidence of particularly good preservation during deglacials, which is especially distinct in the coarse fraction record, and poor preservation during ice growth intervals, marked by low % $\text{CaCO}_3$  and %whole planktonic foraminifers. We observe a generally consistent pattern of higher coarse fraction percentages during glacial intervals, and particularly during deglaciations (e.g., during transitions from  $\delta^{18}\text{O}$  stages 22 to 21, 16 to 15, and 10 to 9) (Fig. 11). High coarse fraction values in the uppermost part of the record are commonly observed in Pacific deep-sea cores and Site 847 is not an exception. To some degree, these high values can be attributed to minimal compaction in the upper sediment column.

Low % $\text{CaCO}_3$  values often coincide with interglacials and with transitions to glacials. For example, the mid-point of interglacial stage 21 corresponds to the mid-point of a low % $\text{CaCO}_3$  event (Fig. 11). In stage 19, the lowest % $\text{CaCO}_3$  values fall not on the center of the isotope stage, but rather on the transition to the subsequent glacial stage 18. We observe low % $\text{CaCO}_3$  values on transitions from stages 19 to 18, 17 to 16, 13 to 12, 11 to 10, and 7 to 6. Smaller % $\text{CaCO}_3$  excursions are observed on other substage glaciations (e.g., 8.5 to 8.4). Interglacial stages 13 and 5 provide an interesting look at the interplay among dissolution indices and the relationship to climate. We see that all of stage 13 is marked by low %whole planktonic values, but the carbonate values decline only at the transition to glacial stage 12. Coarse fraction values in this interval are low to intermediate and do not show a clear link to the other records. Within stage 5, we see three "valleys" of relatively low values of percent  $\text{CaCO}_3$ , coarse fraction, and whole planktonic foraminifers, which are separated by two "peaks" of higher values (Fig. 11). The three intervals of low values are associated with the transition to stage 4 and with the three substages of interglacial stage 5 (5.1, 5.3, and 5.5). The three indices show generally consistent changes, with only slight offsets in phasing relative to each other.

Close examination of the dissolution indices shows a complex and somewhat inconsistent relationship. Part of the reason for this complexity is that none of the indices is exclusively a dissolution index. Each is also affected by variations in plankton ecology, productivity, and variations in the environment of deposition. For example, coarse fraction values will increase if the average size of the microfossils in the sample increases as a result of ecological shifts or if winnowing of the sediments on the seafloor preferentially removes the fine sediment. Differences in sediment processing (i.e., oven-drying samples as opposed to freeze-drying), or among operators wet-sieving the sediment, can also introduce shifts in coarse fraction values, though none were observed in this study. Variations in % $\text{CaCO}_3$  reflect dissolution, dilution, and productivity. Dilution can be accounted for by expressing the % $\text{CaCO}_3$  in terms of the mass accumulation rate (MAR) of  $\text{CaCO}_3$  (in terms of  $\text{g}/\text{cm}^2/\text{k.y.}$ ). Murray et al. (this volume) show that most of the intervals of low % $\text{CaCO}_3$  at Site 847 are also intervals with low  $\text{CaCO}_3$  MARs. Another reason why the links among the dissolution indices appear complicated is that the responses of these indices to dissolution, as measured in the laboratory (Adelseck, 1978; Ku and Oba, 1978), are nonlinear, though we often present them as linear. For example, a linear loss of  $\text{CaCO}_3$  by dissolution is expressed nonlinearly by % $\text{CaCO}_3$  (Heath and Culbertson, 1970). Le and Shackleton (1992) argued that the %whole planktonic

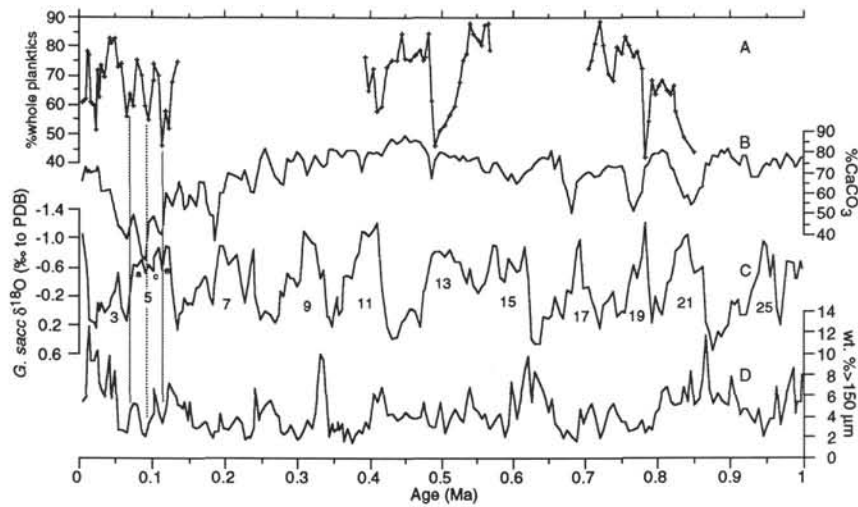


Figure 11. The links between  $\text{CaCO}_3$  preservation and climate at Site 847 are seen in this comparison of %whole planktonic foraminifers (A), % $\text{CaCO}_3$  (B), and %coarse fraction dissolution indices (D) to *G. sacculifer*  $\delta^{18}\text{O}$  (C) vs. age. Enhanced preservation is indicated by the high values in the three indices. Odd numbers denote interglacial stages. Substage covariation between dissolution and isotopes is delineated in stage 5.

index is nonlinear because the number of fragments into which a whole test can break needs to be considered.

We have shown the complex relationships that exist among various dissolution indices and between dissolution and isotopes in the Site 847 record. We conclude that dissolution has had a significantly smaller influence on the Site 847 isotope records than on those from the CEP and the WEP, where the seawater isotopic signal and the chronostratigraphy have been severely distorted in some cores (e.g., Wu et al., 1990). Perhaps the clearest indication of this difference is that the WEP *G. sacculifer* records show a long-term  $\delta^{18}\text{O}$  decrease since 1 Ma, and reduced  $\delta^{18}\text{O}$  amplitude during interglacials, whereas neither is observed in Site 847 record (Fig. 10).

### On Calculating Isotopic Differences

The  $\delta^{18}\text{O}$  and  $\delta^{13}\text{C}$  differences between *G. sacculifer* and *N. dutertrei* largely reflect the contrast in the water temperature and nutrient concentration between the surface mixed layer and the upper thermocline. Ideally, other factors have had minimal effects, or have been constant over time, or have acted with equal impact on both species (such as global ice volume fluctuations), thus not influencing the isotopic difference between them. The complicating factors that may preferentially influence the isotopic composition of one species relative to the other can be grouped into three types: predepositional, postdepositional, and analytical. Previously discussed examples of predepositional factors include differences in the  $\delta^{18}\text{O}$  of the ambient water ( $d_w$ , often associated with salinity changes) at the different calcification depths, disequilibrium calcification from the metabolic effects of respiration, gametogenic calcification, and seasonal variations in foraminifer flux. Complicating factors that arise after the sediments have been deposited on the seafloor include dissolution, bioturbation, and perhaps diagenetic recrystallization within the sedimentary column. Analytical complications, the third type, are probably the easiest to overcome in this study, because all measurements were made in the same laboratory over a short time span.

The isotopic difference between the two species was calculated in two ways. In the simpler approach, we ignored the small lead-lag offsets in isotopic structure between the two  $\delta^{18}\text{O}$  records and calculated the difference in the depth series, that is the isotopic difference between the two species in each sample. The time series of the  $\delta^{18}\text{O}$  difference, where the *G. sacculifer*  $\delta^{18}\text{O}$  is subtracted from the *N.*

*dutertrei*  $\delta^{18}\text{O}$  (thus  $\Delta\delta^{18}\text{O}_{d-s}$ ), is plotted vs. *G. sacculifer*  $\delta^{18}\text{O}$  age in Figure 12A. We smoothed this record with a three-point Gaussian filter to minimize spikes that result from extremes in isotope values and from small differences in the age models, especially at steep transitions between  $\delta^{18}\text{O}$  stages (Fig. 12B).

The second, and more complex calculation of the isotope difference required three steps, but addressed the lead-lag offsets in isotopic structure. We first converted the two isotope records from depth series to time series, based on their independently constructed  $\delta^{18}\text{O}$  chronostratigraphies (Table 1 and Fig. 5). We then interpolated both isotope records to a common time step. We chose 2000 yr such that isotope structure would be retained without excessive signal degradation in sections with high sedimentation rates. Finally, we calculated the isotope difference between the interpolated isotope values of the two species at each time step. The resulting  $\Delta\delta^{18}\text{O}_{d-s}$  time series is plotted vs. the interpolated time steps in Figure 12C. We applied a five-point Gaussian filter to smooth the complex  $\Delta\delta^{18}\text{O}_{d-s}$  time series (Fig. 12D) to about the same degree as the simple time series (Fig. 12B).

To a first approximation, the results from the two methods are similar, suggesting that the offset in isotope stratigraphy does not have a significant influence on the shape and amplitude of the isotope contrast (Fig. 12E). With only a few exceptions, the  $\Delta\delta^{18}\text{O}_{d-s}$  calculated from the simple approach is within  $\pm 0.2\text{‰}$  of the  $\Delta\delta^{18}\text{O}_{d-s}$  calculated from the complex approach. As expected, the exceptions to this occur where the depth offsets between the isotope records are the greatest, for example,  $\delta^{18}\text{O}$  stages 9, 13 through 15, and 20. The isotope lead-lag in stage 3 (Fig. 7) is not noticeable in the  $\Delta\delta^{18}\text{O}_{d-s}$  because the value ranges are similarly low. We consider the difference between the simple and the complex  $\Delta\delta^{18}\text{O}_{d-s}$  time series relatively insignificant, given the large signal-to-noise ratio and the generally small lead-lag offsets (with the one exception at stage 14). As such, the  $\delta^{18}\text{O}$  and  $\delta^{13}\text{C}$  contrasts discussed in the remainder of this chapter are those calculated by the simple approach.

### $\Delta\delta^{18}\text{O}$

The  $\Delta\delta^{18}\text{O}_{d-s}$  reflects the water temperature difference between the surface and the thermocline. The unsmoothed  $\Delta\delta^{18}\text{O}_{d-s}$  values range from  $-0.01\text{‰}$  to  $1.77\text{‰}$ , with a mean of  $0.91\text{‰}$  (Fig. 12A). In the smoothed version, the range narrows to between  $0.05\text{‰}$  and  $1.67\text{‰}$  (Fig. 12B). Temporal variations in the contrast show a pattern (Fig.

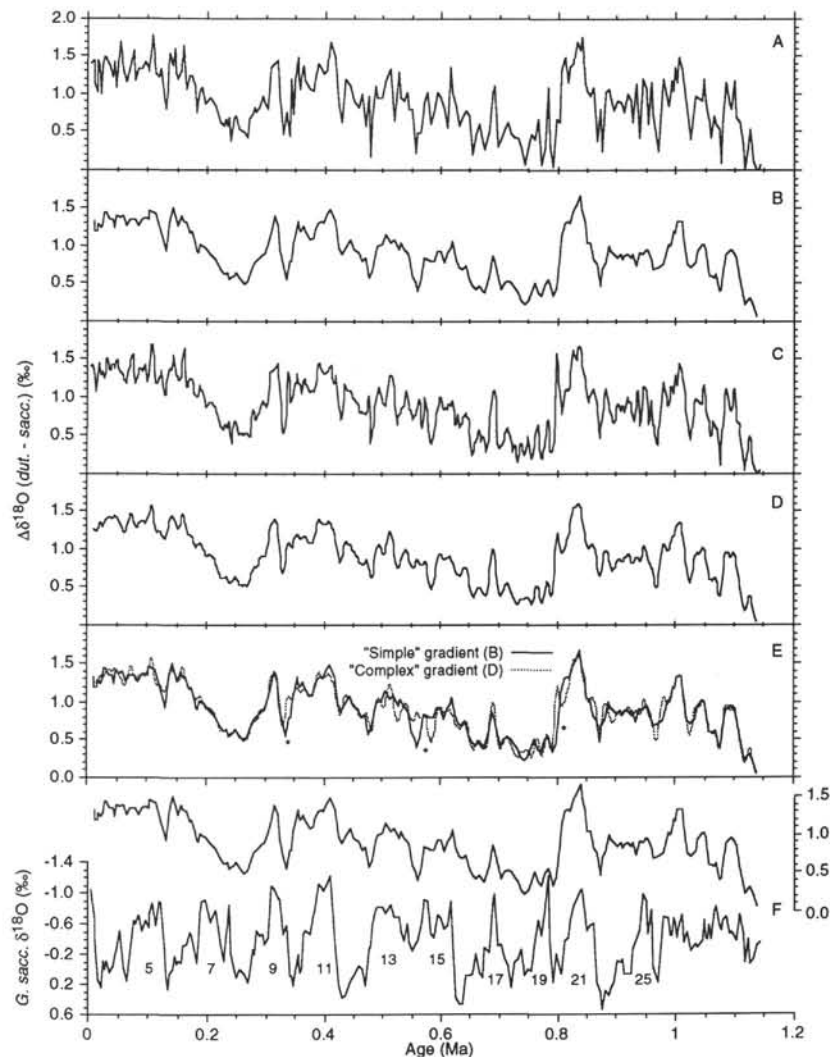


Figure 12. Age vs.  $\delta^{18}\text{O}$  difference (*N. dutertrei* minus *G. sacculifer*) at Site 847. The "simple" difference in Figure 12A is smoothed in Figure 12B. The "complex" difference in Figure 12C is smoothed in Figure 12D. The two smoothed versions are similar, as shown by comparison in Figure 12E. Stars denote offsets between the two versions. The "simple" smoothed version in Figure 12F is compared to the *G. sacculifer*  $\delta^{18}\text{O}$  record.

12F) that is often characterized by higher  $\Delta\delta^{18}\text{O}_{d-s}$  values during interglacials (e.g., stages 5, 9, 11, and 21) and lower values during glacials (e.g., stages 8, 14, 16, and 18). The simple interpretation of this pattern is a larger temperature contrast during interglacials and a smaller one during glacials. However, the glacial/interglacial pattern is not observed consistently over the entire record.

The  $\Delta\delta^{18}\text{O}_{d-s}$  values from the top of the record down to stage 6 are large and nearly invariant (Fig. 12). This results from the relatively heavy  $\delta^{18}\text{O}$  values in this portion of the *N. dutertrei* record, compared to the rest, and from the similar relative amplitudes of the two records (Fig. 7). From stage 6 to 20, there is a long-term decrease in the  $\Delta\delta^{18}\text{O}_{d-s}$  from about 1.5‰ to 0.3‰. Superimposed on this decline is the glacial/interglacial pattern, mentioned above, which is especially clear from stage 8 to 18. Stages 7 and 8 are characterized by a prolonged interval of low  $\Delta\delta^{18}\text{O}_{d-s}$ , with the lowest centered on the isotopic transition between these stages. The  $\Delta\delta^{18}\text{O}_{d-s}$  between early stage 18 and late stage 20 is also marked by low and invariant values. This small isotopic difference results from the anomalously light *N. dutertrei*  $\delta^{18}\text{O}$  values, especially in stage 19, compared to the rest of the record (Fig. 5). The largest  $\Delta\delta^{18}\text{O}_{d-s}$  occurs in stage 21, and is attributed to the heavy *N. dutertrei*  $\delta^{18}\text{O}$  values. Beneath stage 21, the

$\Delta\delta^{18}\text{O}_{d-s}$  again decreases gradually, eventually diminishing to nearly zero at the bottom of the record, where *N. dutertrei* values are low.

A strikingly similar  $\Delta\delta^{18}\text{O}_{d-s}$  pattern was observed to the west, at Site 851 ( $2^{\circ}46'\text{N}$ ,  $110^{\circ}34'\text{W}$ , 3760 m depth) (Ravelo and Shackleton, this volume) (Fig. 13). Except in the uppermost 150 k.y., the timing of the pattern and the absolute  $\Delta\delta^{18}\text{O}_{d-s}$  values are remarkably similar in both records, despite differences in location, sedimentation rate, faunal variations, age models, and laboratories.

### Variations in Temperature Contrast

We converted the  $\Delta\delta^{18}\text{O}_{d-s}$  into two estimates of the water temperature difference between the calcification depths of *G. sacculifer* (mixed layer) and *N. dutertrei* (thermocline). The first, is simply calculated from the paleotemperature equation of Erez and Luz (1983), where a  $\Delta\delta^{18}\text{O}_{d-s}$  value of 0.22‰ is equivalent to a temperature change of 1°C. The results show that the Pleistocene mixed layer is warmer than the thermocline by an average of 4.2°C and varies from 0.2° to 7.6°C (Fig. 14A). In the Site 851 record, Ravelo and Shackleton (this volume) observed a temperature difference of 5°C during interglacials and 3°C during glacials, similar to our values.

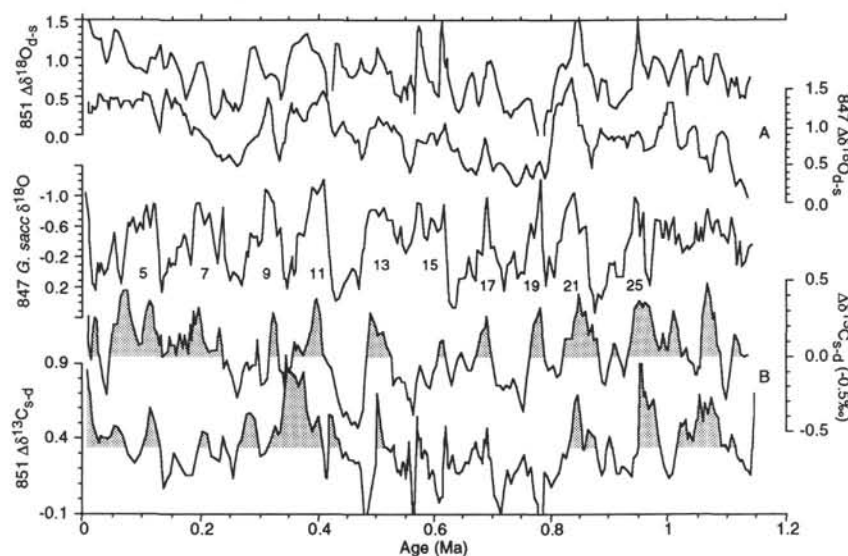


Figure 13. Similarities in  $\delta^{18}\text{O}$  (A) and  $\delta^{13}\text{C}$  (B) differences between *G. sacculifer* and *N. dutertrei* at Sites 847 and 851, as compared to the Site 847 *G. sacculifer*  $\delta^{18}\text{O}$  record. Odd numbers denote interglacial stages.

Our second estimate of the water temperature difference is more complex, because it tries to account for other factors that influence the  $\delta^{18}\text{O}$  contrast between *G. sacculifer* and *N. dutertrei*. We converted the fossil shell  $\delta^{18}\text{O}$  values into equilibrium seawater  $\delta^{18}\text{O}$  values by considering the effects of gametogenic calcification, differential dissolution, and offsets from equilibrium caused by the metabolic influence of foraminifer and algal respiration.

First, we subtracted 0.9‰ from the Site 847 *G. sacculifer*  $\delta^{18}\text{O}$  values to account for gametogenic calcification and differential dissolution, which increase the  $\delta^{18}\text{O}$  away from the equilibrium value in the surface mixed layer (Duplessy et al., 1981). Application of this adjustment to all downcore samples assumes that the magnitude of the offset is correct and that it was constant over time, which is obviously an oversimplification. Our second adjustment accounts for the observed negative offset of *G. sacculifer*  $\delta^{18}\text{O}$  from  $\text{CaCO}_3$   $\delta^{18}\text{O}$  precipitated in equilibrium with seawater  $\delta^{18}\text{O}$ . We added 0.5‰ to our *G. sacculifer*  $\delta^{18}\text{O}$  values to adjust for the disequilibrium calcification attributed to symbiotic algae and metabolic activity. Therefore, the net correction factor is -0.4‰.

We also subtracted 0.9‰ from our *N. dutertrei*  $\delta^{18}\text{O}$  values to account for gametogenic calcification and differential dissolution (Bouvier-Soumagnac and Duplessy, 1985). Support for the direction and magnitude of this correction comes from a comparison of Panama Basin sediment trap results with core top values. The mean *N. dutertrei*  $\delta^{18}\text{O}$  in the Holocene samples from Core A1154-25PC (Pedersen et al., 1991) is 0.20‰, which is 0.86‰ greater than the mean *N. dutertrei*  $\delta^{18}\text{O}$  value of -0.66‰ observed in the sediment traps (Curry et al., 1983). No further adjustments were needed because, unlike *G. sacculifer*, *N. dutertrei* is thought to calcify in equilibrium with  $d_w$  (Curry and Matthews, 1981; Fairbanks et al., 1982).

For simplicity, we also assumed that the  $d_w$  difference between the mixed layer and the thermocline ( $\Delta d_w$ ) did not change over time. If temporal changes in the balance between precipitation and evaporation occurred at Site 847, then the mixed layer salinity and  $d_w$  may have changed (Crowley, 1991), thereby influencing the  $\Delta\delta^{18}\text{O}_{d-s}$  without affecting the temperature contrast. Alternatively, a shift in the salinity of the EUC, which ventilates the thermocline at Site 847, may have altered the  $d_w$  where *N. dutertrei* calcify, but not the  $d_w$  in the surface waters. Today, the  $\Delta d_w$  is nearly constant throughout the year; variations in surface-water and upper thermocline salinity at Site 847 are less than 0.4‰ (Fig. 2). A relationship between  $d_w$  and salinity in the Panama Basin shows an  $\delta^{18}\text{O}$  increase of 0.26‰ for a 1‰ increase in

salinity (Fairbanks et al., 1982). Similarly, in the western Pacific (Kuroshio Current),  $\delta^{18}\text{O}$  increases by 0.20‰ per 1‰ increase in salinity (Oba, 1988). If these relationships hold true at Site 847, then they suggest that the salinity contrast (a proxy for the  $\Delta d_w$ ) between the depths where *G. sacculifer* and *N. dutertrei* calcified has to change significantly to produce an observable change in  $\Delta\delta^{18}\text{O}_{d-s}$ . Given the small  $\Delta d_w$  observed today, and no evidence for significant changes in the past, our assumption of a constant  $\Delta d_w$  is the conservative approach, which we have adopted.

Our final assumption is that the faunal assemblage is composed of *G. sacculifer* and *N. dutertrei* specimens that represent the average annual conditions of the mixed layer and thermocline, respectively. This means that the flux of these species to the seafloor does not vary over the year such that the foraminifers in the sediments reflect a particular season rather than the integrated annual flux. Since the intra-annual climatic and hydrographic conditions are relatively constant at this site, we do not expect to see significant seasonality in the foraminiferal flux to the sea floor. This assumption simplifies the conversion of the  $\Delta\delta^{18}\text{O}_{d-s}$  to a temperature contrast because we can assume that the sedimentary faunal  $\delta^{18}\text{O}$  represents an annual average temperature, rather than a seasonally weighted one.

Application of these assumptions and adjustments to the core top *G. sacculifer*  $\delta^{18}\text{O}$  value (-1.05‰) in the Site 847 record gives an equilibrium value of -1.45‰, which implies calcification in the mixed layer (~10 m) based on the annual average temperature and salinity data at 0°N, 95°W of Levitus (1982), the salinity to  $d_w$  relationship of Fairbanks et al. (1982), and the temperature equation of Erez and Luz (1983) (Fig. 3A). When the core top *N. dutertrei*  $\delta^{18}\text{O}$  value (0.35‰) is converted to an equilibrium value (-0.55‰), a calcification depth of about 39 m is indicated (Fig. 3A). This falls within a steep portion of the upper thermocline. In equilibrium values, the core top  $\Delta\delta^{18}\text{O}_{d-s}$  at Site 847 equals 0.9‰, which is equivalent to a temperature difference of 4.1°C, the difference between 10 and 40 m. We postulate that our assumptions and adjustments are valid for the Holocene, because the converted core top  $\delta^{18}\text{O}$  values from Site 847 are consistent with the modern upper ocean hydrography.

Based on the complex temperature difference estimate, the surface waters at Site 847 average 1.9°C warmer than the thermocline waters and range from 5.3° to -2.0°C warmer (Fig. 14B). This mean value is smaller than that calculated by the simple approach (Fig. 14A), but the range is identical. The merit of the simple approach is that the contrast is never negative, indicating that the thermocline temperature is never

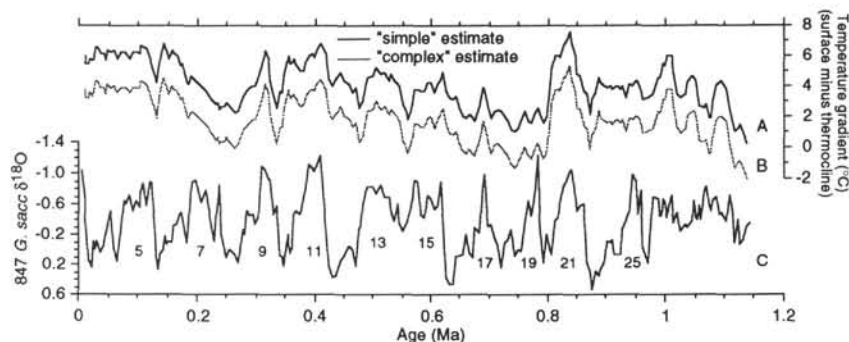


Figure 14. Temporal variations in the temperature difference between the upper thermocline and the surface mixed layer in the EEP based on the Site 847  $\Delta\delta^{18}\text{O}_{\text{d-s}}$  record. A. "Simple" estimate calculated from the Erez and Luz (1983) relationship, in which a change of 0.22‰ equals a 1°C temperature change. B. "Complex" estimate, which attempts to account for the effects of other processes, as described in the text. C. Temperature contrasts compared to the Site 847 *G. sacculifer*  $\delta^{18}\text{O}$  record. Odd numbers denote interglacial stages.

warmer than the mixed layer. Nevertheless, the depth of calcification for *G. sacculifer* and *N. dutertrei* inferred from the simple approach, is 25 and 70 m, respectively, which is somewhat deeper than expected at Site 847. Although a temperature difference of 0°C between the mixed layer and the thermocline seems possible, especially if the thermocline broke through to the surface during enhanced upwelling, the temperature inversions from the complex estimate are unlikely. The negative temperature differences from 0.65 to 0.80 Ma and from 1.10 to 1.15 Ma (Fig. 14B) indicate errors in the assumptions or the adjustments made in the complex estimate. A possible explanation is that the *G. sacculifer* vital effect correction of 0.5‰ is too large in these intervals or that gametogenic calcification was greater. Because carbonate preservation is relatively good in these intervals (Fig. 11), a larger adjustment for differential dissolution is not warranted.

From 1.15 to 1.00 Ma, the temperature difference from the simple estimate increased from about 0° to 6°C, and the glacial/interglacial pattern first appeared (stage 27) (Fig. 14A). Glacials are characterized by small temperature differences, interglacials by larger ones. The largest difference occurred at about 0.84 Ma (stage 21), when the surface waters were between 5.5° and 7.5°C warmer than the thermocline, depending on the method of calculation. The subsequent interval, between 0.7 and 0.8 Ma, is marked by the lowest persistent temperature difference of the record. A distinct glacial/interglacial pattern returns at 0.75 Ma and lasts for about 500 k.y. This pattern is superimposed on a long-term increase in the temperature contrast, which is also seen at Site 851. The contrast since 130 ka has been large and invariant, suggesting stability of the thermal regime.

### $\Delta\delta^{13}\text{C}$

The  $\Delta\delta^{13}\text{C}$  difference was calculated by subtracting the *N. dutertrei*  $\delta^{13}\text{C}$  from the *G. sacculifer*  $\delta^{13}\text{C}$ , thus  $\Delta\delta^{13}\text{C}_{\text{s-d}}$ . The direction of this subtraction is opposite of that used for the  $\Delta\delta^{18}\text{O}_{\text{d-s}}$ , but was adopted simply for the purpose of having positive excursions in the same direction. Two versions of the  $\Delta\delta^{13}\text{C}_{\text{s-d}}$  are presented in Figure 15. The unsmoothed version ranges from -0.73‰ to 0.78‰ around a mean of 0.035‰ (Fig. 15A). In the smoothed version, the range narrows to between -0.48‰ and 0.47‰ (Figs. 15B and 15C). In essence, the average  $\Delta\delta^{13}\text{C}_{\text{s-d}}$  is zero because the *G. sacculifer* and the *N. dutertrei*  $\delta^{13}\text{C}$  values are generally similar. This zero difference may be interpreted in several ways. No difference suggests that the  $\delta^{13}\text{C}$  of  $\Sigma\text{CO}_2$  is the same in the mixed layer and in the thermocline. Alternatively, and more likely, we think the  $\delta^{13}\text{C}$  of  $\Sigma\text{CO}_2$  was heavier in the mixed layer, but this difference was negated in the isotopic composition of the foraminifers by factors such as disequilibrium fractionation, or foraminifer test size differences, as discussed below. Regardless of the absolute values, the  $\Delta\delta^{13}\text{C}_{\text{s-d}}$  pattern that emerges is

clearly one of low values during glacials and high values during interglacials. If fact, this glacial/interglacial pattern is stronger and more consistent than the  $\Delta\delta^{18}\text{O}_{\text{d-s}}$  pattern (Fig. 16).

Based on our understanding of foraminiferal ecology and  $\delta^{13}\text{C}$  systematics (e.g., Broecker and Peng, 1982; Curry and Crowley, 1987), we did not expect to see negative excursions in  $\Delta\delta^{13}\text{C}_{\text{s-d}}$ , where the *N. dutertrei*  $\delta^{13}\text{C}$  values are heavier than the *G. sacculifer* values. Because preferential uptake of  $^{12}\text{C}$  during photosynthesis in the mixed layer results in higher  $\delta^{13}\text{C}$  of  $\Sigma\text{CO}_2$ , we expected to consistently observe heavier *G. sacculifer*  $\delta^{13}\text{C}$  values. This nutrient scenario may in fact be correct, because the negative  $\Delta\delta^{13}\text{C}_{\text{s-d}}$  excursions can be explained by thermodynamic or ecologic processes. For example, they may occur when thermocline waters are enriched in  $^{13}\text{C}$  by thermodynamic processes rather than by nutrient cycling (Broecker and Peng, 1982; Charles et al., 1993). If greater gas equilibration occurred between the atmosphere and the southwest Pacific surface waters that form subantarctic mode waters, the source of the EUC and thus ultimately the thermocline waters at Site 847, then the initial  $\delta^{13}\text{C}$  of  $\Sigma\text{CO}_2$  of this water would be heavier, whereas surface-water  $\delta^{13}\text{C}$  of  $\Sigma\text{CO}_2$  at Site 847 may not have changed, or at least not to the same degree. Greater equilibration in the southwest Pacific could have resulted from colder temperatures, faster  $\text{CO}_2$  exchange rates, longer surface-water residence times, and other factors that promote gas exchange. A simpler explanation for the occasional negative  $\Delta\delta^{13}\text{C}_{\text{s-d}}$  excursions is based on the strong positive correlation between foraminifer size and  $\delta^{13}\text{C}$ , and on the apparent offset of *N. dutertrei*  $\delta^{13}\text{C}$  from the  $\delta^{13}\text{C}$  of  $\Sigma\text{CO}_2$ . Based on previous studies, we assume that the  $\delta^{13}\text{C}$  of the *G. sacculifer* specimens used in this study (300–355  $\mu\text{m}$ ) approximated the  $\delta^{13}\text{C}$  of  $\Sigma\text{CO}_2$  in the mixed layer, whereas the *N. dutertrei* (355–425  $\mu\text{m}$ )  $\delta^{13}\text{C}$  values were 0.5‰ heavier than thermocline waters (e.g., Ravelo, 1991; Ravelo and Shackleton, this volume). We might expect that deep-water gametogenic calcification by *N. dutertrei* would result in lighter, rather than heavier, calcite  $\delta^{13}\text{C}$  because of the lighter  $\delta^{13}\text{C}$  of  $\Sigma\text{CO}_2$ , as observed by others (Williams et al., 1977; Erez and Honjo, 1981; Bouvier-Soumagnac and Duplessy, 1985). Nevertheless, it is possible that the size trend and the strong link to photosynthesis possibly offset this effect (Spero, 1992) and result in a net disequilibrium of +0.5‰. When 0.5‰ is subtracted from the *N. dutertrei* values, the resulting  $\Delta\delta^{13}\text{C}_{\text{s-d}}$  is always positive and the largest difference is about 1‰. The -0.5‰ adjusted core-top  $\Delta\delta^{13}\text{C}_{\text{s-d}}$  value is 1‰, which is comparable to the difference in the  $\delta^{13}\text{C}$  of  $\Sigma\text{CO}_2$  between the surface waters and the thermocline based on EEP water column profiles (Kroopnick, 1974; Quay et al., 1992).

The  $\Delta\delta^{13}\text{C}_{\text{s-d}}$  pattern at Site 847 matches the  $\Delta\delta^{13}\text{C}_{\text{s-d}}$  pattern at Site 851, but not as well as the  $\Delta\delta^{18}\text{O}_{\text{d-s}}$  patterns (Fig. 13). Although both  $\Delta\delta^{13}\text{C}_{\text{s-d}}$  records generally show higher positive values during interglacials, this pattern is not as consistent at Site 851. Also, the mean

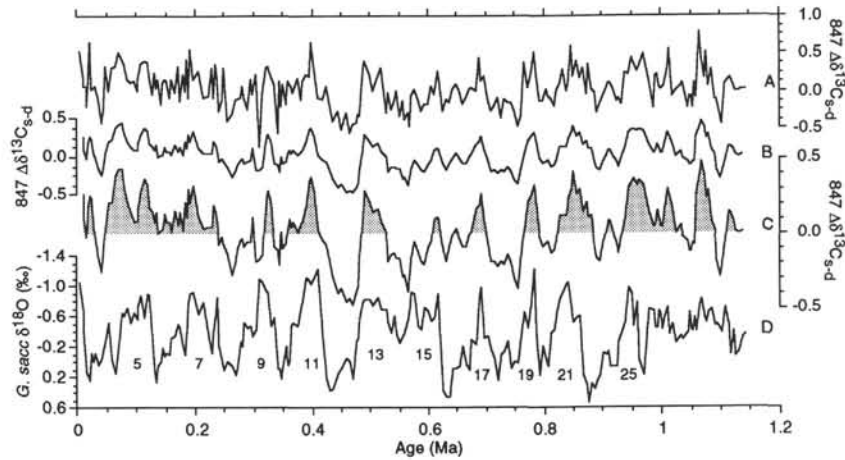


Figure 15. The carbon isotope difference between the thermocline and the mixed layer at Site 847, calculated as  $\delta^{13}\text{C}_{G. sacculifer}$  minus  $\delta^{13}\text{C}_{N. dutertrei}$ . **A.** Difference in  $\delta^{13}\text{C}$ . **B.** Smoothed version of Figure 15A. **C.** Expanded scaling of Figure 15B. **D.** *G. sacculifer*  $\delta^{18}\text{O}$  record shown for comparison. Odd numbers denote interglacial stages. A distinct climatic signal is apparent and is characterized by positive excursions during interglacial and negative ones during glacial.

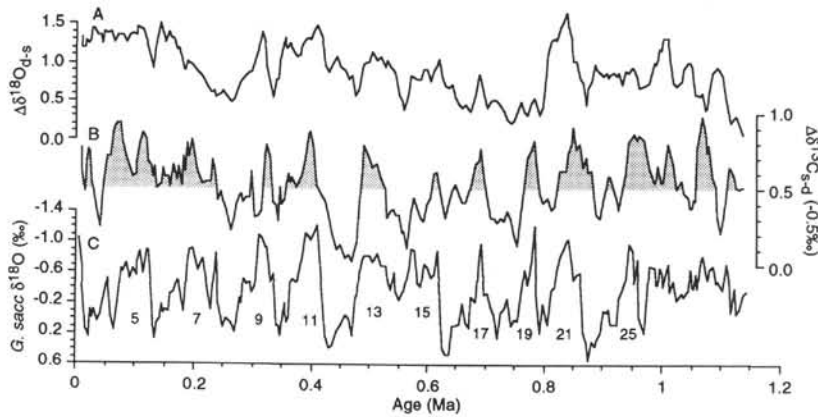


Figure 16. The Pleistocene link between climate and differences in temperature and nutrient concentration between the surface and the thermocline at Site 847. Interglacial stages, denoted by odd numbers in *G. sacculifer*  $\delta^{18}\text{O}$  record (Fig. 16C), are often characterized by large temperature differences (inferred from  $\Delta\delta^{18}\text{O}_{s-t}$  in Fig. 16A) and increases in the nutrient difference (inferred from  $\Delta\delta^{13}\text{C}_{s-t}$  in Fig. 16B). The subtraction of 0.5‰ from the  $\Delta\delta^{13}\text{C}_{s-t}$  values is discussed in the text.

$\Delta\delta^{13}\text{C}_{s-t}$  at Site 851 is about 0.33‰ greater than that at Site 847, indicating a larger difference in the  $\delta^{13}\text{C}$  of  $\Sigma\text{CO}_2$  between the mixed layer and the thermocline. This may be attributed to a lower nutrient injection into the mixed layer at this site, where the thermocline is deeper.

### Interpretation of the $\Delta\delta^{18}\text{O}_{d-s}$ and $\Delta\delta^{13}\text{C}_{s-t}$ Records

Any interpretation of the  $\Delta\delta^{18}\text{O}_{d-s}$  and  $\Delta\delta^{13}\text{C}_{s-t}$  records must explain three observations: (1) smaller thermal contrasts (low  $\Delta\delta^{18}\text{O}_{d-s}$ ) between the mixed layer and the thermocline during many glacial periods, but not all; (2) reduced vertical contrasts in the  $\delta^{13}\text{C}$  of  $\Sigma\text{CO}_2$  (low  $\Delta\delta^{13}\text{C}_{s-t}$ ) during all glacial periods; and (3) long-term (>100 k.y.) variability in  $\Delta\delta^{18}\text{O}_{d-s}$  that does not coincide with the  $\Delta\delta^{13}\text{C}_{s-t}$ . We present several possible explanations of the glacial/interglacial isotope patterns that are based on climate-driven changes in oceanography and on ecological variability. Our preferred causal mechanism is a change in the upwelling rate, which is discussed first. Longer term  $\delta^{18}\text{O}$  contrast patterns are more difficult to interpret, but are tenta-

tively linked to changes in the westward horizontal influx of cooler waters from the Peru Current.

### Glacial/interglacial Pattern: Upwelling Rate

We attribute the glacial/interglacial isotope pattern to variations in the upwelling regime at the equatorial divergence. Greater upwelling during glacial times would have reduced the thermal contrast by cooling the surface waters relative to the thermocline. Barring a change in cloudiness, the radiative heating of the surface mixed layer probably remained constant. This suggests that mixed layer conditions were controlled by waters advected from below, rather than by the atmospheric changes from above. If the thermocline temperature remained constant, then the upwelling-induced decrease in the  $\Delta\delta^{18}\text{O}_{d-s}$  during glacial implies a surface-water cooling of between 1° and 3°C (Fig. 14). This is consistent with the degree of cooling inferred from alkenone records from Site 847 (K. Emeis, pers. comm., 1993) and from the CEP (Lyle et al., 1992) (Fig. 3C). Based on an SST cooling

of 2°C, and a simple heat balance box model, Lyle et al. (1992) suggested that the CEP upwelling rate was as much as 2.5 times higher during glacial periods. This was considered responsible for the SST cooling and is consistent with the increase in new production inferred from the higher organic carbon burial rates during glacials (Lyle et al., 1992).

Increased upwelling during glacials would also explain a reduced  $\Delta\delta^{13}\text{C}_{\text{s-d}}$ . Greater injection of nutrient-rich, low- $\delta^{13}\text{C}$  waters from the thermocline into the mixed layer would have weakened the steep vertical gradient in  $\delta^{13}\text{C}$  of  $\Sigma\text{CO}_2$  that is observed today. In this scenario, input rate of nutrients from the upwelling exceeded the rate at which photosynthesis stripped the nutrients from the surface water. This implies that the excess of nutrients, such as  $\text{NO}_3^-$ , observed in the highly productive equatorial region today (Feely et al., 1987; Murray et al., 1989; Fiedler and Philbrick, 1991; Peña et al., 1994), was even greater during glacials. Though not necessarily the case, greater nutrient input into the mixed layer suggests increased biological productivity and greater export production. The paleoceanographic record shows strong evidence of increased productivity in the equatorial Pacific during glacial times (e.g., Pedersen, 1983; Finney et al., 1988; Lyle, 1988; Pedersen et al., 1988; Herguera and Berger, 1991; Pedersen et al., 1991). Whether or not the higher productivity was augmented by increased input of micronutrients, such as iron (Martin, 1990), remains uncertain. Two possible sources of micronutrients during glacial times are increased eolian dust input and enhanced erosion of the Galápagos Islands caused by lowered sea level and greater westward advection of island-derived nutrients.

Greater equatorial upwelling in the Pacific during glacials has commonly been inferred (Arrhenius, 1952, 1988; Quinn, 1971; Valencia, 1977; Müller and Suess, 1979; Moore et al., 1980; Sarnthein and Winn, 1988; Lyle et al., 1992), and has been attributed to intensified atmospheric and oceanic circulation; particularly a compression of the low latitudinal temperature gradient, linked to expanded ice sheets and ultimately orbital forcing (CLIMAP, 1981; Imbrie et al., 1992). Stronger trade winds during glacial periods would have increased EUC flow because of the steepened sea surface slope along the equator. Increased flow would also be supported by greater subantarctic mode water formation at high southern latitudes in response to stronger westerlies (Imbrie et al., 1992). The high latitude waters were colder during glacials (CLIMAP, 1981), but northward displacement of the westerlies may have shifted the locus of mode water formation toward the equator (Howard and Prell, 1992), possibly offsetting the temperature decrease.

The geologic record of eolian sedimentation in ice cores is consistent with the idea of stronger atmospheric circulation and greater aridity in source regions during glacial times (e.g., Petit et al., 1990; Jouzel et al., 1993). Dust concentrations and accumulations were significantly larger at the high latitudes of both hemispheres during glacial periods. Similarly, the eolian accumulation rate in deep-sea sediment cores from the North Pacific (Hovan et al., 1991) and the Arabian Sea (Clemens and Prell, 1990) were as much as four times greater during glacial times than during interglacials. Interestingly, similar results have not been observed in the equatorial Pacific, where the record of eolian accumulation is ambiguous. Chuey et al. (1987) observed generally higher eolian accumulation during glacials, whereas Murray et al. (1993) and Janecek and Rea (1985) saw the opposite. Rea (1990) noted that eolian accumulation maxima occurred during both glacial and interglacial times and suggested that the common assumption of stronger atmospheric circulation during glacial periods may be incorrect. Equatorial Pacific eolian records are more difficult to interpret for several reasons. First, there may be eolian source regions other than Central and South America. This is implied by the average eolian accumulation rates (0–1 Ma) at Core RC11-210 (1°49'N, 140°03'W) (Chuey et al., 1987), which are equal to or higher than those at Sites 848 (3°S, 110°29'W) and 849 (0°11'N, 110°31'W) (Hovan, this volume), which are located closer to the presumed dust source region

(Nakai et al., 1993). All three sites are south of the ITCZ, where eolian deposition is greater because of wet-depositional scavenging of aerosols and stronger downward mixing (Rea, 1990). Second, latitudinal shifts in the ITCZ on a  $10^3$  to  $10^4$  year time scale (Schramm, 1985) may have complicated the 100-k.y. signal observed outside the equatorial region. Third, ambiguities in chronostratigraphy (affecting eolian mass flux estimates), indistinct  $\delta^{18}\text{O}$  structure, and analytical difficulties influencing the accuracy and precision of the eolian concentration measurements (e.g., Chuey et al., 1987) also contribute to the difficulty in interpreting the equatorial Pacific eolian flux record. The eolian grain-size record, an index of trade-wind strength (Rea, 1990), does not clarify the situation. For example, a coherent link at a 31-k.y. periodicity was observed in the CEP between trade-wind strength inferred from eolian grain size, and equatorial divergence inferred from the radiolarian fauna (Pisias and Rea, 1988). This periodicity is not linearly linked with climate change inferred from the  $\delta^{18}\text{O}$  record, nor with orbital forcing, thus a simple glacial/interglacial pattern in trade-wind strength and equatorial divergence is not observed. Nevertheless, the paleoceanographic record (Pisias and Rea, 1988) indicates that stronger trade winds resulted in more intense upwelling.

The upwelling hypothesis is also supported by the Site 847 sedimentary and faunal record (Fig. 17). The reduced oxygen and carbon isotopic differences during glacials coincide with higher  $\text{CaCO}_3$  MARs (Murray et al., this volume) and greater accumulation rates of *N. dutertrei* (calculated from the data in McKenna et al., this volume). Higher  $\text{CaCO}_3$  MAR during glacials suggests greater carbonate production, although decreased carbonate dissolution from a less corrosive bottom water may have also contributed. The absolute abundance and the flux of divergence-indicative *N. dutertrei* increases dramatically during glacials. Glacial values are commonly in excess of 6000 tests/cm<sup>2</sup>/k.y. whereas interglacial values are generally less than a third of this. Higher production of *N. dutertrei* is attributed to improved ecological conditions that were brought about by greater upwelling. Since *N. dutertrei* is dissolution-resistant, the signal is considered more indicative of production changes rather than variations in dissolution intensity. The *G. sacculifer* flux also shows a glacial/interglacial pattern with higher values during glacials, but the values never rise above 1000 tests/cm<sup>2</sup>/k.y. and this species is never more than 13% of the total fauna whereas *N. dutertrei* averages 45%. Compared to the *N. dutertrei* flux, that of dissolution-susceptible *G. sacculifer* shows a closer correspondence to dissolution fluctuations, as indicated by the stronger association of high fluxes with high percentages of whole foraminifers.

#### **Glacial/interglacial Pattern: Water Property, Advection, and Ecological Interpretations**

Could the glacial isotopic contrast patterns be explained by upwelling of colder and  $^{13}\text{C}$ -enriched waters even though the rate of upwelling remained unchanged? One plausible scenario is the formation of colder subantarctic mode water with a lower  $\delta^{13}\text{C}$  of  $\Sigma\text{CO}_2$  caused by a higher preformed nutrient concentration or less  $\text{CO}_2$  gas exchange. These properties would be transferred to the EUC, the source of thermocline water at Site 847. Another possibility is a change in the relative proportion of upper and lower tier waters that comprise the EUC. Without corresponding records from the southwest Pacific, these hypotheses cannot be tested.

If both the upwelling rate and the properties of the upwelled waters remained constant over time, then the reduced thermal contrast during glacials could be explained by a cooling of the surface waters because of (1) decreased radiative heating, (2) increased evaporative cooling, or (3) greater westward advection of cooler surface waters from the Peru Current. However, these mechanisms would not explain the concomitant decrease in  $\Delta\delta^{13}\text{C}_{\text{s-d}}$ . The first two mechanisms can be excluded because they would not change the  $\delta^{13}\text{C}$  contrast. The third, advection of Peru Current water, would most likely increase the  $\Delta\delta^{13}\text{C}_{\text{s-d}}$  rather than decrease it because the  $\delta^{13}\text{C}$  of these surface

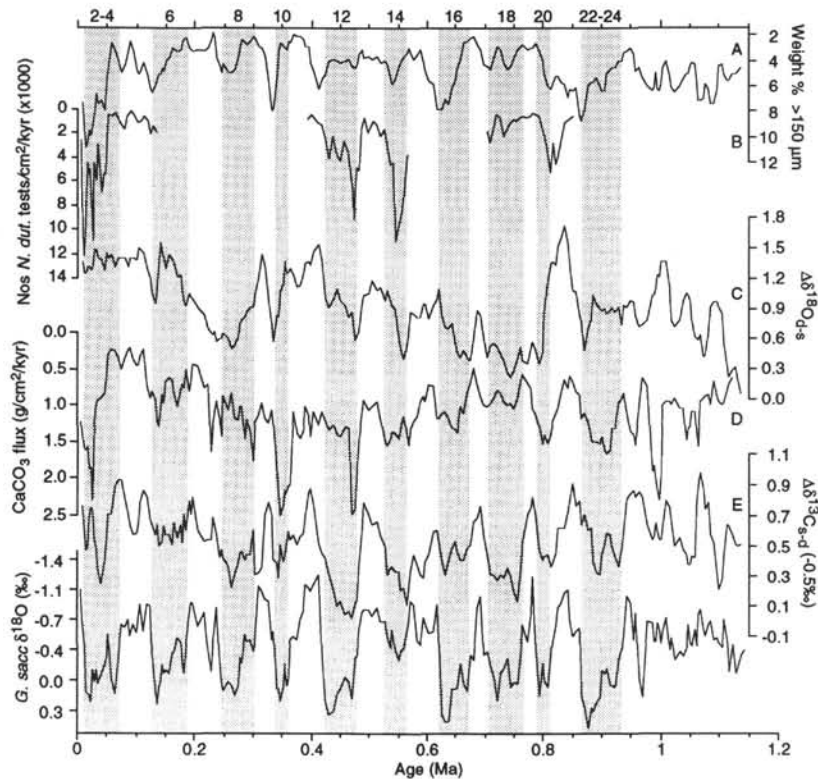


Figure 17. Climatic links among isotopic contrasts, biogenic accumulation rates, and carbonate preservation at Site 847. Increased upwelling and export production in the EEP during glacial periods (shaded regions), and less dissolution, are inferred from generally greater preservation (wt% > 150  $\mu\text{m}$ ; A), higher accumulation rates of *N. dutertrei* (B) and  $\text{CaCO}_3$  (D), lower  $\Delta\delta^{18}\text{O}_{\text{d-s}}$  (C), and lower  $\Delta\delta^{13}\text{C}_{\text{s-d}}$  (E).

waters is higher than in the equatorial divergence (Kroopnick, 1974), and gas exchange and biological uptake would further enrich the  $^{13}\text{C}$  content during westward advection toward Site 847.

A change in the preferred depth habitat of the foraminifers is an ecologically based explanation of low  $\Delta\delta^{18}\text{O}_{\text{d-s}}$  and  $\Delta\delta^{13}\text{C}_{\text{s-d}}$  values during glacials. The reduced isotopic contrasts could have resulted from the shoaling of *N. dutertrei* into the warmer, nutrient-depleted mixed layer or, from the migration of *G. sacculifer* into the thermocline. We consider *N. dutertrei* movement more plausible, because even a small shoaling of the calcification depth would have had a measurable impact on the isotopic composition of the shell given the steep gradients in thermocline temperature and  $\delta^{13}\text{C}$ . Nevertheless, we consider this explanation unlikely for two reasons. First, the large increase in the absolute abundance and the accumulation rate of *N. dutertrei* during glacials argues against movement into significantly warmer water, outside this species optimal ecological habitat. Second, a similar shift in the calcification depth would have had to occur throughout the entire EEP, given the similarity of the EEP *N. dutertrei* isotope records and the similar isotopic contrasts at ODP Sites 847 and 851.

#### Nonglacial/interglacial Isotope Contrast Patterns

Two  $\Delta\delta^{18}\text{O}_{\text{d-s}}$  patterns that do not show an obvious link to glacial/interglacial variations are the long-term increase in the thermal contrast from stage 19 to 9 and the relatively constant contrast from stage 5 to 1. The long-term increase, superimposed on the glacial/interglacial pattern, is not a local feature because it is also observed at Site 851. A gradual decrease in the upwelling rate is unlikely because this is inconsistent with the  $\Delta\delta^{13}\text{C}_{\text{s-d}}$  record, which does not show a corresponding increase. The decoupling of the temperature and the nutrient contrasts

may represent some change in the character of the upwelled water, either in terms of the  $\delta^{13}\text{C}$  of  $\Sigma\text{CO}_2$ , or in the temperature. Alternatively, it may represent a progressively smaller infusion of cold surface waters advected from outside the western Galápagos region. This explanation is supported by the foraminiferal faunal assemblage data (McKenna et al., this volume). The lowest  $\Delta\delta^{18}\text{O}_{\text{d-s}}$  values, indicating the smallest temperature difference between the mixed layer and the thermocline, occur between 0.7 and 0.8 Ma, where the faunal assemblage is characterized by unusually large abundances of *Neogloboquadrina pachyderma* left-coiling. This species is commonly found in polar waters, and co-occurs with only a small number of species. The fact that the relative abundance of this species was as high as 30% in this interval, and co-occurred with a diverse collection of equatorial species, attests to an unusual hydrographic setting at this time. Greater advection of cold Peru Current waters into the Galápagos region at this time is a viable explanation of both the faunal and isotopic data, though the apparent decoupling from the  $\Delta\delta^{13}\text{C}_{\text{s-d}}$  record is more difficult to explain.

The temperature contrast in the upper part of our record (stages 1 through 5) is generally invariant, and does not show a distinct glacial/interglacial pattern. Interestingly, this interval shows the poorest match to the Site 851 temperature difference record, which has distinct changes (Fig. 13). The  $\delta^{18}\text{O}$  structure from stages 1 through 5 is unambiguous in both the Site 847 and Site 851  $\delta^{18}\text{O}$  records, suggesting stratigraphic continuity. The Site 847  $\Delta\delta^{13}\text{C}_{\text{s-d}}$  record shows significant glacial/interglacial variability over this interval as well as in previous ones. We cannot easily explain the  $\Delta\delta^{18}\text{O}_{\text{d-s}}$  constancy in this portion of the record. At this point, we note that this interval is also anomalous in comparison to the rest of the Pleistocene with respect to other paleoceanographic records. For example, the *N. dutertrei*  $\delta^{18}\text{O}$  values are uncharacteristically heavy over stages 1 to 5, suggesting

relatively colder thermocline temperatures (Figs. 5 and 9). This interval is also marked at Site 847 by the highest opal concentrations of the previous million years and by unusually high opal MARs (Murray et al., this volume). A similar increase in opal MAR is not observed at Site 851, whereas the CaCO<sub>3</sub> MAR at both ODP sites is approximately the same (1 g/cm<sup>2</sup>/k.y.) (Farrell et al., this volume). Finally, the shift to an invariant isotope contrast at the end of stage 6 coincides with a distinct shift toward less upwelling in the EEP based on fluctuations in the radiolarian faunal assemblage (Schramm, 1985).

### CONCLUSIONS

The Pleistocene sedimentary record at Site 847 is continuous and the  $\delta^{18}\text{O}$ -based sedimentation rate since 1.15 Ma averaged about 3 cm/k.y. The  $\delta^{18}\text{O}$  chronostratigraphy serves as an independent check of the GRAPE age model (Shackleton et al., this volume). GRAPE age estimates are similar to those based on  $\delta^{18}\text{O}$ , but offsets as large as 30,000 yr occur in some intervals. Although generally small, the offsets will affect the spectral evaluation of oceanographic processes on the Milankovitch-scale. Nevertheless, given the time, effort, and expense involved in generating isotope records, the GRAPE approach is promising.

Estimates of global ice volume based on  $\delta^{18}\text{O}$  records from *N. dutertrei* are inconsistent with those based on records from low latitude "warm pool" *G. sacculifer*. This calls into question one or more of the following assumptions: (1) *N. dutertrei* calcifies at a constant water temperature; (2) the WEP SST has remained constant; (3) gametogenic calcification does not significantly overprint the isotopic signal incorporated by *G. sacculifer* in the mixed layer or by *N. dutertrei* in the thermocline; (4) the equatorial Pacific sedimentary assemblages reflect annual average oceanographic conditions; and (5) dissolution does not significantly distort the seawater record.

Comparison of *G. sacculifer*  $\delta^{18}\text{O}$  records from Site 847 and Core RC17-177 suggests that the surface waters in the EEP have constantly remained about 5°C colder than those in the WEP since 250 ka. Before this, the amplitude of the EEP isotope record is larger, which suggests relatively warmer interglacial SSTs in the EEP or greater dissolution in the WEP.

Temporal variability in the temperature and nutrient contrast between the surface waters and the thermocline was inferred from the  $\delta^{18}\text{O}$  and  $\delta^{13}\text{C}$  differences between *G. sacculifer* and *N. dutertrei*. Holocene isotopic contrasts are consistent with modern hydrographic conditions and with foraminiferal ecology. During the past million years, the surface waters were between 0° and 7°C warmer than the upper thermocline waters. Glacial periods are generally characterized by smaller thermal and nutrient contrasts. We attribute this pattern to increased upwelling of colder and nutrient-enriched waters during glacials. Superimposed on the glacial/interglacial temperature pattern are more complex trends, some of which co-occur with unusual planktonic foraminifer assemblages. Similar isotopic contrasts have been observed further west at Site 851 (Ravelo and Shackleton, this volume), suggesting that the inferred hydrographic changes were widespread.

### ACKNOWLEDGMENTS

We thank the crew and scientific party of Leg 138 for their hard work and generous collaboration that enabled the collection of such fine data. The authors are most grateful to C. Cors, R. Fifer, A. Martin, C. Star, M. Waldorf, and M. Zani, for their dedicated effort and expert technical assistance. S. Clemens, H. Spero, J. Le, and T. Pedersen provided helpful information, stimulating email conversation, and useful suggestions. We acknowledge N. Shackleton and A. Mix for graciously providing unpublished isotope data. The manuscript benefited by thoughtful reviews from D. Rea, N. Slowey, and W. Howard. The wise advice kindly given by Tj. van Andel is greatly appreciated. Financial support from the U.S. National Science Foundation (through JOI/USSAC Grant No. TAMRF-20528) to JF is gratefully acknowledged.

### REFERENCES\*

- Adelseck, C.G., Jr., 1977. Recent and late Pleistocene sediments from the eastern equatorial Pacific Ocean: sedimentation and dissolution [Ph.D. dissert.]. Univ. of California, San Diego.
- , 1978. Dissolution of deep-sea carbonate: preliminary calibration of preservational and morphological aspects. *Deep-Sea Res. Part A*, 24:1167–1185.
- Arrhenius, G., 1952. Sediment cores from the East Pacific. In Pettersson, H. (Ed.), *Rep. Swed. Deep-Sea Exped. 1947–1948*, 1–228.
- , 1988. Rate of production, dissolution and accumulation of biogenic solids in the ocean. *Palaeogeogr., Palaeoclimatol., Palaeoecol.*, 67:119–146.
- Baksi, A.K., Hsu, V., McWilliams, M.O., and Farrar, E., 1992. <sup>40</sup>Ar/<sup>39</sup>Ar dating of the Brunhes-Matuyama geomagnetic field reversal. *Science*, 256:356–357.
- Barber, R.T., and Chavez, F.P., 1983. Biological consequences of El Niño. *Science*, 222:1203–1210.
- Bé, A.W.H., 1980. Gametogenic calcification in a spinose planktonic foraminifer, *Globigerinoides sacculifer* (Brady). *Mar. Micropaleontol.*, 5:283–310.
- Bé, A.W.H., Bishop, J.K.B., Swerdlove, M.S., and Gardner, W.D., 1985. Standing stock, vertical distribution and flux of planktonic foraminifera in the Panama Basin. *Mar. Micropaleontol.*, 9:307–333.
- Bé, A.W.H., and Duplessy, J.-C., 1976. Subtropical convergence fluctuations and Quaternary climates in the middle latitudes of the Indian Ocean. *Science*, 194:419–422.
- Berger, A., and Loutre, M.F., 1991. Insolation values for the climate of the last 10 million years. *Quat. Sci. Rev.*, 10:297–317.
- Berger, W.H., 1971. Sedimentation of planktonic foraminifera. *Mar. Geol.*, 11:325–358.
- Berger, W.H., and Killingley, J.S., 1977. Glacial-Holocene transition in deep-sea carbonates: selective dissolution and the stable isotope signal. *Science*, 197:563–566.
- Berger, W.H., Killingley, J.S., and Edith, V., 1978. Stable isotopes in deep-sea carbonates: Box Core ERDC-92, west equatorial Pacific. *Oceanol. Acta*, 1:203–216.
- Blomqvist, S., 1991. Quantitative sampling of soft-bottom sediments: problems and solutions. *Mar. Ecol. Prog. Ser.*, 72:295–304.
- Bouvier-Soumagnac, Y., and Duplessy, J.-C., 1985. Carbon and oxygen isotopic composition of planktonic foraminifera from laboratory culture, plankton tows and recent sediment: implications for the reconstruction of paleoclimatic conditions and of the global carbon cycle. *J. Foraminiferal Res.*, 15:302–320.
- Broecker, W.S., and Peng, T.-H., 1982. *Tracers in the Sea*: Palisades, NY (Eldigio Press).
- Bryden, H.L., and Brady, E.C., 1985. Diagnostic model of the three-dimensional circulation in the upper Equatorial Pacific Ocean. *J. Phys. Oceanogr.*, 15:1255–1273.
- Cane, M.A., 1983. Oceanographic events during El Niño. *Science*, 222:1189–1210.
- Charles, C.D., Wright, J.D., and Fairbanks, R.G., 1993. Thermodynamic influences on the marine carbon isotope record. *Paleoceanography*, 8:691–697.
- Chavez, F.P., and Barber, R.T., 1987. An estimate of new production in the equatorial Pacific. *Deep-Sea Res. Part A*, 34:1229–1243.
- Chuey, J.M., Rea, D.K., and Pisias, N.G., 1987. Late Pleistocene paleoclimatology of the central Equatorial Pacific: a quantitative record of eolian and carbonate deposition. *Quat. Res. (N.Y.)*, 28:323–339.
- Clemens, S.C., and Prell, W.L., 1990. Late Pleistocene variability of Arabian Sea summer monsoon winds and continental aridity: eolian records from the lithogenic component of deep-sea sediments. *Paleoceanography*, 5:109–145.
- CLIMAP Project Members, 1981. Seasonal reconstructions of the Earth's surface at the last glacial maximum. *Geol. Soc. Am., Map and Chart Ser.*, MC36:1–18.

\*Abbreviations for names of organizations and publications in ODP reference lists follow the style given in *Chemical Abstracts Service Source Index* (published by American Chemical Society).

- Craig, H., 1957. Isotopic standards for carbon and oxygen correction factors for mass spectrometric analysis of CO<sub>2</sub>. *Geochim. Cosmochim. Acta*, 12:133–149.
- Crowley, T., 1991. Past CO<sub>2</sub> changes and tropical sea surface temperatures. *Paleoceanography*, 6:387–394.
- Curry, W.B., and Crowley, T.J., 1987. The δ<sup>13</sup>C of equatorial Atlantic surface waters: implications for ice-age pCO<sub>2</sub> levels. *Paleoceanography*, 2:489–517.
- Curry, W.B., and Matthews, R.K., 1981. Paleooceanographic utility of oxygen isotopic measurements on planktonic foraminifera: Indian Ocean core top evidence. *Paleoceanogr., Palaeoclimatol., Palaeoecol.*, 33:173–192.
- Curry, W.B., Thunell, R.C., and Honjo, S., 1983. Seasonal changes in the isotopic composition of planktonic foraminifera collected in Panama Basin sediment traps. *Earth Planet. Sci. Lett.*, 64:33–43.
- Deuser, W.G., 1987. Seasonal variations in isotopic composition and deep-water fluxes of the tests of perennially abundant planktonic foraminifera of the Sargasso Sea: results from sediment-trap collections and their paleoceanographic significance. *J. Foraminiferal Res.*, 17:14–29.
- Deuser, W.G., Ross, E.H., Hemleben, C., and Spindler, M., 1981. Seasonal changes in species composition numbers, mass, size and isotopic composition of planktonic foraminifera settling into the deep Sargasso Sea. *Paleoceanogr., Palaeoclimatol., Palaeoecol.*, 33:103–127.
- Duplessy, J.C., 1978. Isotope studies. In Gribbin, J. (Ed.), *Climate Change*: Cambridge (Cambridge Univ. Press), 46–67.
- Duplessy, J.C., Bé, A.W.H., and Blanc, P.L., 1981. Oxygen and carbon isotopic composition and the biogeographic distribution of planktonic foraminifera in the Indian Ocean. *Paleoceanogr., Palaeoclimatol., Palaeoecol.*, 33:9–47.
- Dymond, J., and Collier, R., 1988. Biogenic particle fluxes in the equatorial Pacific: evidence for both high and low productivity during the 1982–1983 El Niño. *Global Biogeochem. Cycles*, 2:129–137.
- Erez, J., 1979. Modification of the oxygen-isotope record in deep-sea cores by Pleistocene dissolution cycles. *Nature*, 281:535–538.
- Erez, J., Almogi-Labin, A., and Avraham, S., 1991. On the life history of planktonic foraminifera: lunar reproduction cycle in *Globigerinoides sacculifer* (Brady). *Paleoceanography*, 6:295–306.
- Erez, J., and Honjo, S., 1981. Comparison of isotopic composition of planktonic foraminifera in plankton tows, sediment traps and sediments. *Paleoceanogr., Palaeoclimatol., Palaeoecol.*, 33:129–156.
- Erez, J., and Luz, B., 1982. Temperature control of oxygen-isotope fractionation of cultured planktonic foraminifera. *Nature*, 297:220–222.
- , 1983. Experimental paleotemperature equation for planktonic foraminifera. *Geochim. Cosmochim. Acta*, 47:1025–1031.
- Fairbanks, R.G., Sverdlow, M., Free, R., Wiebe, P.H., and Bé, A.W.H., 1982. Vertical distribution and isotopic fractionation of living planktonic foraminifera from the Panama Basin. *Nature*, 298:841–844.
- Fairbanks, R.G., Wiebe, P.H., and Bé, A.W.H., 1980. Vertical distribution and isotopic composition of living planktonic foraminifera in the western North Atlantic. *Science*, 207:61–63.
- Farrell, J.W., and Prell, W.L., 1989. Climatic change and CaCO<sub>3</sub> preservation: an 800,000 year bathymetric reconstruction from the central equatorial Pacific Ocean. *Paleoceanography*, 4:447–466.
- Feely, R.A., Gammon, R.H., Taft, B.A., Pullen, P.E., Waterman, L.S., Conway, T.J., Gendron, J.F., and Wisegarver, D.P., 1987. Distribution of chemical tracers in the eastern equatorial Pacific during and after the 1982–1983 El Niño/Southern Oscillation Event. *J. Geophys. Res.*, 92:6545–6558.
- Fiedler, P.C., Philbrick, V., and Chavez, F.P., 1991. Oceanic upwelling and productivity in the eastern tropical Pacific. *Limnol. Oceanogr.*, 36:1834–1850.
- Finney, B.P., Lyle, M.W., and Heath, G.R., 1988. Sedimentation at MANOP Site H (eastern equatorial Pacific) over the past 400,000 years: climatically induced redox variations and their effects on transition metal cycling. *Paleoceanography*, 3:169–189.
- Gastrich, M.D., 1988. Ultrastructure of a new intracellular symbiotic alga found within planktonic foraminifera. *J. Phycol.*, 23:623–632.
- Hagelberg, T., Shackleton, N., Pisias, N., and Shipboard Scientific Party, 1992. Development of composite depth sections for Sites 844 through 854. In Mayer, L., Pisias, N., Janecek, T., et al., *Proc. ODP, Init. Repts.*, 138 (Pt. 1): College Station, TX (Ocean Drilling Program), 79–85.
- Hall, C.M., and Farrell, J.W., 1993. Laser <sup>40</sup>Ar/<sup>39</sup>Ar age from ash D of ODP Site 758: dating the Brunhes-Matuyama reversal and oxygen isotope stage 19.1. *Eos*, 74 (Suppl.):110.
- Halpern, D., 1987. Observations of annual and El Niño thermal and flow variations at 0°, 110°W and 0°, 95°W during 1980–1985. *J. Geophys. Res.*, 92:8197–8212.
- Hayes, S.P., Mangum, L.J., Barber, R.T., Huyer, A., and Smith, R.L., 1986. Hydrographic variability west of the Galápagos Islands during the 1982–83 El Niño. *Prog. Oceanogr.*, 17:137–162.
- Heath, G.R., and Culbertson, C., 1970. Calcite: degree of saturation, rate of dissolution and the compensation depth in the deep oceans. *Geol. Soc. Am. Bull.*, 81:3157–3160.
- Hemleben, C., Spindler, M., and Anderson, O.R., 1989. *Modern Planktonic Foraminifera*: New York (Springer-Verlag).
- Herbert, T.D., and Mayer, L.A., 1991. Long climatic time series from sediment physical property measurements. *J. Sediment. Petrol.*, 61:1089–1108.
- Herguera, J.C., and Berger, W.H., 1991. Paleoproductivity: glacial to post-glacial change in the western equatorial Pacific, from benthic foraminifera. *Geology*, 19:1173–1176.
- Hovan, S.A., Rea, D.K., and Pisias, N.G., 1991. Late Pleistocene continental climate and oceanic variability recorded in northwest Pacific sediments. *Paleoceanography*, 6:349–370.
- Howard, W.R., and Prell, W.L., 1992. Late Quaternary surface circulation of the southern Indian Ocean and its relationship to orbital variations. *Paleoceanography*, 7:79–117.
- Hutson, W.H., 1980. Bioturbation of deep-sea sediments: oxygen isotopes and stratigraphic uncertainty. *Geology*, 8:127–130.
- Imbrie, J., Boyle, E.A., Clemens, S.C., Duffy, A., Howard, W.R., Kukla, G., Kutzbach, J., Martinson, D.G., McIntyre, A., Mix, A.C., Molino, B., Morley, J.J., Peterson, L.C., Pisias, N.G., Prell, W.L., Raymo, M.E., Shackleton, N.J., and Toggweiler, J.R., 1993. On the structure and origin of major glacial cycles, 1. Linear responses to Milankovitch forcing. *Paleoceanography*, 7:701–738.
- Imbrie, J., Hays, J.D., Martinson, D.G., McIntyre, A., Mix, A.C., Morley, J.J., Pisias, N.G., Prell, W.L., and Shackleton, N.J., 1984. The orbital theory of Pleistocene climate: support from a revised chronology of the marine δ<sup>18</sup>O record. In Berger, A., Imbrie, J., Hays, J., Kukla, G., and Saltzman, B. (Eds.), *Milankovitch and Climate* (Pt. 1): Dordrecht (D. Reidel), 269–305.
- Janecek, T.R., and Rea, D.K., 1985. Quaternary fluctuation in the Northern Hemisphere trade winds and westerlies. *Quat. Res.*, 24:150–163.
- Johnson, R.G., 1982. Brunhes-Matuyama magnetic reversal dated at 790,000 yr B.P. by marine-astronomical correlations. *Quat. Res.*, 17:135–147.
- Jouzel, J., Barkov, N.I., Barnola, J.M., Bender, M., Chappellaz, J., Genthon, C., Kotlyakov, V.M., Lipenkov, V., Lorius, C., Petit, J.R., Raynaud, D., Raisbeck, G., Ritz, C., Sowers, T., Stievenard, M., Yiou, F., and Yiou, P., 1993. Extending the Vostok ice-core record of palaeoclimate to the penultimate glacial period. *Nature*, 364:407–411.
- Kahn, M.I., 1979. Non-equilibrium oxygen and carbon isotopic fractionation in tests of living planktonic foraminifera. *Oceanol. Acta*, 2:195–208.
- Karlin, R., Lyle, M., and Zahn, R., 1992. Carbonate variations in the northeast Pacific during the late Quaternary. *Paleoceanography*, 7:43–61.
- Keigwin, L.D., and Jones, G.A., 1990. Deglacial climatic oscillations in the Gulf of California. *Paleoceanography*, 5:1009–1023.
- Kroopnick, P., 1974. The dissolved O<sub>2</sub>-CO<sub>2</sub>-<sup>13</sup>C system in the eastern equatorial Pacific. *Deep-Sea Res. Part A*, 21:211–227.
- Ku, T.-L., and Oba, T., 1978. A method for quantitative evaluation of carbonate dissolution in deep-sea sediments and its application to paleoceanographic reconstruction. *Quat. Res.*, 10:112–129.
- Le, J., and Shackleton, N.J., 1992. Carbonate dissolution fluctuations in the western equatorial Pacific during the late Quaternary. *Paleoceanography*, 7:21–42.
- Levitus, S., 1982. *Climatological Atlas of the World Ocean*. NOAA Prof. Pap., 13.
- Lohmann, G.P., 1993. Unmixing the chemistry of planktonic foraminifera. *Eos*, 74 (Suppl):183.
- Lohmann, P.G., 1992. Glacial-interglacial changes in the upper ocean recorded by deep-living planktonic foraminifera. *Fourth Int. Conf. on Paleoceanogr.*, 185. (Abstract)
- Lukas, R., 1986. The termination of the equatorial undercurrent in the Eastern Pacific. *Prog. Oceanogr.*, 16:63–90.
- Lyle, M., 1988. Climatically forced organic carbon burial in the equatorial Atlantic and Pacific oceans. *Nature*, 335:529–532.
- Lyle, M.W., Prahl, F.G., and Sparrow, M.A., 1992. Upwelling and productivity changes inferred from temperature record in the central equatorial Pacific. *Nature*, 355:812–815.
- Martin, J.H., 1990. Glacial-interglacial CO<sub>2</sub> change: the iron hypothesis. *Paleoceanography*, 5:1–13.
- Matthews, R.K., and Poore, R.Z., 1980. Tertiary δ<sup>18</sup>O record and glacio-eustatic sea-level fluctuations. *Geology*, 8:501–504.

- Mayer, L., Pisias, N., Janecek, T., et al., 1992. *Proc. ODP, Init. Repts.*, 138 (Pts. 1 and 2): College Station, TX (Ocean Drilling Program).
- Mayer, L.A., 1991. Extraction of high-resolution carbonate data for paleoclimate reconstruction. *Nature*, 352:148–150.
- McCartney, M.S., 1982. The subtropical recirculation of mode waters. *J. Mar. Res.*, 40:427–464.
- McPhaden, M.J., and Hayes, S.P., 1990. Variability in the eastern equatorial Pacific Ocean during 1986–1988. *J. Geophys. Res.*, 95:13195–13208.
- Mix, A.C., Pisias, N.G., Zahn, R., Rugh, W., Lopez, C., and Nelson, K., 1991. Carbon-13 in Pacific deep and intermediate waters, 0–370 ka: implications for ocean circulation and Pleistocene CO<sub>2</sub>. *Paleoceanography*, 6:205–226.
- Montgomery, R.B., and Stroup, E.D., 1962. Equatorial waters and currents at 150°W in July–August 1952. *Johns Hopkins Oceanogr. Stud.*
- Moore, T.C., Jr., Burckle, L.H., Geitzenauer, K., Luz, B., Molina-Cruz, A., Robertson, J.H., Sachs, H., Sancetta, C., Thiede, J., Thompson, P., and Wenkam, C., 1980. The reconstruction of sea surface temperatures in the Pacific Ocean of 18,000 B.P. *Mar. Micropaleontol.*, 5:215–247.
- Müller, P.J., and Suess, E., 1979. Productivity, sedimentation rate, and sedimentary organic matter in the oceans. I. Organic carbon preservation. *Deep-Sea Res. Part A*, 26:1347–1362.
- Murray, D.W., 1987. Spatial and temporal variations in sediment accumulation in the central tropical Pacific [Ph.D. dissert.], Oregon State Univ., Corvallis, OR.
- Murray, J.W., Downs, J.N., Strom, S., Wei, C.L., and Jannasch, H.W., 1989. Nutrient assimilation, export production and <sup>234</sup>Th scavenging in the eastern equatorial Pacific. *Deep-Sea Res. Part A*, 36:1471–1489.
- Murray, R.W., Leinen, M., and Isern, A.R., 1993. Biogenic flux of Al to sediment in the central equatorial Pacific Ocean: evidence for increased productivity during glacial periods. *Paleoceanography*, 8:651–670.
- Nakai, S., Halliday, A.N., and Rea, D.K., 1993. Provenance of dust in the Pacific Ocean. *Earth Planet. Sci. Lett.*, 119:143–157.
- Oba, T., 1988. Paleocceanographic information obtained by the isotopic measurement of individual foraminiferal specimens. *Proc. First Int. Conf. Asian Mar. Geol.*, 169–180.
- Oppo, D.W., and Fairbanks, R.G., 1989. Carbon isotope composition of tropical surface water during the past 22,000 years. *Paleoceanography*, 4:333–351.
- Pedersen, T.F., 1983. Increased productivity in the eastern equatorial Pacific during the last glacial maximum (19,000 to 14,000 yr B.P.). *Geology*, 11:16–19.
- Pedersen, T.F., Nielsen, B., and Pickering, M., 1991. Timing of late Quaternary productivity pulses in the Panama Basin and implications for atmospheric CO<sub>2</sub>. *Paleoceanography*, 6:657–678.
- Pedersen, T.F., Pickering, M., Vogel J.S., Southon, J.N., and Nelson, D.E., 1988. The response of benthic foraminifera to productivity cycles in the eastern equatorial Pacific: faunal and geochemical constraints on glacial bottom water oxygen levels. *Paleoceanography*, 3:157–168.
- Peña, A., Lewis, M.R., and Cullen, J.J., 1994. New production in the warm waters of the tropical Pacific Ocean. *J. Geophys. Res.*, 99:14255–14268.
- Petit, J.R., Mounier, L., Jouzel, J., Korotkevich, Y.S., Kotlyakov, V.I., and Lorius, C., 1990. Paleoclimatological and chronological implications of the Vostok core dust record. *Nature*, 343:56–58.
- Philander, S.G.H., 1990. *El Niño, La Niña and the Southern Oscillation*: San Diego (Academic Press).
- Pisias, N.G., and Rea, D.K., 1988. Late Pleistocene paleoclimatology of the central equatorial Pacific: sea surface response to the southeast Trade Winds. *Paleoceanography*, 3:21–37.
- Popp, B.N., Podosek, F.A., Brannon, J.C., Anderson, T.F., and Pier, J., 1986. <sup>87</sup>Sr/<sup>86</sup>Sr ratios in Permo-Carboniferous sea water from the analyses of well-preserved brachiopod shells. *Geochim. Cosmochim. Acta*, 50:1321–1328.
- Prell, W.L., Imbrie, J., Martinson, D.G., Morley, J.J., Pisias, N.G., Shackleton, N.J., and Stretter, H.F., 1986. Graphic correlation of oxygen isotope stratigraphy: application to the late Quaternary. *Paleoceanography*, 1:137–162.
- Prentice, M.L., and Matthews, R.K., 1988. Cenozoic ice-volume history: development of a composite oxygen isotope record. *Geology*, 16:963–966.
- Quay, P.D., Tilbrook, B., and Wong, C.S., 1992. Oceanic uptake of fossil fuel CO<sub>2</sub>: carbon-13 evidence. *Science*, 256:74–79.
- Quinn, W.H., 1971. Late Quaternary meteorological and oceanographic developments in the equatorial Pacific. *Nature*, 229:330–331.
- Ravelo, A.C., 1991. Reconstructing the tropical Atlantic seasonal thermocline using planktonic foraminifera [Ph.D. thesis]. Columbia Univ., NY.
- Ravelo, A.C., and Fairbanks, R.G., 1992. Oxygen isotopic composition of multiple species of planktonic foraminifera: recorders of the modern photic zone temperature gradient. *Paleoceanography*, 7:815–831.
- Rea, D.K., 1990. Aspects of atmospheric circulation: the late Pleistocene (0–950,000 yr) record of eolian deposition in the Pacific Ocean. *Palaeogeogr., Palaeoclimatol., Palaeoecol.*, 78:217–227.
- Robinson, M.K., 1976. *Atlas of North Pacific Ocean Monthly Mean Temperatures and Mean Salinities of the Surface Layer*: Washington (Dept. of the Navy).
- Ruddiman, W.F., Raymo, M.E., Martinson, D.G., Clement, B.M., and Backman, J., 1989. Pleistocene evolution: Northern Hemisphere ice sheets and North Atlantic Ocean. *Paleoceanography*, 4:353–412.
- Sarnthein, M., and Winn, K., 1988. Global variations of surface ocean productivity in low and mid latitudes: influence on CO<sub>2</sub> reservoirs of the deep ocean and atmosphere during the last 21,000 years. *Paleoceanography*, 3:361–399.
- Schiffelbein, P., 1984. Effect of benthic mixing on the information content of deep-sea stratigraphical signals. *Nature*, 311:651–653.
- , 1985. An interactive global optimization algorithm for geological problems. *Math. Geol.*, 17:703–728.
- Schramm, C.T., 1985. Implications of radiolarian assemblages for the Late Quaternary paleoceanography of the eastern equatorial Pacific. *Quat. Res.*, 24:204–218.
- Shackleton, N.J., 1977. Carbon-13 in *Uvigerina*: tropical rain forest history and the equatorial Pacific carbonate dissolution cycles. In Andersen, N.R., and Malahoff, A. (Eds.), *The Fate of Fossil Fuel CO<sub>2</sub> in the Oceans*: New York (Plenum), 401–427.
- , 1987. Oxygen isotopes, ice volume, and sea level. *Quat. Sci. Rev.*, 6:183–190.
- Shackleton, N.J., Berger, A., and Peltier, W.R., 1990. An alternative astronomical calibration of the lower Pleistocene time scale based on ODP Site 677. *Trans. R. Soc. Edinburgh, Earth Sci.*, 81:251–261.
- Shackleton, N.J., and Opydyke, N.D., 1973. Oxygen isotope and paleomagnetic stratigraphy of equatorial Pacific core V28-238: oxygen isotope temperatures and ice volumes on a 10<sup>5</sup> year and 10<sup>6</sup> year scale. *Quat. Res.*, 3:39–55.
- Shackleton, N.J., Wiseman, J.D.H., and Buckley, H.A., 1973. Nonequilibrium isotopic fractionation between seawater and planktonic foraminiferal tests. *Nature*, 242:177–179.
- Spero, H.J., 1992. Do planktic foraminifera accurately record shifts in the carbon isotopic composition of seawater ΣCO<sub>2</sub>? *Mar. Micropaleontol.*, 19:275–285.
- Spero, H.J., and Lea, D.W., 1993. Intraspecific stable isotope variability in the planktic foraminifera Globigerinoides sacculifer—results from laboratory experiments. *Mar. Micropaleontol.*, 22:221–234.
- Spero, H.J., and Williams, D.F., 1988. Extracting environmental information from planktonic foraminiferal δ<sup>13</sup>C data. *Nature*, 335:717–719.
- Taylor, R.C., 1973. *An Atlas of Pacific Islands Rainfall*. Hawaiian Inst. Geophys., 2573-9.
- Thompson, P.R., and Saito, T., 1974. Pacific Pleistocene sediments: planktonic foraminifera dissolution cycles and geochronology. *Geology*, 2:333–335.
- Thunell, R.C., Curry, W.B., and Honjo, S., 1983. Seasonal variation in the flux of planktonic foraminifera: time series trap results from the Panama Basin. *Earth Planet. Sci. Lett.*, 64:44–55.
- Thunell, R.C., and Reynolds, L.A., 1984. Sedimentation of planktonic foraminifera: seasonal changes in species flux in the Panama Basin. *Micropaleontology*, 30:243–262.
- Toggweiler, J.R., Dixon, K., and Broecker, W.S., 1991. The Peru upwelling and the ventilation of the south Pacific thermocline. *J. Geophys. Res.*, 96:20467–20497.
- Tsuchiya, M., 1968. Upper waters of the intertropical Pacific Ocean. *Johns Hopkins Oceanogr. Stud.*, 4.
- Tsuchiya, M., Lukas, R., Fine, R.A., Firing, E., and Lindstrom, E., 1990. Source waters of the Pacific equatorial undercurrent. *Progr. Oceanogr.*, 23:101–147.
- Valencia, M., 1977. Pleistocene stratigraphy of the western equatorial Pacific. *Geol. Soc. Am. Bull.*, 85:1789–1802.
- Watkins, J.M., Mix, A.C., and Wilson, J., 1993. Relating equatorial Pacific planktic foraminifera species standing stocks to physical and biological parameters. *Eos*, 74:371.
- Williams, D.F., Bé, A.W.H., and Fairbanks, R.G., 1979. Seasonal oxygen isotopic variations in living planktonic foraminifera off Bermuda. *Science*, 206:447–449.
- , 1981. Seasonal stable isotopic variations in living planktonic foraminifera from Bermuda plankton tows. *Palaeogeogr., Palaeoclimatol., Palaeoecol.*, 33:71–102.
- Williams, D.F., Sommer, M.A., II, and Bender, M.L., 1977. Carbon isotopic compositions of Recent planktonic foraminifera of the Indian Ocean. *Earth Planet. Sci. Lett.*, 36:391–403.

- Wooster, W.S., and Gilmartin, M., 1961. The Peru-Chile Undercurrent. *J. Mar. Res.*, 19:97-122.
- Wooster, W.S., and Guillen, O., 1974. Characteristics of El Niño in 1972. *J. Mar. Res.*, 32:387-404.
- Wu, G., and Berger, W.H., 1989. Planktonic foraminifera: differential dissolution and the Quaternary stable isotope record in the west-equatorial Pacific. *Paleoceanography*, 4:181-198.
- , 1991. Pleistocene  $\delta^{18}\text{O}$  records from Ontong-Java Plateau: effects of winnowing and dissolution. *Mar. Geol.*, 96:193-209.
- Wu, G., Herguera, J.C., and Berger, W.H., 1990. Differential dissolution: modification of late Pleistocene oxygen isotope records in the western equatorial Pacific. *Paleoceanography*, 5:581-594.
- Wyrski, K., 1963. The horizontal and vertical field of motion in the Peru Current. *Bull. Scripps Inst. Oceanogr.*, 8:313-346.
- , 1966. Oceanography of the eastern equatorial Pacific Ocean. *Oceanogr. Mar. Biol. Ann. Rev.*, 4:33-68.
- , 1967. Circulation and water masses in the eastern equatorial Pacific Ocean. *Int. J. Oceanol. Limnol.*, 1:117-147.
- Wyrski, K., Firing, E., Halpern, D., Knox, R., McNally, G.D., Patzert, W.C., Stroup, E.D., Taft, B.A., and Williams, R., 1981. The Hawaii to Tahiti shuttle experiment. *Science*, 211:22-28.

**Date of initial receipt: 15 June 1993**

**Date of acceptance: 22 April 1994**

**Ms 138SR-115**

**APPENDIX A**  
*N. dutertrei*  $\delta^{13}\text{C}$  and  $\delta^{18}\text{O}$  (355–425  $\mu\text{m}$ ) from Site 847

Core, section, interval (cm)	ODP depth (mbsf)	Shipboard composite depth (mcd)	Shore-based composite depth (rmcd)	This study composite depth (Bmcd)	$\delta^{13}\text{C}$ (‰) (PDB)	$\delta^{18}\text{O}$ (‰) (PDB)	Comment
138-847B-							
IH-1, 2	0.02	0.02	0.02	0.02	1.64	0.35	
IH-1, 19	0.19	0.19	0.19	0.19	1.52	0.76	
IH-1, 30	0.30	0.30	0.30	0.30	1.53	0.74	
IH-1, 30	0.30	0.30	0.30	0.30	1.56	0.67	
IH-1, 47	0.47	0.47	0.47	0.47	1.30	1.27	
IH-1, 47	0.47	0.47	0.47	0.47	1.38	1.05	
IH-1, 59	0.59	0.59	0.59	0.59	1.46	1.61	
IH-1, 77	0.77	0.77	0.77	0.77	1.53	1.52	
IH-1, 77	0.77	0.77	0.77	0.77	1.54	1.55	
IH-1, 92	0.92	0.92	0.92	0.92	1.29	1.22	
IH-1, 92	0.92	0.92	0.92	0.92	1.69	1.27	
IH-1, 107	1.07	1.07	1.07	1.07	1.70	1.26	
IH-1, 107	1.07	1.07	1.07	1.07	1.72	1.24	
IH-1, 123	1.23	1.23	1.24	1.23	1.64	1.50	
IH-1, 137	1.37	1.37	1.40	1.37	1.64	1.49	
IH-1, 137	1.37	1.37	1.40	1.37	1.73	1.21	
IH-2, 2	1.52	1.52	1.55	1.52	1.59	1.42	
IH-2, 24	1.74	1.74	1.75	1.74	1.75	1.18	
IH-2, 37	1.87	1.87	1.87	1.87	1.36	1.25	
IH-2, 52	2.02	2.02	2.02	2.02	1.43	0.96	
IH-2, 52	2.02	2.02	2.02	2.02	1.54	0.70	
IH-2, 67	2.17	2.17	2.17	2.17	1.58	1.15	
IH-2, 67	2.17	2.17	2.17	2.17	1.59	1.18	
IH-2, 80	2.30	2.30	2.30	2.30	1.31	1.29	
IH-2, 92	2.42	2.42	2.42	2.42	1.57	1.50	
IH-2, 92	2.42	2.42	2.42	2.42	1.38	1.11	
IH-2, 107	2.57	2.57	2.57	2.57	1.68	1.12	
IH-2, 123	2.73	2.73	2.73	2.73	1.93	0.93	
IH-2, 137	2.87	2.87	2.87	2.87	1.68	0.46	
IH-2, 137	2.87	2.87	2.87	2.87	1.78	0.68	
IH-3, 2	3.02	3.02	3.02	3.02	1.65	0.63	
IH-3, 17	3.17	3.17	3.17	3.17	1.65	0.82	
IH-3, 30	3.30	3.30	3.30	3.30	1.64	0.76	
IH-3, 30	3.30	3.30	3.30	3.30	1.74	0.79	
IH-3, 30	3.30	3.30	3.30	3.30	1.57	0.81	
IH-3, 47	3.47	3.47	3.47	3.47	1.73	0.82	
IH-3, 47	3.47	3.47	3.47	3.47	1.66	0.75	
IH-3, 64	3.64	3.64	3.64	3.64	1.50	0.67	Not in composite
IH-3, 77	3.77	3.77	3.77	3.77	1.62	0.45	Not in composite
IH-3, 92	3.92	3.92	3.92	3.92	1.27	0.48	Not in composite
IH-3, 107	4.07	4.07	4.07	4.07	1.51	-0.36	Not in composite
IH-3, 123	4.23	4.23	4.23	4.23	1.15	-0.01	Not in composite
IH-3, 137	4.37	4.37	4.37	4.37	0.75	0.96	Not in composite
138-847C-							
IH-1, 2	2.02	2.42	2.02	2.30	1.60	1.19	Not in composite
IH-1, 17	2.17	2.57	2.16	2.45	1.52	1.04	Not in composite
IH-1, 32	2.32	2.72	2.27	2.60	1.68	1.39	Not in composite
IH-1, 47	2.47	2.87	2.33	2.75	1.59	1.68	Not in composite
IH-1, 62	2.62	3.02	2.40	2.90	1.73	1.38	Not in composite
IH-1, 77	2.77	3.17	2.59	3.05	1.63	1.29	Not in composite
IH-1, 92	2.92	3.32	3.08	3.20	1.69	1.17	Not in composite
IH-1, 107	3.07	3.47	3.41	3.35	1.76	0.65	Not in composite
IH-1, 122	3.22	3.62	3.60	3.50	1.66	0.57	
IH-1, 137	3.37	3.77	3.74	3.65	1.53	0.90	
IH-2, 2	3.52	3.92	3.87	3.80	1.41	0.69	
IH-2, 17	3.67	4.07	4.00	3.95	1.32	0.34	
IH-2, 32	3.82	4.22	4.14	4.10	1.25	0.47	
IH-2, 47	3.97	4.37	4.30	4.25	1.23	0.67	
IH-2, 65	4.15	4.55	4.51	4.43	1.03	0.76	
IH-2, 65	4.15	4.55	4.51	4.43	1.18	1.08	
IH-2, 77	4.27	4.67	4.67	4.55	1.02	1.28	
IH-2, 92	4.42	4.82	4.87	4.70	1.43	1.70	
IH-2, 92	4.42	4.82	4.87	4.70	1.35	1.49	
IH-2, 107	4.57	4.97	5.05	4.85	1.43	1.39	
IH-2, 122	4.72	5.12	5.20	5.00	1.31	1.41	
IH-2, 122	4.72	5.12	5.20	5.00	1.28	1.45	
IH-2, 137	4.87	5.27	5.32	5.15	1.50	1.20	
IH-3, 2	5.02	5.42	5.44	5.30	1.43	1.10	
IH-3, 17	5.17	5.57	5.57	5.45	1.27	1.24	
IH-3, 32	5.32	5.72	5.71	5.60	1.34	1.39	
IH-3, 32	5.32	5.72	5.71	5.60	1.23	1.24	
IH-3, 47	5.47	5.87	5.87	5.75	1.68	0.73	
IH-3, 62	5.62	6.02	6.03	5.90	1.28	0.82	
IH-3, 62	5.62	6.02	6.03	5.90	1.42	0.69	
IH-3, 77	5.77	6.17	6.19	6.05	1.43	0.79	
IH-3, 92	5.92	6.32	6.34	6.20	1.21	0.93	
IH-3, 107	6.07	6.47	6.48	6.35	1.44	0.67	
IH-3, 122	6.22	6.62	6.61	6.50	1.36	0.56	
IH-3, 137	6.37	6.77	6.76	6.65	1.73	0.28	
IH-4, 2	6.52	6.92	6.91	6.80	1.59	0.19	
IH-4, 17	6.67	7.07	7.07	6.95	1.54	-0.03	

## APPENDIX A (continued).

Core, section, interval (cm)	ODP depth (mbsf)	Shipboard composite depth (mcd)	Shore-based composite depth (rmcd)	This study composite depth (Bmcd)	$\delta^{13}\text{C}$ (‰) (PDB)	$\delta^{18}\text{O}$ (‰) (PDB)	Comment
1H-4, 32	6.82	7.22	7.22	7.10	1.58	0.32	
1H-4, 47	6.97	7.37	7.36	7.25	1.45	0.04	
1H-4, 47	6.97	7.37	7.36	7.25	1.52	0.11	
1H-4, 62	7.12	7.52	7.51	7.40	1.35	0.29	
1H-4, 77	7.27	7.67	7.67	7.55	1.35	0.48	
1H-4, 92	7.42	7.82	7.84	7.70	1.65	0.26	
1H-4, 107	7.57	7.97	8.03	7.85	1.57	-0.01	
1H-4, 122	7.72	8.12	8.20	8.00	1.44	-0.16	
1H-4, 137	7.87	8.27	8.36	8.15	1.32	0.19	
1H-5, 2	8.02	8.42	8.52	8.30	1.45	0.69	
1H-5, 17	8.17	8.57	8.68	8.45	1.31	0.78	
1H-5, 17	8.17	8.57	8.68	8.45	1.08	0.85	
1H-5, 32	8.32	8.72	8.83	8.60	1.79	0.55	
1H-5, 47	8.47	8.87	8.98	8.75	1.33	0.71	
1H-5, 47	8.47	8.87	8.98	8.75	1.53	0.39	
1H-5, 62	8.62	9.02	9.11	8.90	1.31	0.55	
1H-5, 62	8.62	9.02	9.11	8.90	1.18	0.64	
1H-5, 77	8.77	9.17	9.24	9.05	1.20	0.72	
1H-5, 92	8.92	9.32	9.39	9.20	1.62	0.46	
1H-5, 107	9.07	9.47	9.56	9.35	1.62	0.63	
1H-5, 122	9.22	9.62	9.77	9.50	1.88	0.43	
1H-5, 122	9.22	9.62	9.77	9.50	1.80	0.05	
1H-5, 137	9.37	9.77	9.97	9.65	1.85	0.32	
1H-5, 137	9.37	9.77	9.97	9.65	1.74	0.39	
1H-6, 2	9.52	9.92	10.12	9.80	1.77	0.51	
1H-6, 17	9.67	10.07	10.25	9.95	1.75	0.55	
1H-6, 32	9.82	10.22	10.37	10.10	1.65	0.33	
1H-6, 32	9.82	10.22	10.37	10.10	1.54	0.40	
1H-6, 47	9.97	10.37	10.51	10.25	1.87	0.35	
1H-6, 47	9.97	10.37	10.51	10.25	1.79	0.17	
1H-6, 62	10.12	10.52	10.70	10.40	1.53	0.35	
1H-6, 62	10.12	10.52	10.70	10.40	1.39	0.37	
1H-6, 77	10.27	10.67	10.93	10.55	1.45	0.52	
1H-6, 92	10.42	10.82	11.13	10.70	1.46	0.13	
1H-6, 92	10.42	10.82	11.13	10.70	1.30	-0.02	
1H-6, 107	10.57	10.97	11.28	10.85	1.04	-0.01	
1H-6, 107	10.57	10.97	11.28	10.85	0.97	0.01	
1H-6, 122	10.72	11.12	11.41	11.00	1.16	0.04	
1H-6, 122	10.72	11.12	11.41	11.00	1.03	0.31	
1H-6, 137	10.87	11.27	11.52	11.15	0.93	0.69	
1H-6, 137	10.87	11.27	11.52	11.15	2.11	0.39	
1H-7, 2	11.02	11.42	11.63	11.30	1.26	1.62	
1H-7, 2	11.02	11.42	11.63	11.30	1.09	1.33	
1H-7, 2	11.02	11.42	11.63	11.30	0.93	0.96	
1H-7, 17	11.17	11.57	11.75	11.45	1.43	0.94	
1H-7, 17	11.17	11.57	11.75	11.45	1.36	0.96	
1H-7, 32	11.32	11.72	11.88	11.60	1.40	1.25	
1H-7, 47	11.47	11.87	12.02	11.75	1.54	1.28	
1H-7, 62	11.62	12.02	12.16	11.90	1.75	0.98	Not in composite
1H-7, 73	11.73	12.13	12.27	12.01	1.81	0.81	Not in composite
2H-1, 2	11.52	13.20	13.06	12.93	1.59	0.57	Not in composite
2H-1, 17	11.67	13.35	13.23	13.08	2.00	0.26	
2H-1, 30	11.80	13.48	13.57	13.21	1.69	0.24	
2H-1, 47	11.97	13.65	13.70	13.38	1.64	0.20	
2H-1, 62	12.12	13.80	13.78	13.53	1.75	0.46	
2H-1, 77	12.27	13.95	13.92	13.68	1.27	1.16	
2H-1, 92	12.42	14.10	14.11	13.83	1.33	1.09	
2H-1, 107	12.57	14.25	14.25	13.98	1.41	1.00	
2H-1, 122	12.72	14.40	14.39	14.13	1.66	1.50	
2H-1, 122	12.72	14.40	14.39	14.13	1.80	1.60	
2H-1, 137	12.87	14.55	14.56	14.28	1.78	1.26	
2H-2, 2	13.02	14.70	14.70	14.43	1.79	1.02	
2H-2, 17	13.17	14.85	14.85	14.58	1.68	0.78	
2H-2, 30	13.30	14.98	14.98	14.71	1.94	1.00	
2H-2, 47	13.47	15.15	15.15	14.88	1.79	0.79	
2H-2, 64	13.64	15.32	15.32	15.05	1.85	0.72	
2H-2, 77	13.77	15.45	15.45	15.18	1.82	-0.13	
2H-2, 92	13.92	15.60	15.60	15.33	1.85	0.11	
2H-2, 107	14.07	15.75	15.75	15.48	1.62	0.33	
2H-2, 122	14.22	15.90	15.90	15.63	1.96	0.14	
2H-2, 137	14.37	16.05	16.05	15.78	1.63	-0.02	
2H-2, 137	14.37	16.05	16.05	15.78	1.95	0.30	
2H-3, 2	14.52	16.20	16.20	15.93	1.97	0.40	
2H-3, 2	14.52	16.20	16.20	15.93	1.96	0.48	
2H-3, 17	14.67	16.35	16.35	16.08	1.96	0.44	
2H-3, 17	14.67	16.35	16.35	16.08	1.99	0.53	
2H-3, 30	14.80	16.48	16.48	16.21	1.65	-0.05	
2H-3, 47	14.97	16.65	16.65	16.38	1.96	0.61	
2H-3, 62	15.12	16.80	16.80	16.53	1.81	0.43	
2H-3, 77	15.27	16.95	16.96	16.68	1.90	0.53	
2H-3, 92	15.42	17.10	17.10	16.83	1.74	0.43	
2H-3, 107	15.57	17.25	17.24	16.98	1.59	0.44	
2H-3, 122	15.72	17.40	17.40	17.13	1.72	0.56	

## APPENDIX A (continued).

Core, section, interval (cm)	ODP depth (mbsf)	Shipboard composite depth (mcd)	Shore-based composite depth (rmcd)	This study composite depth (Bmcd)	$\delta^{13}\text{C}$ (‰) (PDB)	$\delta^{18}\text{O}$ (‰) (PDB)	Comment
2H-3, 137	15.87	17.55	17.57	17.28	1.57	-0.12	
2H-4, 2	16.02	17.70	17.71	17.43	1.86	0.09	
2H-4, 2	16.02	17.70	17.71	17.43	1.96	0.15	
2H-4, 17	16.17	17.85	17.85	17.58	2.03	-0.06	
2H-4, 17	16.17	17.85	17.85	17.58	2.14	-0.10	
2H-4, 32	16.32	18.00	17.99	17.73	2.06	-0.08	
2H-4, 47	16.47	18.15	18.14	17.88	1.81	-0.03	
2H-4, 62	16.62	18.30	18.31	18.03	1.85	0.14	
2H-4, 77	16.77	18.45	18.46	18.18	1.79	0.12	
2H-4, 92	16.92	18.60	18.60	18.33	1.70	0.37	
2H-4, 107	17.07	18.75	18.76	18.48	1.80	0.31	
2H-4, 122	17.22	18.90	18.91	18.63	1.97	0.30	
2H-4, 137	17.37	19.05	19.05	18.78	1.83	0.26	
2H-5, 2	17.52	19.20	19.20	18.93	1.62	0.06	
2H-5, 2	17.52	19.20	19.20	18.93	1.60	-0.08	
2H-5, 17	17.67	19.35	19.36	19.08	1.48	0.47	
2H-5, 30	17.80	19.48	19.49	19.21	1.27	0.59	
2H-5, 47	17.97	19.65	19.65	19.38	1.32	1.23	
2H-5, 62	18.12	19.80	19.79	19.53	1.24	1.00	
2H-5, 62	18.12	19.80	19.79	19.53	1.36	1.06	
2H-5, 77	18.27	19.95	19.95	19.68	1.29	1.15	
2H-5, 92	18.42	20.10	20.10	19.83	1.20	0.87	
2H-5, 107	18.57	20.25	20.25	19.98	1.12	0.81	
2H-5, 122	18.72	20.40	20.40	20.13	0.93	0.26	
2H-5, 137	18.87	20.55	20.55	20.28	1.22	0.27	
2H-6, 2	19.02	20.70	20.70	20.43	1.11	0.63	
2H-6, 17	19.17	20.85	20.87	20.58	1.23	0.48	
2H-6, 30	19.30	20.98	21.00	20.71	1.32	-0.03	
2H-6, 47	19.47	21.15	21.14	20.88	1.30	0.24	
2H-6, 47	19.47	21.15	21.14	20.88	1.67	0.29	
2H-6, 64	19.64	21.32	21.35	21.05	1.58	0.16	
2H-6, 77	19.77	21.45	21.55	21.18	1.51	0.12	
2H-6, 92	19.92	21.60	21.71	21.33	1.32	-0.12	
2H-6, 92	19.92	21.60	21.71	21.33	1.39	0.13	
2H-6, 107	20.07	21.75	21.84	21.48	1.55	0.06	
2H-6, 122	20.22	21.90	22.02	21.63	1.53	0.37	
2H-6, 137	20.37	22.05	22.19	21.78	1.59	0.59	
2H-7, 2	20.52	22.20	22.34	21.93	1.52	0.70	
2H-7, 17	20.67	22.35	22.46	22.08	1.71	0.33	
2H-7, 30	20.80	22.48	22.54	22.21	1.71	0.28	
2H-7, 47	20.97	22.65	22.64	22.38	0.91	0.07	Not in composite
2H-7, 62	21.12	22.80	22.79	22.53	1.29	0.19	Not in composite
3H-1, 2	21.02	23.42	23.24	23.16	1.52	0.28	Not in composite
3H-1, 17	21.17	23.57	23.48	23.31	1.52	-0.39	
3H-1, 32	21.32	23.72	23.62	23.46	1.37	-0.41	
3H-1, 32	21.32	23.72	23.62	23.46	1.38	-0.50	
3H-1, 47	21.47	23.87	23.72	23.61	1.42	-0.12	
3H-1, 62	21.62	24.02	23.84	23.76	1.45	-0.04	
3H-1, 77	21.77	24.17	24.01	23.91	1.27	0.21	
3H-1, 92	21.92	24.32	24.27	24.06	1.12	0.47	
3H-1, 107	22.07	24.47	24.47	24.21	1.21	0.61	
3H-1, 122	22.22	24.62	24.62	24.36	1.19	1.24	
3H-1, 122	22.22	24.62	24.62	24.36	1.16	1.50	
3H-1, 137	22.37	24.77	24.77	24.51	1.38	1.11	
3H-2, 2	22.52	24.92	24.92	24.66	1.40	0.73	
3H-2, 17	22.67	25.07	25.07	24.81	1.40	0.72	
3H-2, 30	22.80	25.20	25.20	24.94	1.42	0.25	
3H-2, 30	22.80	25.20	25.20	24.94	1.30	0.87	
3H-2, 47	22.97	25.37	25.37	25.11	1.32	0.84	
3H-2, 47	22.97	25.37	25.37	25.11	1.14	0.69	
3H-2, 47	22.97	25.37	25.37	25.11	1.30	0.84	
3H-2, 65	23.15	25.55	25.55	25.29	1.23	0.85	
3H-2, 65	23.15	25.55	25.55	25.29	1.24	0.26	
3H-2, 77	23.27	25.67	25.67	25.41	1.31	0.81	
3H-2, 77	23.27	25.67	25.67	25.41	1.32	0.61	
3H-2, 92	23.42	25.82	25.82	25.56	0.94	0.43	
3H-2, 107	23.57	25.97	25.97	25.71	1.39	0.53	
3H-2, 122	23.72	26.12	26.12	25.86	1.14	0.28	
3H-2, 122	23.72	26.12	26.12	25.86	1.22	0.53	
3H-2, 137	23.87	26.27	26.27	26.01	0.91	0.62	
3H-2, 137	23.87	26.27	26.27	26.01	0.82	0.33	
3H-3, 2	24.02	26.42	26.42	26.16	0.72	0.53	
3H-3, 2	24.02	26.42	26.42	26.16	0.94	0.56	
3H-3, 17	24.17	26.57	26.57	26.31	1.00	1.10	
3H-3, 32	24.32	26.72	26.72	26.46	0.51	0.79	
3H-3, 47	24.47	26.87	26.87	26.61	1.02	1.31	
3H-3, 62	24.62	27.02	27.02	26.76	1.07	1.41	
3H-3, 76	24.76	27.16	27.16	26.90	1.29	1.21	
3H-3, 92	24.92	27.32	27.32	27.06	1.33	0.96	
3H-3, 107	25.07	27.47	27.47	27.21	1.16	0.68	
3H-3, 107	25.07	27.47	27.47	27.21	1.18	0.89	
3H-3, 122	25.22	27.62	27.61	27.36	1.09	0.75	
3H-3, 122	25.22	27.62	27.61	27.36	1.18	0.85	
3H-3, 137	25.37	27.77	27.75	27.51	0.99	0.42	

## APPENDIX A (continued).

Core, section, interval (cm)	ODP depth (mbsf)	Shipboard composite depth (mcd)	Shore-based composite depth (rmcd)	This study composite depth (Bmcd)	$\delta^{13}\text{C}$ (‰) (PDB)	$\delta^{18}\text{O}$ (‰) (PDB)	Comment
3H-3, 137	25.37	27.77	27.75	27.51	1.15	1.00	
3H-4, 2	25.52	27.92	27.91	27.66	0.84	0.82	
3H-4, 17	25.67	28.07	28.06	27.81	0.94	1.05	
3H-4, 32	25.82	28.22	28.22	27.96	1.18	0.98	
3H-4, 47	25.97	28.37	28.37	28.11	1.13	0.41	
3H-4, 47	25.97	28.37	28.37	28.11	1.14	0.31	
3H-4, 62	26.12	28.52	28.52	28.26	1.55	0.77	
3H-4, 62	26.12	28.52	28.52	28.26	1.43	0.74	
3H-4, 76	26.26	28.66	28.66	28.40	1.51	-0.10	
3H-4, 92	26.42	28.82	28.82	28.56	1.38	0.22	
3H-4, 107	26.57	28.97	28.97	28.71	1.17	0.18	
3H-4, 122	26.72	29.12	29.12	28.86	1.15	0.12	
3H-4, 137	26.87	29.27	29.27	29.01	0.93	0.38	
3H-5, 2	27.02	29.42	29.42	29.16	1.08	0.67	
3H-5, 17	27.17	29.57	29.57	29.31	1.35	0.55	
3H-5, 17	27.17	29.57	29.57	29.31	1.39	0.31	
3H-5, 32	27.32	29.72	29.72	29.46	1.74	0.53	
3H-5, 47	27.47	29.87	29.87	29.61	1.74	0.06	
3H-5, 47	27.47	29.87	29.87	29.61	1.83	0.29	
3H-5, 62	27.62	30.02	30.02	29.76	1.48	0.54	
3H-5, 76	27.76	30.16	30.16	29.90	1.48	0.73	
3H-5, 92	27.92	30.32	30.32	30.06	1.74	0.38	
3H-5, 107	28.07	30.47	30.47	30.21	1.58	0.89	
3H-5, 107	28.07	30.47	30.47	30.21	1.42	0.63	
3H-5, 122	28.22	30.62	30.62	30.36	1.43	0.74	
3H-5, 137	28.37	30.77	30.77	30.51	1.44	0.92	
3H-6, 2	28.52	30.92	30.92	30.66	1.44	0.62	
3H-6, 17	28.67	31.07	31.07	30.81	1.35	0.79	
3H-6, 30	28.80	31.20	31.20	30.94	1.72	0.15	
3H-6, 30	28.80	31.20	31.20	30.94	1.64	0.37	
3H-6, 47	28.97	31.37	31.37	31.11	1.65	0.05	
3H-6, 47	28.97	31.37	31.37	31.11	1.40	0.24	
3H-6, 65	29.15	31.55	31.55	31.29	1.28	0.64	
3H-6, 77	29.27	31.67	31.66	31.41	1.24	0.67	
3H-6, 92	29.42	31.82	31.81	31.56	1.37	0.53	
3H-6, 107	29.57	31.97	31.99	31.71	1.32	0.56	
3H-6, 122	29.72	32.12	32.17	31.86	1.33	0.49	
3H-6, 137	29.87	32.27	32.34	32.01	1.52	0.33	
3H-7, 2	30.02	32.42	32.48	32.16	1.36	0.06	
3H-7, 17	30.17	32.57	32.59	32.31	1.35	0.03	
3H-7, 30	30.30	32.70	32.68	32.44	1.32	-0.06	
3H-7, 47	30.47	32.87	32.84	32.61	1.19	-0.22	
3H-7, 62	30.62	33.02	33.05	32.76	1.31	-0.04	
3H-7, 77	30.77	33.17	33.33	32.91	1.23	-0.19	Not in composite
4H-1, 32	30.82	34.12	34.22	33.94	1.45	-0.38	
4H-1, 32	30.82	34.12	34.22	33.94	1.60	0.22	
4H-1, 47	30.97	34.27	34.58	34.09	1.29	-0.13	
4H-1, 61	31.11	34.41	34.68	34.23	0.93	-0.09	
4H-1, 77	31.27	34.57	34.76	34.39	1.16	-0.08	
4H-1, 92	31.42	34.72	34.85	34.54	0.92	0.17	
4H-1, 92	31.42	34.72	34.85	34.54	1.13	0.72	
4H-1, 107	31.57	34.87	34.95	34.69	1.17	-0.02	
4H-1, 122	31.72	35.02	35.08	34.84	1.18	-0.31	
4H-1, 137	31.87	35.17	35.22	34.99	1.18	-0.30	
138-847D-							
2H-3, 62	10.22	12.02	12.04	11.76	1.41	1.23	
2H-3, 77	10.37	12.17	12.16	11.91	1.38	1.11	
2H-3, 92	10.52	12.32	12.28	12.06	1.52	1.23	
2H-3, 107	10.67	12.47	12.41	12.21	1.74	0.91	
2H-3, 122	10.82	12.62	12.55	12.36	1.72	0.67	
2H-3, 137	10.97	12.77	12.68	12.51	1.76	0.61	
2H-4, 2	11.12	12.92	12.82	12.66	1.80	0.33	
2H-4, 17	11.27	13.07	13.00	12.81	1.75	0.41	
2H-4, 32	11.42	13.22	13.20	12.96	1.84	0.31	
3H-3, 62	19.72	22.72	22.72	22.38	1.63	0.02	
3H-3, 77	19.87	22.87	22.86	22.53	1.46	0.15	
3H-3, 92	20.02	23.02	23.01	22.68	1.48	0.30	
3H-3, 107	20.17	23.17	23.17	22.83	1.70	0.49	
3H-3, 122	20.32	23.32	23.32	22.98	1.62	0.07	
3H-3, 137	20.47	23.47	23.47	23.13	1.30	0.02	
4H-3, 47	29.07	33.07	33.07	32.86	1.16	-0.41	
4H-3, 62	29.22	33.22	33.22	33.01	1.40	0.01	
4H-3, 77	29.37	33.37	33.37	33.16	1.28	0.47	
4H-3, 77	29.37	33.37	33.37	33.16	1.28	0.47	
4H-3, 92	29.52	33.52	33.51	33.31	1.56	0.33	
4H-3, 92	29.52	33.52	33.51	33.31	1.44	0.47	
4H-3, 107	29.67	33.67	33.66	33.46	1.37	0.35	
4H-3, 107	29.67	33.67	33.66	33.46	1.43	0.26	
4H-3, 122	29.82	33.82	33.82	33.61	1.61	0.75	
4H-3, 122	29.82	33.82	33.82	33.61	1.57	0.76	

**APPENDIX B**  
*G. sacculifer*  $\delta^{13}\text{C}$  and  $\delta^{18}\text{O}$  data from Site 847

Core, section, interval (cm)	ODP depth (mbsf)	Shipboard composite depth (mcd)	Shore-based composite depth (rmcd)	This study composite depth (Bmcd)	Foraminifer size ( $\mu\text{m}$ )	$\delta^{13}\text{C}$ (‰) (PDB)	$\delta^{18}\text{O}$ (‰) (PDB)	Comment
138-847B-								
1H-1, 2	0.02	0.02	0.02	0.02	300-425	2.17	-1.05	
1H-1, 19	0.19	0.19	0.19	0.19	300-355	1.71	-0.69	
1H-1, 30	0.30	0.30	0.30	0.30	300-355	1.62	-0.44	
1H-1, 47	0.47	0.47	0.47	0.47	300-355	1.40	0.13	
1H-1, 59	0.59	0.59	0.59	0.59	300-355	1.34	0.16	
1H-1, 59	0.59	0.59	0.59	0.59	355-425	1.17	0.16	
1H-1, 77	0.77	0.77	0.77	0.77	300-355	1.31	0.57	
1H-1, 77	0.77	0.77	0.77	0.77	300-355	2.00	-0.23	
1H-1, 92	0.92	0.92	0.92	0.92	355-425	2.13	0.25	
1H-1, 107	1.07	1.07	1.07	1.07	300-355	1.72	-0.11	
1H-1, 123	1.23	1.23	1.24	1.23	300-355	1.68	0.01	
1H-1, 137	1.37	1.37	1.40	1.37	300-355	1.75	-0.11	
1H-2, 2	1.52	1.52	1.55	1.52	300-355	1.47	0.04	
1H-2, 24	1.74	1.74	1.75	1.74	300-355	1.33	-0.05	
1H-2, 37	1.87	1.87	1.87	1.87	300-355	0.99	-0.15	
1H-2, 37	1.87	1.87	1.87	1.87	355-425	1.28	-0.21	
1H-2, 52	2.02	2.02	2.02	2.02	300-355	1.82	-0.26	
1H-2, 67	2.17	2.17	2.17	2.17	300-355	1.59	-0.52	
1H-2, 80	2.30	2.30	2.30	2.30	300-355	1.61	-0.03	
1H-2, 92	2.42	2.42	2.42	2.42	300-355	1.82	0.15	
1H-2, 107	2.57	2.57	2.57	2.57	300-355	2.20	-0.23	
1H-2, 123	2.73	2.73	2.73	2.73	300-355	2.36	-0.64	
1H-2, 137	2.87	2.87	2.87	2.87	300-355	2.08	-0.60	
1H-3, 2	3.02	3.02	3.02	3.02	300-355	1.81	-0.70	
1H-3, 17	3.17	3.17	3.17	3.17	300-355	1.77	-0.51	
1H-3, 30	3.30	3.30	3.30	3.30	300-355	1.79	-0.64	
1H-3, 47	3.47	3.47	3.47	3.47	300-355	1.89	-0.43	
1H-3, 47	3.47	3.47	3.47	3.47	300-355	1.49	-0.66	
1H-3, 64	3.64	3.64	3.64	3.64	300-355	1.32	-0.77	Not in composite
1H-3, 77	3.77	3.77	3.77	3.77	300-355	1.43	-0.83	Not in composite
1H-3, 92	3.92	3.92	3.92	3.92	300-355	1.44	-0.94	Not in composite
1H-3, 107	4.07	4.07	4.07	4.07	300-355	1.44	-1.39	Not in composite
1H-3, 107	4.07	4.07	4.07	4.07	300-355	1.83	-1.21	Not in composite
1H-3, 123	4.23	4.23	4.23	4.23	300-355	1.20	-0.52	Not in composite
1H-3, 137	4.37	4.37	4.37	4.37	300-355	1.07	-0.67	Not in composite
1H-3, 137	4.37	4.37	4.37	4.37	300-355	1.14	-0.25	Not in composite
138-847C-								
1H-1, 2	2.02	2.42	2.02	2.30	300-355	1.51	-0.10	Not in composite
1H-1, 2	2.02	2.42	2.02	2.30	300-425	2.04	-0.19	Not in composite
1H-1, 17	2.17	2.57	2.16	2.45	300-355	1.53	-0.14	Not in composite
1H-1, 17	2.17	2.57	2.16	2.45	300-425	1.80	-0.24	Not in composite
1H-1, 32	2.32	2.72	2.27	2.60	300-425	1.81	-0.31	Not in composite
1H-1, 47	2.47	2.87	2.33	2.75	300-355	1.67	-0.23	Not in composite
1H-1, 47	2.47	2.87	2.33	2.75	300-425	1.77	-0.50	Not in composite
1H-1, 62	2.62	3.02	2.40	2.90	300-425	1.56	-0.28	Not in composite
1H-1, 77	2.77	3.17	2.59	3.05	300-425	1.85	-0.32	Not in composite
1H-1, 107	3.07	3.47	3.41	3.35	300-425	1.97	-0.65	Not in composite
1H-1, 122	3.22	3.62	3.60	3.50	300-355	1.59	-0.55	
1H-1, 122	3.22	3.62	3.60	3.50	300-425	1.98	-0.89	
1H-1, 137	3.37	3.77	3.74	3.65	300-425	1.88	-0.87	
1H-2, 2	3.52	3.92	3.87	3.80	300-355	1.72	-0.43	
1H-2, 2	3.52	3.92	3.87	3.80	300-355	1.88	-0.71	
1H-2, 17	3.67	4.07	4.00	3.95	300-355	1.69	-0.88	
1H-2, 32	3.82	4.22	4.14	4.10	300-355	1.46	-0.86	
1H-2, 47	3.97	4.37	4.30	4.25	300-355	1.19	-0.29	
1H-2, 65	4.15	4.55	4.51	4.43	300-425	1.36	0.12	
1H-2, 77	4.27	4.67	4.67	4.55	300-355	1.06	0.27	
1H-2, 92	4.42	4.82	4.87	4.70	300-355	1.54	0.07	
1H-2, 107	4.57	4.97	5.05	4.85	300-355	1.25	0.01	
1H-2, 122	4.72	5.12	5.20	5.00	300-355	1.41	-0.17	
1H-2, 137	4.87	5.27	5.32	5.15	300-355	1.44	0.12	
1H-2, 137	4.87	5.27	5.32	5.15	300-355	1.87	-0.26	
1H-3, 2	5.02	5.42	5.44	5.30	300-355	1.52	0.04	
1H-3, 2	5.02	5.42	5.44	5.30	300-425	1.61	-0.25	
1H-3, 17	5.17	5.57	5.57	5.45	300-425	1.19	-0.08	
1H-3, 32	5.32	5.72	5.71	5.60	300-425	1.45	-0.32	
1H-3, 47	5.47	5.87	5.87	5.75	300-425	1.65	-0.34	
1H-3, 62	5.62	6.02	6.03	5.90	300-355	1.69	-0.48	
1H-3, 77	5.77	6.17	6.19	6.05	300-355	1.29	-0.45	
1H-3, 92	5.92	6.32	6.34	6.20	300-425	1.43	-0.19	
1H-3, 107	6.07	6.47	6.48	6.35	300-425	1.43	-0.08	
1H-3, 122	6.22	6.62	6.61	6.50	300-425	1.78	-0.38	
1H-3, 137	6.37	6.77	6.76	6.65	300-355	1.64	-0.76	
1H-4, 2	6.52	6.92	6.91	6.80	300-425	2.15	-0.89	
1H-4, 17	6.67	7.07	7.07	6.95	300-355	1.69	-0.90	
1H-4, 32	6.82	7.22	7.22	7.10	300-355	1.84	-0.63	
1H-4, 47	6.97	7.37	7.36	7.25	300-355	1.41	-0.77	
1H-4, 62	7.12	7.52	7.51	7.40	300-355	1.28	-0.34	
1H-4, 77	7.27	7.67	7.67	7.55	300-355	1.65	-0.10	
1H-4, 92	7.42	7.82	7.84	7.70	300-425	1.57	-0.41	

## APPENDIX B (continued).

Core, section, interval (cm)	ODP depth (mbsf)	Shipboard composite depth (mcd)	Shore-based composite depth (rmcd)	This study composite depth (Bmcd)	Foraminifer size ( $\mu\text{m}$ )	$\delta^{13}\text{C}$ (‰) (PDB)	$\delta^{18}\text{O}$ (‰) (PDB)	Comment
1H-4, 107	7.57	7.97	8.03	7.85	300-425	1.92	-0.59	
1H-4, 122	7.72	8.12	8.20	8.00	300-355	1.61	-0.84	
1H-4, 137	7.87	8.27	8.36	8.15	300-355	1.05	-0.19	
1H-5, 2	8.02	8.42	8.52	8.30	300-355	1.32	0.01	
1H-5, 17	8.17	8.57	8.68	8.45	300-355	1.52	0.12	
1H-5, 32	8.32	8.72	8.83	8.60	300-425	1.38	0.01	
1H-5, 47	8.47	8.87	8.98	8.75	300-355	1.12	0.06	
1H-5, 62	8.62	9.02	9.11	8.90	300-355	1.13	0.18	
1H-5, 77	8.77	9.17	9.24	9.05	300-355	1.08	0.06	
1H-5, 92	8.92	9.32	9.39	9.20	300-425	1.53	-0.26	
1H-5, 107	9.07	9.47	9.56	9.35	300-425	1.69	-0.20	
1H-5, 122	9.22	9.62	9.77	9.50	300-355	1.76	-0.52	
1H-5, 137	9.37	9.77	9.97	9.65	300-355	1.49	-0.25	
1H-5, 137	9.37	9.77	9.97	9.65	300-355	1.60	-0.65	
1H-6, 2	9.52	9.92	10.12	9.80	300-425	1.92	-0.46	
1H-6, 17	9.67	10.07	10.25	9.95	300-425	1.70	-0.34	
1H-6, 32	9.82	10.22	10.37	10.10	300-425	1.83	-0.43	
1H-6, 47	9.97	10.37	10.51	10.25	300-355	1.10	-1.09	
1H-6, 62	10.12	10.52	10.70	10.40	300-355	1.44	-1.04	
1H-6, 77	10.27	10.67	10.93	10.55	300-355	1.77	-0.93	
1H-6, 92	10.42	10.82	11.13	10.70	300-355	1.72	-0.97	
1H-6, 92	10.42	10.82	11.13	10.70	300-355	1.72	-0.84	
1H-6, 107	10.57	10.97	11.28	10.85	300-355	1.03	-0.43	
1H-6, 107	10.57	10.97	11.28	10.85	300-425	1.38	-0.49	
1H-6, 122	10.72	11.12	11.41	11.00	300-355	1.14	-0.63	
1H-6, 122	10.72	11.12	11.41	11.00	300-355	1.23	-0.51	
1H-6, 137	10.87	11.27	11.52	11.15	300-355	0.96	0.09	
1H-7, 2	11.02	11.42	11.63	11.30	300-355	1.23	0.09	
1H-7, 17	11.17	11.57	11.75	11.45	300-355	1.20	0.23	
1H-7, 32	11.32	11.72	11.88	11.60	300-355	1.48	0.07	
1H-7, 47	11.47	11.87	12.02	11.75	300-355	1.36	-0.20	
1H-7, 62	11.62	12.02	12.16	11.90	300-425	1.84	-0.34	Not in composite
1H-7, 73	11.73	12.13	12.27	12.01	300-355	1.89	-0.39	Not in composite
2H-1, 2	11.52	13.20	13.06	12.93	300-425	1.97	-0.68	Not in composite
2H-1, 17	11.67	13.35	13.23	13.08	300-355	1.97	-0.86	
2H-1, 17	11.67	13.35	13.23	13.08	300-355	2.42	-1.27	
2H-1, 30	11.80	13.48	13.57	13.21	300-355	2.33	-1.03	
2H-1, 47	11.97	13.65	13.70	13.38	300-355	1.92	-1.11	
2H-1, 62	12.12	13.80	13.78	13.53	300-355	1.46	-1.38	
2H-1, 62	12.12	13.80	13.78	13.53	300-355	1.85	-1.06	
2H-1, 77	12.27	13.95	13.92	13.68	300-355	1.16	-0.31	
2H-1, 92	12.42	14.10	14.11	13.83	300-355	1.40	0.23	
2H-1, 107	12.57	14.25	14.25	13.98	300-355	1.22	0.38	
2H-1, 122	12.72	14.40	14.39	14.13	300-355	1.33	0.35	
2H-1, 137	12.87	14.55	14.56	14.28	300-355	1.50	0.15	
2H-2, 2	13.02	14.70	14.70	14.43	300-355	1.28	0.10	
2H-2, 17	13.17	14.85	14.85	14.58	300-355	1.38	-0.04	
2H-2, 30	13.30	14.98	14.98	14.71	300-355	1.37	0.01	
2H-2, 47	13.47	15.15	15.15	14.88	300-355	1.35	0.22	
2H-2, 64	13.64	15.32	15.32	15.05	300-355	1.43	-0.26	
2H-2, 77	13.77	15.45	15.45	15.18	300-355	1.54	-0.15	
2H-2, 77	13.77	15.45	15.45	15.18	300-355	1.56	-0.47	
2H-2, 77	13.77	15.45	15.45	15.18	355-425	1.39	-0.29	
2H-2, 92	13.92	15.60	15.60	15.33	300-355	1.28	-0.72	
2H-2, 92	13.92	15.60	15.60	15.33	300-355	1.52	-0.34	
2H-2, 92	13.92	15.60	15.60	15.33	300-355	1.74	-0.64	
2H-2, 107	14.07	15.75	15.75	15.48	300-355	1.67	-0.82	
2H-2, 107	14.07	15.75	15.75	15.48	300-355	2.01	-0.74	
2H-2, 122	14.22	15.90	15.90	15.63	300-355	2.37	-0.82	
2H-2, 137	14.37	16.05	16.05	15.78	300-355	2.02	-0.81	
2H-3, 2	14.52	16.20	16.20	15.93	300-355	1.96	-0.74	
2H-3, 17	14.67	16.35	16.35	16.08	300-425	2.18	-0.84	
2H-3, 30	14.80	16.48	16.48	16.21	300-355	1.97	-0.69	
2H-3, 47	14.97	16.65	16.65	16.38	300-355	1.66	-0.68	
2H-3, 62	15.12	16.80	16.80	16.53	300-355	1.78	-0.52	
2H-3, 77	15.27	16.95	16.96	16.68	300-355	1.65	-0.37	
2H-3, 92	15.42	17.10	17.10	16.83	300-355	1.60	-0.59	
2H-3, 107	15.57	17.25	17.24	16.98	300-355	1.58	-0.36	
2H-3, 122	15.72	17.40	17.40	17.13	300-355	1.38	-0.24	
2H-3, 137	15.87	17.55	17.57	17.28	300-355	1.43	-0.34	
2H-4, 2	16.02	17.70	17.71	17.43	300-355	1.52	-0.37	
2H-4, 17	16.17	17.85	17.85	17.58	300-355	1.80	-0.56	
2H-4, 32	16.32	18.00	17.99	17.73	300-355	1.59	-0.69	
2H-4, 47	16.47	18.15	18.14	17.88	300-355	1.75	-0.91	
2H-4, 62	16.62	18.30	18.31	18.03	300-355	1.88	-0.88	
2H-4, 77	16.77	18.45	18.46	18.18	300-355	1.67	-0.47	
2H-4, 92	16.92	18.60	18.60	18.33	300-355	1.44	-0.41	
2H-4, 107	17.07	18.75	18.76	18.48	300-355	1.61	-0.72	
2H-4, 122	17.22	18.90	18.91	18.63	300-355	1.78	-0.66	
2H-4, 137	17.37	19.05	19.05	18.78	300-355	1.90	-0.54	
2H-5, 2	17.52	19.20	19.20	18.93	300-355	1.57	-0.57	
2H-5, 17	17.67	19.35	19.36	19.08	300-355	1.74	-0.88	
2H-5, 30	17.80	19.48	19.49	19.21	300-355	1.39	-0.44	
2H-5, 47	17.97	19.65	19.65	19.38	300-355	1.04	0.39	

## APPENDIX B (continued).

Core, section, interval (cm)	ODP depth (mbsf)	Shipboard composite depth (mcd)	Shore-based composite depth (rmcd)	This study composite depth (Bmcd)	Foraminifer size ( $\mu\text{m}$ )	$\delta^{13}\text{C}$ (‰) (PDB)	$\delta^{18}\text{O}$ (‰) (PDB)	Comment
2H-5, 62	18.12	19.80	19.79	19.53	300-355	1.18	0.46	
2H-5, 77	18.27	19.95	19.95	19.68	300-355	1.14	0.46	
2H-5, 92	18.42	20.10	20.10	19.83	300-355	1.22	0.09	
2H-5, 107	18.57	20.25	20.25	19.98	300-355	1.21	0.10	
2H-5, 122	18.72	20.40	20.40	20.13	300-355	0.92	0.07	
2H-5, 137	18.87	20.55	20.55	20.28	300-355	1.04	-0.19	
2H-6, 2	19.02	20.70	20.70	20.43	300-355	1.02	0.04	
2H-6, 17	19.17	20.85	20.87	20.58	300-355	1.24	0.11	
2H-6, 30	19.30	20.98	21.00	20.71	300-355	1.37	-0.29	
2H-6, 47	19.47	21.15	21.14	20.88	300-355	1.48	-0.23	
2H-6, 64	19.64	21.32	21.35	21.05	300-425	2.03	-0.84	
2H-6, 77	19.77	21.45	21.55	21.18	300-355	1.64	-0.98	
2H-6, 92	19.92	21.60	21.71	21.33	300-355	1.57	-0.30	
2H-6, 107	20.07	21.75	21.84	21.48	300-355	1.44	-0.33	
2H-6, 122	20.22	21.90	22.02	21.63	300-355	1.26	-0.16	
2H-6, 137	20.37	22.05	22.19	21.78	300-355	1.39	-0.04	
2H-7, 2	20.52	22.20	22.34	21.93	300-355	1.42	0.24	
2H-7, 17	20.67	22.35	22.46	22.08	300-355	1.36	-0.09	
2H-7, 30	20.80	22.48	22.54	22.21	300-355	1.60	-0.14	
2H-7, 47	20.97	22.65	22.64	22.38	300-355	1.53	-0.17	Not in composite
2H-7, 62	21.12	22.80	22.79	22.53	300-355	1.02	-0.11	Not in composite
3H-1, 2	21.02	23.42	23.24	23.16	300-355	1.35	-0.10	Not in composite
3H-1, 17	21.17	23.57	23.48	23.31	300-355	1.56	-0.45	
3H-1, 32	21.32	23.72	23.62	23.46	300-355	1.60	-0.75	
3H-1, 47	21.47	23.87	23.72	23.61	300-355	1.94	-1.23	
3H-1, 47	21.47	23.87	23.72	23.61	300-425	1.92	-1.19	
3H-1, 62	21.62	24.02	23.84	23.76	300-355	1.68	-0.34	
3H-1, 77	21.77	24.17	24.01	23.91	300-355	1.13	0.17	
3H-1, 92	21.92	24.32	24.27	24.06	300-355	0.98	-0.20	
3H-1, 107	22.07	24.47	24.47	24.21	300-355	1.23	0.00	
3H-1, 122	22.22	24.62	24.62	24.36	300-355	1.11	0.07	
3H-1, 137	22.37	24.77	24.77	24.51	300-355	1.27	-0.38	
3H-2, 2	22.52	24.92	24.92	24.66	300-355	1.19	-0.43	
3H-2, 17	22.67	25.07	25.07	24.81	300-355	1.40	-0.63	
3H-2, 30	22.80	25.20	25.20	24.94	300-355	1.45	-0.83	
3H-2, 47	22.97	25.37	25.37	25.11	300-355	1.54	-0.90	
3H-2, 65	23.15	25.55	25.55	25.29	300-355	1.23	-1.01	
3H-2, 77	23.27	25.67	25.67	25.41	300-355	1.41	-1.05	
3H-2, 92	23.42	25.82	25.82	25.56	300-355	1.55	-0.71	
3H-2, 107	23.57	25.97	25.97	25.71	300-355	1.59	-0.51	
3H-2, 122	23.72	26.12	26.12	25.86	300-355	1.59	-0.57	
3H-2, 137	23.87	26.27	26.27	26.01	300-355	1.05	-0.60	
3H-3, 2	24.02	26.42	26.42	26.16	300-355	1.15	0.17	
3H-3, 17	24.17	26.57	26.57	26.31	300-355	0.95	0.31	
3H-3, 32	24.32	26.72	26.72	26.46	300-355	0.93	0.57	
3H-3, 32	24.32	26.72	26.72	26.46	300-355	0.81	0.50	
3H-3, 47	24.47	26.87	26.87	26.61	300-355	1.04	0.30	
3H-3, 62	24.62	27.02	27.02	26.76	300-355	1.05	0.35	
3H-3, 76	24.76	27.16	27.16	26.90	300-355	0.99	0.26	
3H-3, 92	24.92	27.32	27.32	27.06	300-355	1.15	0.19	
3H-3, 107	25.07	27.47	27.47	27.21	300-355	1.10	-0.12	
3H-3, 122	25.22	27.62	27.61	27.36	300-355	1.18	-0.08	
3H-3, 137	25.37	27.77	27.75	27.51	300-355	1.18	-0.14	
3H-4, 2	25.52	27.92	27.91	27.66	300-355	0.95	0.06	
3H-4, 17	25.67	28.07	28.06	27.81	300-355	0.95	0.06	
3H-4, 32	25.82	28.22	28.22	27.96	300-355	1.05	0.07	
3H-4, 47	25.97	28.37	28.37	28.11	300-355	1.05	-0.26	
3H-4, 62	26.12	28.52	28.52	28.26	300-355	1.31	-0.37	
3H-4, 76	26.26	28.66	28.66	28.40	300-425	1.76	-0.51	
3H-4, 92	26.42	28.82	28.82	28.56	300-425	1.61	-0.97	
3H-4, 107	26.57	28.97	28.97	28.71	300-355	1.61	-0.89	
3H-4, 122	26.72	29.12	29.12	28.86	300-355	1.53	-0.47	
3H-4, 137	26.87	29.27	29.27	29.01	300-355	1.33	-0.84	
3H-4, 137	26.87	29.27	29.27	29.01	300-355	1.06	-0.69	
3H-5, 2	27.02	29.42	29.42	29.16	300-355	1.42	-0.17	
3H-5, 2	27.02	29.42	29.42	29.16	355-425	1.37	0.12	
3H-5, 17	27.17	29.57	29.57	29.31	300-425	1.86	0.19	
3H-5, 32	27.32	29.72	29.72	29.46	300-425	1.90	-0.68	
3H-5, 47	27.47	29.87	29.87	29.61	300-355	1.57	-0.66	
3H-5, 62	27.62	30.02	30.02	29.76	300-355	1.67	-0.44	
3H-5, 76	27.76	30.16	30.16	29.90	300-355	1.71	-0.45	
3H-5, 92	27.92	30.32	30.32	30.06	300-355	1.80	-0.67	
3H-5, 107	28.07	30.47	30.47	30.21	300-355	1.52	-0.59	
3H-5, 122	28.22	30.62	30.62	30.36	300-355	1.47	-0.42	
3H-5, 137	28.37	30.77	30.77	30.51	300-355	1.51	-0.56	
3H-6, 2	28.52	30.92	30.92	30.66	300-355	1.72	-0.72	
3H-6, 17	28.67	31.07	31.07	30.81	300-355	1.91	-0.36	
3H-6, 30	28.80	31.20	31.20	30.94	300-355	1.62	-0.49	
3H-6, 47	28.97	31.37	31.37	31.11	300-355	1.52	-0.24	
3H-6, 65	29.15	31.55	31.55	31.29	300-355	1.35	-0.33	
3H-6, 77	29.27	31.67	31.66	31.41	300-355	1.35	-0.28	
3H-6, 92	29.42	31.82	31.81	31.56	300-355	1.14	-0.37	
3H-6, 107	29.57	31.97	31.99	31.71	300-355	1.26	-0.65	
3H-6, 122	29.72	32.12	32.17	31.86	300-355	1.26	-0.43	

## APPENDIX B (continued).

Core, section, interval (cm)	ODP depth (mbsf)	Shipboard composite depth (mcd)	Shore-based composite depth (rmcd)	This study composite depth (Bmcd)	Foraminifer size ( $\mu\text{m}$ )	$\delta^{13}\text{C}$ (‰) (PDB)	$\delta^{18}\text{O}$ (‰) (PDB)	Comment
3H-6, 137	29.87	32.27	32.34	32.01	300-355	1.29	-0.39	
3H-7, 2	30.02	32.42	32.48	32.16	300-425	1.46	-0.58	
3H-7, 17	30.17	32.57	32.59	32.31	300-355	1.26	-0.39	
3H-7, 30	30.30	32.70	32.68	32.44	300-355	2.10	-0.76	
3H-7, 47	30.47	32.87	32.84	32.61	300-355	1.66	-0.81	
3H-7, 62	30.62	33.02	33.05	32.76	300-355	1.48	-0.58	
3H-7, 77	30.77	33.17	33.33	32.91	300-355	1.55	-0.62	Not in composite
4H-1, 32	30.82	34.12	34.22	33.94	300-355	1.72	-0.68	
4H-1, 32	30.82	34.12	34.22	33.94	300-355	1.52	-0.74	
4H-1, 47	30.97	34.27	34.58	34.09	300-355	1.44	-0.32	
4H-1, 47	30.97	34.27	34.58	34.09	300-355	1.45	-0.59	
4H-1, 61	31.11	34.41	34.68	34.23	300-355	1.10	-0.09	
4H-1, 77	31.27	34.57	34.76	34.39	300-355	1.22	-0.40	
4H-1, 92	31.42	34.72	34.85	34.54	300-355	1.02	-0.03	
4H-1, 92	31.42	34.72	34.85	34.54	300-355	1.03	-0.11	
4H-1, 107	31.57	34.87	34.95	34.69	300-355	1.16	-0.13	
4H-1, 122	31.72	35.02	35.08	34.84	300-355	1.20	-0.30	
4H-1, 137	31.87	35.17	35.22	34.99	300-355	1.20	-0.36	
138-847D-								
2H-3, 62	10.22	12.02	12.04	11.76	300-355	1.30	-0.09	
2H-3, 77	10.37	12.17	12.16	11.91	300-355	1.51	0.05	
2H-3, 92	10.52	12.32	12.28	12.06	300-355	1.61	-0.02	
2H-3, 107	10.67	12.47	12.41	12.21	300-425	1.81	-0.47	
2H-3, 122	10.82	12.62	12.55	12.36	300-425	1.70	-0.50	
2H-3, 137	10.97	12.77	12.68	12.51	300-425	1.94	-0.46	
2H-4, 2	11.12	12.92	12.82	12.66	300-355	1.69	-0.71	
2H-4, 17	11.27	13.07	13.00	12.81	300-355	1.89	-0.79	
2H-4, 32	11.42	13.22	13.20	12.96	300-425	2.07	-1.10	
3H-3, 62	19.72	22.72	22.72	22.38	300-355	1.47	-0.26	
3H-3, 77	19.87	22.87	22.86	22.53	300-355	1.31	0.08	
3H-3, 92	20.02	23.02	23.01	22.68	300-355	1.20	0.01	
3H-3, 107	20.17	23.17	23.17	22.83	300-355	1.22	0.03	
3H-3, 122	20.32	23.32	23.32	22.98	300-355	1.28	-0.33	
3H-3, 137	20.47	23.47	23.47	23.13	300-355	1.67	-0.64	
4H-3, 47	29.07	33.07	33.07	32.86	300-355	1.66	-0.50	
4H-3, 62	29.22	33.22	33.22	33.01	300-355	1.47	-0.64	
4H-3, 77	29.37	33.37	33.37	33.16	300-355	1.57	-0.68	
4H-3, 92	29.52	33.52	33.51	33.31	300-355	1.38	-0.46	
4H-3, 107	29.67	33.67	33.66	33.46	300-355	1.29	-0.49	
4H-3, 122	29.82	33.82	33.82	33.61	300-355	1.26	-0.42	
4H-3, 137	29.97	33.97	33.97	33.76	300-355	1.44	-0.38	